Dissertation zur Erlangung des Doktorgrades

der Fakultät für Chemie und Pharmazie

der Ludwig-Maximilians-Universität München

A Structural View on Ligands at the Ribosomal Tunnel Exit

Christoph Friedrich Leidig

aus

Tübingen, Deutschland

2012

Parts of this thesis have been submitted to scientific journals for publication:

Christoph Leidig*, Gert Bange*, Jürgen Kopp, Stefan Amlacher, Ajay Aravind, Stephan Wickles, Gregor Witte, Ed Hurt, Roland Beckmann and Irmgard Sinning

* These authors contribute equally to the work

"Structural characterization of a eukaryotic co-translational chaperone, the ribosome-associated complex (RAC)"

Bettina Bradatsch*, **Christoph Leidig***, Sander Granneman, Marén Gnädig, David Tollervey, Bettina Böttcher, Roland Beckmann, and Ed Hurt

* These authors contribute equally to the work

"Structure of late pre-60S ribosomal subunits with nuclear export factor Arx1 bound at the peptide exit tunnel"

Parts of this thesis have been presented at international conferences:

FEBS Advanced Course: Advanced Methods in Protein Crystallization IV
Nové Hrady, Czech Republic, 2009

Christoph Leidig, Marco Gartmann, Gregor Witte and Roland Beckmann (Poster)

"Structural Characterization of RAC and its Ribosomal Interaction"

FASEB conference: Protein Folding in the Cell
Saxtons River, USA, 2009

Christoph Leidig, Marco Gartmann, Gregor Witte and Roland Beckmann (Poster)

"Structural Characterization of RAC and its Ribosomal Interaction"

Table of Contents

Abstract

Protein biosynthesis in all organisms is achieved by ribosomes, universally conserved macromolecular machines composed of ribonucleic acids and proteins. Nascent polypeptides that emerge from the ribosome need to fold into their native states to become biologically active. A ribosome-associated complex (RAC), consisting of the chaperones Zuotin and Ssz1 in *Saccharomyces cerevisiae*, together with the Hsp70 protein Ssb was found to assist the folding process of nascent polypeptide chains. Various biochemical data are available on this system, however, structural information on RAC is scarce and the chaperone complex has not yet been visualized. The results presented in this study demonstrate that as few as 30 amino acids in the N-terminus of Zuotin are sufficient to form a stable complex with Ssz1 and that the head domain located at Zuotin's C-terminus is crucial for efficient binding of RAC to the ribosome. Small-angle x-ray scattering (SAXS) analysis of RAC give insights into the arrangement of Zuotin and Ssz1 inside the complex, and the 3D cryo-EM reconstruction of the *Chaetomium thermophilum* RAC-ribosome complex reveals RAC's binding site close to the ribosomal tunnel exit. In addition, the crystal structure of the Ssz1 ATPase domain explains its inability to hydrolyze ATP and suggests a non-canonical role as a low-affinity holding chaperone.

Cellular ribosome biogenesis is a highly complex and coordinated process. In eukaryotes, the two ribosomal subunits are assembled in the nucleus and are then individually exported to the cytoplasm for translation. Several export factors are required to allow the passage of pre-ribosomal particles through the nuclear pore complexes, including Nmd3, Mex67-Mtr2, and Arx1 in the yeast *Saccharomyces cerevisiae*. The underlying principles and mechanisms of ribosome biogenesis are not well understood. In particular, almost no structural information is available on premature ribosomal subunits. In this study, the first high-resolution three-dimensional (3D) cryo-electron microscopy (cryo-EM) reconstruction of a maturating pre-60S particle is presented. It displays a scattered distribution of non-ribosomal factors across its surface and reveals features of the premature subunit itself. The export factor Arx1 was found to bind to the immature subunit directly at the ribosomal tunnel exit.

The results presented here stress the functional importance of the ribosomal tunnel exit site. A chaperone complex was found to occupy it on the mature ribosome, while it is occupied by an export factor on the premature 60S subunit. The rRNA expansion segment $ES27^L$ seems to be contacting the respective ligands in both cases, suggesting a role in coordination of tunnel exit ligands or signal transmission between those ligands and the ribosome.

Abbreviations

2D	two-dimensional
3D	three-dimensional
AA	amino acid
Ac	acetate
B. taurus	*Bos taurus*
C. thermophilum	*Chaetomium thermophilum*
CP	central protuberance
cryo-EM	cryo-electron microscopy
C-terminus	carboxy-terminus
CTF	contrast transfer function
CV	column volume
DNA	deoxyribonucleic acid
DTT	dithiothreitol
E. coli	*Escherichia coli*
eEF	eukaryotic elongation factor
EF-G	elongation factor G
EF-Tu	elongation factor Tu
eIF	eukaryotic initiation factor
eRF	eukaryotic release factor
ES#$^{\text{L}}$	rRNA expansion segment # of the large subunit
FPLC	fast protein liquid chromatography
FSC	Fourier shell correlation
GFP	green fluorescent protein
H#	rRNA helix #
His	histidine
IF	initiation factor
IPTG	isopropyl β-D-1-thiogalactopyranoside
M. musculus	*Mus musculus*
MBP	maltose-binding protein
MWCO	molecular weight cut-off
NEF	nucleotide exchange factor

NES	nuclear export sequence
NPC	nuclear pore complex
N-terminus	amino-terminus
OD$_{600}$	optical density measured at a wavelength of $\lambda = 600$ nm
PAGE	polyacrylamide gel electrophoresis
PCR	polymerase chain reaction
pH	negative decimal logarithm of hydrogen ion activity
pI	isoelectric point
PMSF	phenylmethylsulfonyl fluoride
RAC	ribosome-associated complex
RF	release factor
RNA	ribonucleic acid
mRNA	messenger ribonucleic acid
rRNA	ribosomal ribonucleic acid
siRNA	small inhibitor RNA
ssRNA	single-stranded ribonucleic acid
tRNA	transfer ribonucleic acid
rpm	rotations per minute
RRF	ribosome release factor
RT	room temperature
S. cerevisiae	*Saccharomyces cerevisiae*
SAXS	small-angle x-ray scattering
SDS	sodium dodecyl sulfate
T. thermophila	*Tetrahymena thermophila*
TCA	trichloroacetic acid
TEV	tobacco etch virus
T$_M$	melting temperature
UAS	universal adapter site
UV	ultraviolet
v/v	volume per volume
w/v	weight per volume
wt	wild-type

Chapter

1 Introduction

1.1 Cellular Biology in a Nutshell

Every organism on this planet is defined by its unique set of nucleic acid molecules. The organization of deoxyribonucleic acid (DNA) strands in complementary double helices enables efficient replication and maintenance of their nucleotide sequences, performed by DNA dependent DNA polymerases and the DNA repair machinery, respectively. Specific DNA sequences, called genes, are transcribed into ribonucleic acid (RNA) molecules by DNA dependent RNA polymerases. This essential process is tightly regulated by transcription factors and repressors. In eukaryotes, the ability to control the accessibility of entire DNA regions by adjusting the chromatin organization provides an additional level of regulation. Important classes of cellular RNAs include messenger RNA (mRNA), ribosomal RNA (rRNA), and transfer RNA (tRNA). Messenger RNAs serve as templates for ribosomes to complete their fascinating task of deciphering the genetic code. During that process they facilitate tRNA molecules to translate a sequence of ribonucleic acid triplets into a chain of amino acids, called protein – a chemically completely unrelated polymer. After folding into their native structures, proteins are involved in virtually all biological functions of the cell. Most proteins have a tightly controlled lifetime and are degraded when they are no longer required, providing the building blocks for new molecules.

1.2 Ribosomes

Ribosomes are large, macromolecular complexes consisting of both, ribosomal proteins and rRNA. They are conserved throughout all domains of life – archaea, eukaryotes and prokaryotes – in their general appearance and primary function: the biosynthesis of proteins. However, they vary considerably in size and composition[1] (Figure 1). The function and architecture of ribosomes are well described due to a large amount of biochemical data and structural information, including three-dimensional (3D) reconstructions from cryo-electron microscopy (cryo-EM) studies and structures derived from x-ray crystallography[2-11] (Figure 2). Ribosomes comprise two subunits: a small and a large ribosomal subunit. In the 70S ribosomes of prokaryotes and archaea, they are referred to as 30S and 50S subunit, according to their respective sedimentation coefficients. For eukaryotic 80S ribosomes, these names change to 40S and 60S subunit, respectively. The subunits are joined during translation initiation (see 1.4) and contain distinct functional sites. The small subunit accommodates the mRNA path and the decoding site, where the anticodons of cognate tRNAs are matched with their respective codons in the mRNA, while the peptidyl transferase center (PTC), that catalyzes the addition of new amino acids to the growing polypeptide chain, is located in the large subunit[6,12]. A continuous channel, called the peptide exit tunnel, extends from the PTC to the solvent side of the 60S subunit. The tRNA binding sites (A-, P- and E-site) are formed by both subunits at their interface. Together, these sites constitute the conserved functional core of the ribosome, formed by roughly 4400 rRNA bases and 34 conserved ribosomal proteins[11,13,14] (Figure 1). Additional conserved

landmarks of the ribosome are the L7/L12-stalk (P-stalk) and the L1-stalk (Figure 1) as well as the ribosomal tunnel exit site. In contrast to the tunnel itself, which is mainly formed by rRNA, the tunnel exit site is almost exclusively surrounded by ribosomal proteins.
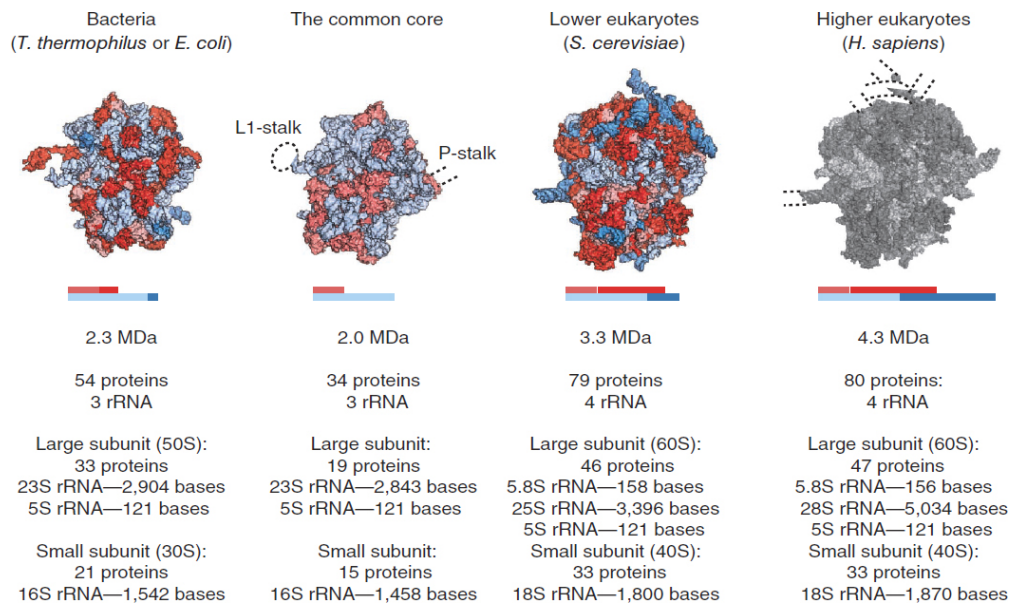
Figure 1. Conservation and composition of ribosomes[1]

Ribosomes from various species and their common core. Ribosomal proteins and rRNA are colored in red and blue, respectively.

Various factors that interact with nascent polypeptide chains need to be coordinated at the tunnel exit. Two major conserved interaction sites shared between several non-ribosomal factors have been identified and were termed universal adapter sites 1 and 2 (UAS1 and UAS2), respectively. The neighboring ribosomal proteins Rpl25/Rpl35 constitute the UAS1 that was shown to serve as docking site for the signal recognition particle (SRP), the protein-conducting channel, ERj1, YidC/Oxa1, and trigger factor[15-19]. The UAS2 is formed by Rpl31/Rpl17 and was shown to facilitate the binding of the nascent polypeptide-associated complex (NAC), the ribosome-associated complex (RAC), and the SRP receptor (SR)[20-22].

Eukaryotic ribosomes feature a multitude of insertions in their rRNA, termed expansion segments. Four very prominent of those expansion segments exist in the 25S/28S rRNA: ES7^L, ES15^L, ES27^L, and ES39^L. Their highly variable lengths between species is one of the major factors responsible for the molecular weight differences found among eukaryotic ribosomes[1,9]. Although ES27^L is clearly the best studied expansion segment, its exact function has not yet been revealed. In *S. cerevisiae*, ES27^L forms a rod-like shape of roughly 150 Å that is flexibly anchored at the ribosome[13]. It can adopt two main conformations, pointing either towards the L1-stalk (named *L1* conformation) or towards the ribosomal tunnel exit site (named *exit* conformation)[15,23]. ES27^L was found to be essential in

S. cerevisiae as well as *T. thermophila*[24,25]. The lethal phenotype can be rescued in *T. thermophila* by insertion of ES27[L] sequences from other species (including *S. cerevisiae*), but not unrelated sequences of similar length[24]. The expansion segment was shown to be functionally important for 60S biogenesis[25]. It was also suggested to coordinate access of ribosomal ligands to the tunnel exit and might even provide a link to translational control[15,18].
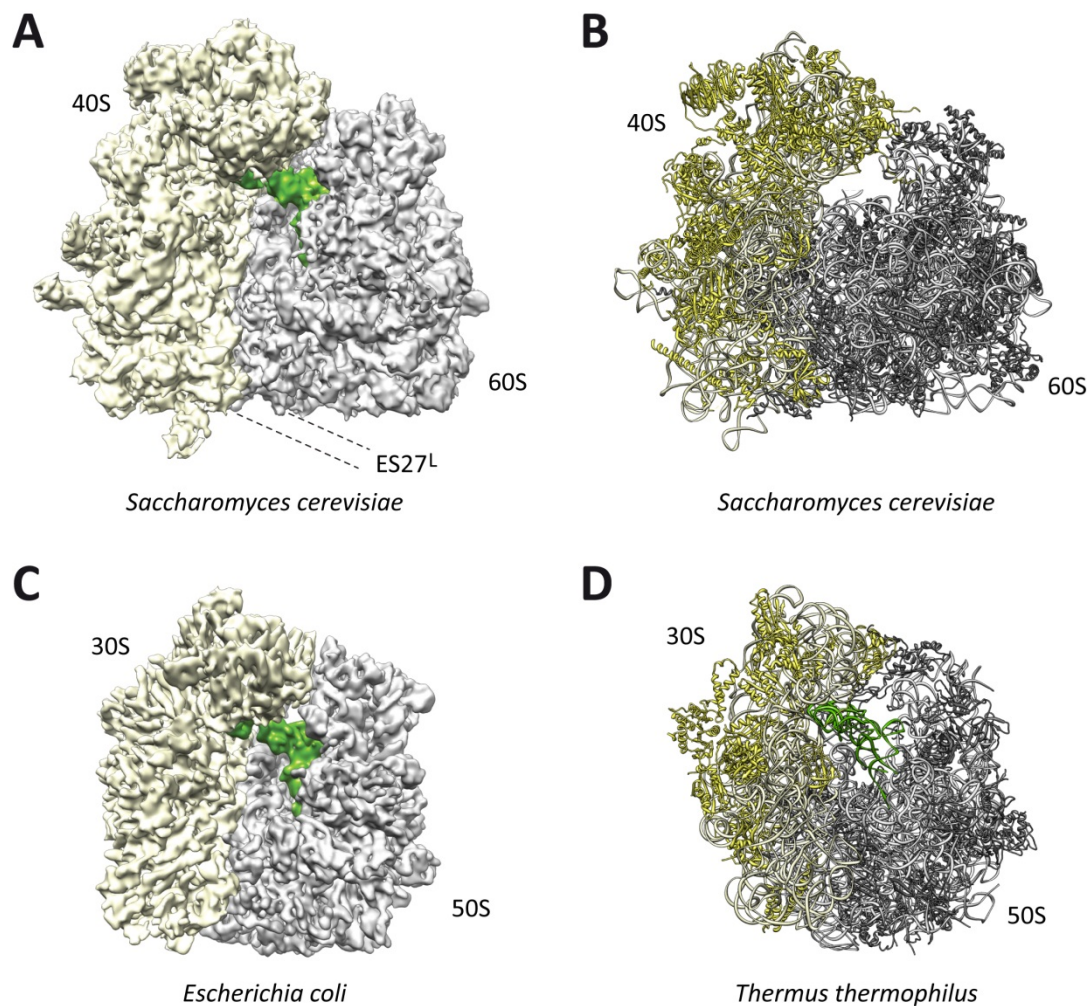
Figure 2. Cryo-EM and crystal structures of 80S and 70S ribosomes[9,11,26,27]

The ribosomal subunits are colored in yellow and grey for the small and the large subunit, respectively. If present, tRNAs are colored in green. **A.** Cryo-EM reconstruction of the *S. cerevisiae* 80S ribosome including a P-site tRNA at 6.1 Å. The approximate position of ES27[L] in the exit conformation is indicated (dotted lines). **B.** Crystal structure of the *S. cerevisiae* 80S ribosome at 3.0 Å resolution (PDB codes: 3U5B, 3U5C, 3U5D and 3U5E). **C.** Cryo-EM reconstruction of the *E. coli* 70S ribosome including a P-site tRNA at 5.8 Å resolution. **D.** Crystal structure of the *Thermus thermophilus* 70S ribosome including tRNAs in the A-, P- and E-site at 2.8 Å resolution (PDB codes: 2J00 and 2J01).

1.3   Ribosome Biogenesis

Despite the similarity of 70S and 80S ribosomes, their assembly pathways are quite different. Prokaryotic ribosome biogenesis is primarily a self-assembly process. This is emphasized by the facts, that the small set of prokaryotic assembly factors is non-essential and that 70S ribosomes can be reconstituted *in vitro*, which in contrast was not yet successfully demonstrated for 80S ribosomes[28,29]. In contrast, most of the more than 200 factors that are involved in eukaryotic ribosome assembly are essential[29]. Another layer of complexity is added in eukaryotes by the compartmentalization of the cell that spatially separates early ribosome biogenesis in the nucleus from the active translation machinery in the cytoplasm. Due to the fundamental differences between both pathways, and since this study was performed in the yeast system, only eukaryotic ribosome assembly will be discussed here.

Ribosome biogenesis in the eukaryote *S. cerevisiae* involves the coordinated assembly of 79 ribosomal proteins and four rRNAs: the 18S rRNA of the small subunit and the 25S, 5.8S and 5S rRNAs of the large subunit[30-32] (Figure 1). The process begins in the nucleolus, where RNA polymerase I transcribes a 35S rRNA precursor transcript, containing the mature sequences of the 18S, 5.8S and 25S rRNAs separated by spacer sequences[33,34]. The 5S rRNA is transcribed separately by RNA polymerase III as a 7S rRNA precursor molecule. After being completely processed, the 5S rRNA is delivered to the nucleolus by the ribosomal proteins Rpl5 and Rpl11 together with the ribosome biogenesis factors Rpf2 and Rrs1[35]. The state at which it actually joins a pre-ribosomal particle is still under debate and may vary between species[36]. The ribosomal proteins are synthesized in the cytoplasm from mRNAs transcribed by RNA polymerase II. They are then targeted to the nucleus and nucleolus. The 35S rRNA precursor transcript is assembled into a 90S pre-ribosomal particle containing early joining ribosomal proteins, the U3 snoRNP and a large number of processing factors of the small subunit. Interestingly, only a few large subunit processing factors are present in this complex. By cleavage at the A_2 site, the 35S transcript is divided into a 20S precursor of the 18S rRNA and a 27S RNA comprising the 5.8S and 25S rRNA sequences. The 43S pre-40S particle and the 66S pre-60S particle are created, containing the 20S pre-rRNA and the 27S pre-rRNA, respectively. They are processed mostly independently and exported from the nucleus as individual pre-subunit particles[28,37].

The pre-40S particle includes a comparatively small number of biogenesis factors in addition to the small subunit proteins and the 20S rRNA. These factors include Rio2, Enp1, Tsr1, Dim1, Dim2, Nob1, Rrp12, Hrr25 and Ltv1[38]. All pre-ribosomal particles are exported from the nucleus through nuclear pore complexes (NPCs). For the pre-40S particle this requires a functional RanGTPase system and Crm1, but additional factors, such as Rrp12, might also contribute[39-41]. The final maturation steps occur in the cytoplasm. The ribosomal protein rpS3 is rearranged in a phosphorylation-dependent manner involving the kinases Hrr25 and Rio2[42]. Correct processing of the 20S pre-rRNA is also dependent on kinases, namely Rio1 and Rio2. The mechanism, however, is not known[31]. Also, the nucleases processing 20S pre-rRNA to 18S rRNA have not been unambiguously identified, yet. Two candidate factors, Nob1 and Fap7, are clearly involved in the process, but nuclease activity has not been

directly demonstrated for either protein[43,44]. A comprehensive low-resolution cryo-EM analysis of various pre-40S particles revealed the binding sites of many important factors[45].
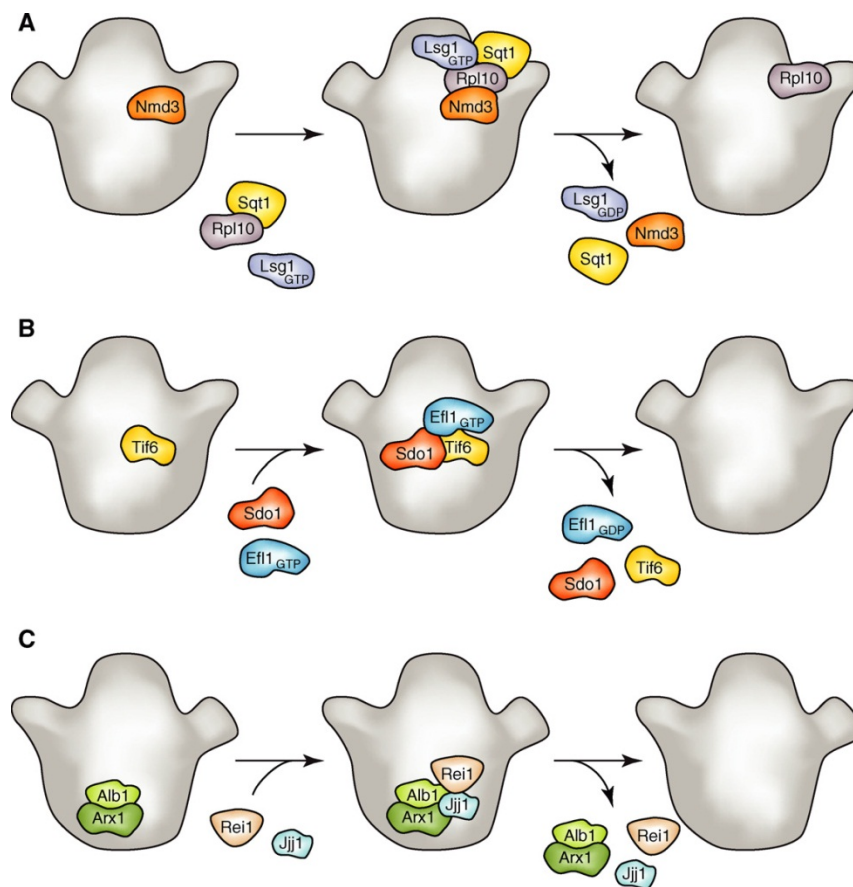
Figure 3. Final steps during cytoplasmic 60S ribosomal subunit maturation in *S. cerevisiae*[31]

Pre-60S particles are depicted as grey shapes. **A.** Release of Nmd3 by Lsg1 and loading of Rpl10, involving Sqt1, are coupled. GTP hydrolysis by Lsg1 is required for Nmd3 release. **B.** Release of Tif6 requires Sdo1 and GTP hydrolysis by Efl1. **C.** Rei1 and Jjj1 are involved in Arx1/Alb1 release.

For pre-60S subunits, rRNA processing is completed in the nucleus[28,46]. Their export through NPCs is also dependent on the RanGTPase system and Crm1 as well as a variety of additional specific export factors[47-49]. One of those, Nmd3, has been shown to interact with Crm1 and its nuclear export sequence (NES) was shown to be necessary for pre-60S export[46,48,50]. Nmd3 binds to the exposed intersubunit surface of mature 60S particles[51].

The protein Arx1 was shown to bind to 60S subunits in the vicinity of the tunnel exit[52]. Together with Alb1, it was suggested to function as a space holder for non-ribosomal factors interacting in this region or as a quality control factor for correct formation of the exit site[31,52]. More recent studies show that Arx1 can interact with the FG repeats of nucleoporins and functions as an export factor for the pre-60S particle[53,54]. The complex of Mex67-Mtr2 is also directly involved in pre-60S nuclear export and is recruited to the 5S rRNA[55,56]. Another factor, Rrp12, that was found to be associated with pre-40S as well as

pre-60S particles, was also suggested to mediate nuclear export of the pre-60S subunit since it contains HEAT repeats, the major structural element involved in RanGTPase dependent nuclear export[38,41,57]. Furthermore Ecm1 and Npl3 were implied to play a role in the process[58,59].

After export to the cytoplasm late ribosomal assembly factors as well as nuclear export factors need to be removed and final ribosomal proteins need to be incorporated to result in a translation competent 60S subunit. Nmd3 is removed from the pre-60S subunit by the GTPase Lsg1 in the presence of Rpl10. This event is closely coupled to the loading of Rpl10 onto the subunit by Sqt1 through an unknown mechanism[60,61] (Figure 3A). The protein Tif6 was found to bind to the intersubunit surface of mature 60S subunits, thereby preventing premature assembly of 80S ribosomes[62]. Removal of the factor requires the presence of Sdo1 and Efl1[63] (Figure 3B). Several proteins have been implicated to play a role in the release and nuclear recycling of the Arx1/Alb1 heterodimer. Rei1 might be required for re-import of Arx1 into the nucleus or may directly facilitate its dissociation from the pre-60S particle[52,64]. Deletion of the Hsp40 protein Jjj1 was found to create defects in Arx1 release, therefore it was speculated that Jjj1, together with its Hsp70 partner protein Ssa1, could also be responsible for this process[31,65] (Figure 3C).

In contrast to the low-resolution cryo-EM data that exists for the pre-40S subunit, little to no structural information is available on pre-60S particles. The determination of the Nmd3 binding site by cryo-EM as well as the Tif6 binding site by cryo-EM and protein crystallography were performed using mature 60S subunits with artificially re-bound factors[51,62,66]. For pre-60S particles isolated from living cells only negative stain EM data in combination with immuno-labeling are available so far[67,68].

1.4 Translation

The process of protein biosynthesis by the ribosome is called translation. It can be functionally divided into initiation, elongation, termination and recycling (Figure 4).

In prokaryotes, during initiation, the 30S subunit forms an active initiation complex at a start site near a Shine-Dalgarno sequence in the mRNA with initiation factors IF1, IF2 and IF3 as well as an initiator tRNA in its P-site[69,70]. Transition to the elongation phase is achieved by ejection of the initiation factors and joining of the large subunit[71]. During this phase, aminoacyl-tRNAs are delivered by elongation factor Tu (EF-Tu) and bound to the A-site of the ribosome, if they display the correct anticodon for the base triplet (codon) of the mRNA located there. After GTP hydrolysis EF-Tu leaves the ribosome and the growing polypeptide chain is transferred to the acceptor stem of the newly bound tRNA in the PTC. Elongation factor G (EF-G) then facilitates the translocation of the mRNA by one codon and the movement of the bound tRNAs from A-site to P-site and from P-site to E-site, respectively. After GTP hydrolysis, EF-G dissociates from the elongation complex, resulting in a vacant A-

site, that is ready to receive the next aminoacyl-tRNA[72,73]. During elongation, ribosomes translating the same mRNA form polysomes. In these large helical structures, ribosomes are arranged with their small subunits facing inwards and their large subunits facing away from each other, resulting in a maximum spacing between their growing polypeptide chains[74]. The elongation cycle is repeated until termination is induced by the presence of a stop codon in the A-site. The stop codon is recognized by either release factor RF1 or RF2, that then triggers the hydrolytic release of the nascent polypeptide chain from the tRNA, before it is removed by RF3[75]. After the ribosome has been recycled by the ribosome release factor (RRF) and EF-G, its subunits are ready to engage into a new round of translation[76,77].
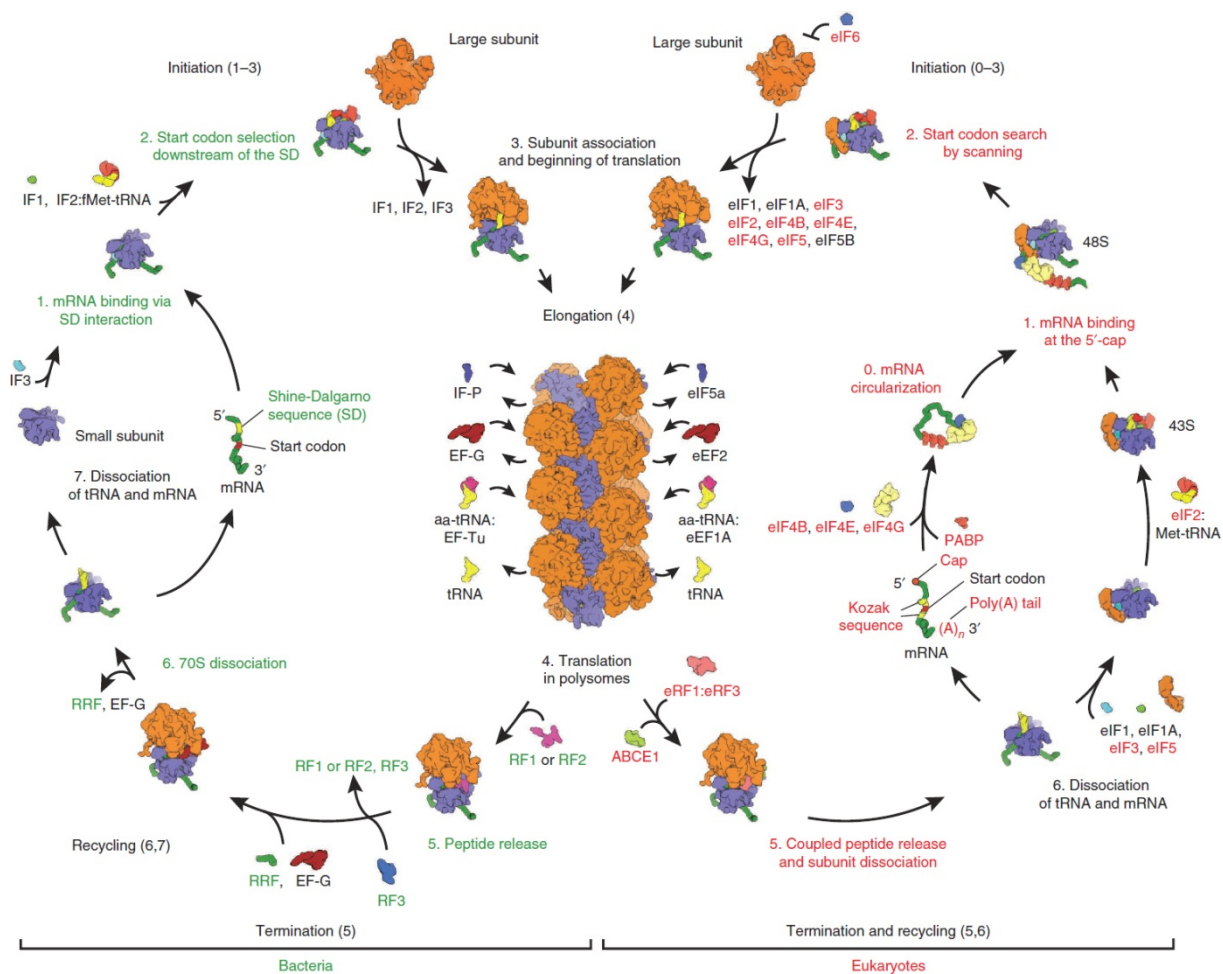
Figure 4. Translation in bacteria and eukaryotes[1]

Names of conserved factors are printed in black, prokaryote or eukaryote specific factors are printed in green or red, respectively.

Although the basic principles of translation in eukaryotes are very similar to those of the bacterial system, there are significant differences and the process involves a highly increased number of regulatory and accessory factors. The most striking differences lie in the mechanisms of initiation and also recycling. In contrast to the targeted mRNA binding of the bacterial 30S subunit at the Shine-Dalgarno sequence and the start codon, the eukaryotic

40S subunit binds to a cap structure at the 5'-end of the mRNA and searches for the start codon by a scanning mechanism. Eukaryotic initiation also involves a significantly larger number of initiation factors[1,70]. As a first step, a 43S preinitiation complex is formed consisting of a 40S subunit, eIF1, eIF1A, eIF3 and GTP bound eIF2, including a methionine initiator tRNA (eIF2–GTP–Met-tRNA$^{Met}_i$). It is likely that eIF5 is also already present in this complex. Then, after mRNA activation by eIF4F and eIF4B, the 43S preinitiation complex binds to the 5'-cap proximal region of the mRNA and starts scanning for a start codon in 5' to 3' direction. Upon start codon recognition by Met-tRNA$^{Met}_i$, a 48S initiation complex is formed, including eIF4A/G and eIF4B as additional subunits. After eIF5-mediated release of the other initiation factors, a 60S subunit joins in to form an active elongation competent 80S ribosome[78]. As the elongation phase itself, the eukaryotic elongation factors (eEF) are well conserved when compared to their prokaryotic homologs. The termination and recycling phases are coupled in eukaryotic translation. The complex of eukaryotic release factors eRF1 and eRF3 together with ABCE1 is responsible for peptide release and subunit dissociation[79].

1.5 Protein Folding and Molecular Chaperones

To become biologically active most nascent polypeptides need to adopt well-defined 3D conformations, their native states. The process of folding can be described as sampling of an energy landscape, in which the native state is the global minimum of the free energy. The native state is defined by the primary sequence of a protein and folding – in particular for small, globular proteins – is a self-guided, spontaneous process[80,81]. However, in the crowded environment of the cell, spontaneous folding is not always successful, resulting in non-native conformations. Such misfolded or partially folded proteins are usually biologically inactive or could even assume new, detrimental activities. The formation of, often extensive, protein aggregates is also a common, misfolding-related problem in the cell, that is linked to various severe diseases[82]. These problems are even more pronounced for larger, multi-domain proteins, which are more frequently found in eukaryotic cells, but also exist in prokaryotes[83]. A special class of proteins has evolved to prevent or rescue such mishaps in the cell: molecular chaperones. They recognize and bind other proteins in their non-native states and help them to adopt their functional conformations[84]. Two of the most important and best understood classes are the Hsp60 chaperonins and the Hsp70 chaperones. Chaperonins form huge barrel-shaped complexes, in which the individual subunits are arranged in symmetric rings. They recognize hydrophobic surfaces of collapsed proteins and individual substrate proteins are bound by globally enclosing them in an internal cavity where they can fold correctly in a confined environment[85]. In contrast, Hsp70 chaperones function as individual proteins. They bind to hydrophobic stretches in extended polypeptide chains, locally enclosing the corresponding regions[86,87].

The overall protein architecture is similar for all Hsp70 chaperones. They comprise a highly conserved N-terminal nucleotide binding domain (NBD, also called ATPase domain) of roughly 44 kDa, followed by a roughly 15 kDa substrate binding domain (SBD) and a less conserved C-terminal domain (CTD) of 10 kDa[84]. Hsp70 family chaperones fulfill a plethora of functions in the cell. Their tasks include folding assistance for nascent polypeptides, trans-membrane transport, disassembly of oligomeric protein structures, support in proteolysis of unstable proteins, and regulation of folded proteins[84]. Interestingly, all of those functions rely on a simple mechanism of binding and release of short exposed hydrophobic stretches[88,89]. The affinity of an Hsp70 chaperone for its substrates is directly regulated by the nucleotide bound to its ATPase domain. While the substrate is tightly bound in the presence of ADP, nucleotide exchange to ATP greatly reduces the binding affinity and increases the dissociation rate. Notably, the association rate is also increased, allowing the formation of new substrate-Hsp70 complexes. These complexes are stabilized upon ATP hydrolysis[86,90-93]. However, the intrinsic ATPase activity of Hsp70 chaperones is too slow to facilitate their functional activity – despite the fact that it is slightly stimulated by substrate binding[91,94,95]. This enables the regulation of Hsp70 activity by the action of Hsp40 co-chaperones (also called J-proteins) and nucleotide exchange factors (NEFs).

Members of the Hsp40 protein family efficiently stimulate Hsp70 ATPase activity[91,96]. These otherwise heterogeneous proteins share a highly conserved domain of roughly 80 amino acids, the J-domain, which is essential for their function[97-99]. The J-domain is characterized by a conserved "HPD" sequence motif that is involved essentially in its interaction with Hsp70[97]. Among other auxiliary domains, Hsp40 proteins often contain their own substrate binding domains, and their efficiency in stimulating Hsp70 ATP hydrolysis is strongly increased in the presence of a substrate. Thereby, Hsp70 ATPase stimulation can be coupled to substrate delivery, preventing unproductive expense of ATP[84,100-102].

Beside ATP hydrolysis, release of ADP and P_i is another regulated step during the chaperone cycle of many Hsp70s, controlled by NEFs of the GrpE family[96,100]. *In vivo*, the actions of both classes of regulatory proteins are coordinated to achieve an optimal equilibrium between substrate binding and release[84]. The complete Hsp70 chaperone cycle (Figure 5) therefore comprises six distinct steps. It starts with (i) the transient substrate interaction with the J-protein or, for J-proteins lacking a SBD, with the ATP-bound state of Hsp70 (Hsp70-ATP). Then, (ii) the J-domain of the co-chaperone binds to Hsp70-ATP and, at the same time, the substrate is transferred to the open binding pocket of Hsp70-ATP. Together, these events (iii) trigger ATP hydrolysis, resulting in a stabilized complex of the substrate with ADP+P_i-bound Hsp70 (Hsp70-ADP) and (iv) dissociation of the J-protein. (v) A NEF can now bind to the complex and stimulate ADP and P_i release. Finally, (vi) upon anew binding of ATP to the Hsp70, the NEF and the bound substrate are released.
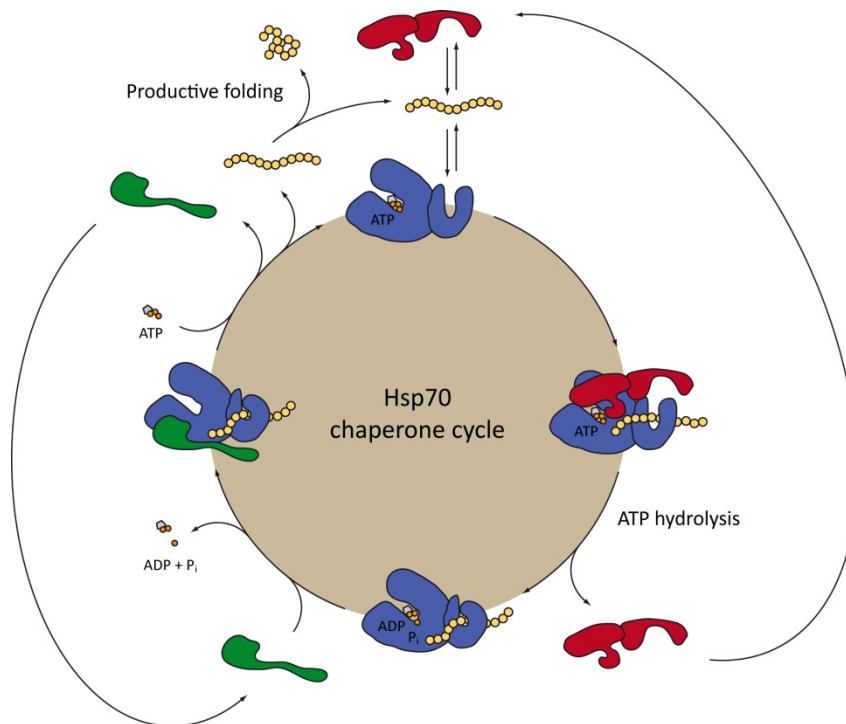
Figure 5. Hsp70 mediated protein folding

Schematic model of the Hsp70 chaperone cycle mediating productive protein folding. The cycle starts with loose interaction of an extended substrate (yellow) with Hsp40 (red) or directly with Hsp70-ATP (blue). A transient complex comprising Hsp70-ATP, Hsp40, and the substrate is formed. ATP hydrolysis is stimulated by the simultaneous interaction of Hsp40's J-domain and the substrate with Hsp70-ATP. As a result, the substrate is tightly bound to Hsp70-ADP and Hsp40 is released. Binding of a NEF (green) leads to the dissociation of ADP and P_i. Re-binding of ATP results in dissociation of the NEF and release of the substrate. The substrate may now fold into its native conformation or re-enter the cycle.

1.6   Co-Translational Folding

Already during its synthesis, the growing polypeptide chain is the subject of modifying enzymes and chaperones. The ribosome, and in particular the tunnel exit region, serves as a platform to coordinate and regulate those factors[103]. The peptide deformylase (PDF) and the methionine aminopeptidase (MAP) are the first enzymes to modify the nascent protein on bacterial ribosomes by successively removing the formyl group from the N-terminal methionine and the methionine itself, respectively[104-106]. In eukaryotes, the N-terminal methionine is not formylated and can be directly removed by a MAP, followed by the N-terminal acetylation of the nascent protein by a member of the Nα-acetyltransferase (NAT) family[107,108]. As soon as the growing polypeptide chain extends past the shielded environment of the ribosomal tunnel, it is exposed to the cytosol and especially prone to aggregation. Therefore, it needs to be shielded until it is long enough to fold into its native conformation[109]. In prokaryotes, this task is fulfilled by trigger factor[110,111]. In eukaryotes, the ribosome-associated NAC was identified as the first factor to interact with the nascent polypeptide chain[112]. In addition, ribosome-associated Hsp70/Hsp40 systems have evolved,

to aid co-translational folding. In the cytosol, the ribosome-associated complex (RAC) works together with cytosolic Hsp70s, while proteins translocated into the lumen of the endoplasmic reticulum (ER) are chaperoned by ER luminal Hsp70s, together with their ribosome-associated membrane protein (RAMP) Hsp40 partners. In *S. cerevisiae*, these systems are constituted by RAC together with the two nearly identical Hsp70 homologs Ssb1 and Ssb2 (referred to as Ssb) and by the Hsp70 Kar2 together with the type I membrane protein Erj5, respectively[113,114].

1.7 The RAC-Ssb System

RAC is the stable, heterodimeric complex of the Hsp70 homolog Ssz1 and the J-protein Zuotin[115]. The chaperone complex is anchored to the ribosome via its Zuotin subunit, which also carries the J-domain required for the stimulation of Ssb[115-118]. Together the chaperones form a functional triad on the ribosome[113]. Their functional dependence is emphasized by the observation that deletion of any of the three chaperones results in the same specific set of phenotypes as their combined deletion[113,117]. Such deletions result in slow growth, sensitivity to cold temperatures (18 °C) as well as high osmolarity, and hypersensitivity to the protein synthesis inhibitor paromomycin, indicating defects in translational fidelity[113,115-117].

Ssb can be cross-linked to ribosome-associated nascent chains[119]. However, these cross-links were shown to be efficient only in the presence of functional RAC[113]. Consistent with its proposed function as co-translational chaperone, a deletion of its SBD domain renders the protein non-functional[120]. Zuotin was originally identified as Z-form DNA-binding protein[121]. Later, it was also shown to tightly interact with tRNA and a small inhibitor RNA (siRNA)[122,123]. Zuotin comprises a unique N-terminal region with no homologies to other Hsp40 proteins, a well conserved J-domain and a highly charged region (CR) close to its C-terminus[118] (Figure 6). The CR was shown to be crucial for ribosome interaction. Since its deletion was found to also abolish tRNA binding, Zuotin was suggested to interact with the ribosome – at least partially – via rRNA contacts[116]. Using a cross-linking approach, Zuotin could be shown to contact Rpl31 at the ribosome. In addition, deletion of Rpl31 displayed similar phenotypes to a RAC or Ssb deletion. However, Zuotin can still bind to ribosomes in the absence of Rpl31. Therefore, the ribosomal protein seems not to be the only contact and seems to be functionally involved in the same process as the chaperones[21].

While the roles of Zuotin and Ssb inside the chaperone triad are quite well established, the exact biological function of Ssz1 needs yet to be determined. It consists of a NBD and a SBD, however, in comparison to other Hsp70s, the SBD is unusually short and Ssz1 is lacking the 10 kDa CTD[115] (Figure 6). Surprisingly, Ssz1 does not require its ability to bind ATP *in vivo* and is not able to hydrolyze ATP[118,124]. Also, its SBD can be deleted without any observable growth defect and only minor defects in translational fidelity *in vivo*[115,117,124]. However, simultaneous disruption of both, nucleotide binding and the SBD, leads to the inactivation of

Ssz1 function *in vivo*[124]. A dual role of Ssz1 in two distinct pathways, related to general growth defects or to translational fidelity, was proposed[124]. It was also found to act in programmed -1 ribosomal frame-shifting[125].
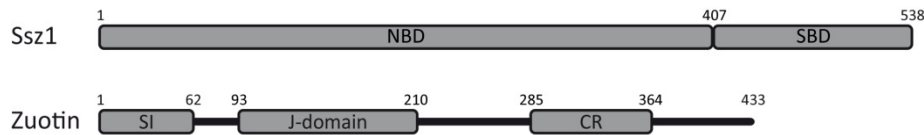
Figure 6. Domain architecture of the subunits of RAC: Ssz1 and Zuotin

The residue numbers indicate domain boundaries. NBD: nucleotide binding domain; SBD: substrate binding domain; SI: Ssz1-interaction domain; CR: charged region.

The stable interaction between a Hsp70 and a Hsp40 found inside RAC is unusual, but not unprecedented. A stable Hsp70 and J-protein complex was previously identified in archaea[126]. RAC is extremely stable and its subunits can only be separated upon their denaturation[124]. Its high stability and the conservation of RAC in higher eukaryotes suggest a functional relevance of the interaction[124,127]. While neither the NBD nor the SBD of Ssz1 could be shown to bind to Zuotin on their own, a region of Zuotin could be identified, that facilitates formation of RAC. The 62 N-terminal residues of Zuotin were shown to be sufficient for its interaction with Ssz1[124,128].

1.8 Motivation

Both, ribosome-associated folding by RAC and eukaryotic ribosome biogenesis have been extensively studied. A lot of biochemical and biophysical data has been acquired on RAC and its interaction with the eukaryotic 80S ribosome. Similarly, the maturation of ribosomal subunits is well described. In contrast, very little structural information is available on either of those topics. For RAC, no 3D structures have been published so far. Negative stain EM studies have been performed on premature ribosomal subunits and low-resolution cryo-EM reconstructions are available for pre-40S particles. However, no high-resolution 3D structures have been determined for pre-60S particles. The aim of this study[129] was to fill this gap. Structural information on RAC or its complex with the ribosome could pave the road towards fully understanding its biological function and might offer insights into the coordination of factors at the tunnel exit. Providing the first 3D structure of a maturation intermediate of a 60S subunit could greatly contribute to our understanding of the fundamental process of ribosome biogenesis in eukaryotes.

Chapter

2 Materials and Methods

2.1 Molecular Cloning

2.1.1 Vectors and Organisms

Specialized vectors (Table 1) and bacterial strains (Table 2) were used for molecular cloning (*E. coli* XL1 blue) or protein expression (*E. coli* Rosetta 2 (DE3)) during this study.

Table 1. Expression vectors

Name	Selection marker	Origin of replication	Company
pET-15b	Ampicillin	pBR322	Novagen
pET-28a	Kanamycin	pBR322	Novagen
pETcoco-2	Ampicillin	oriV, oriS	Novagen
pMal-c2X	Ampicillin	pBR322, M13	New England BioLabs
pProEX HTb	Ampicillin		Invitrogen

Table 2. Organisms

Strain	Description / genotype
E. coli Rosetta 2 (DE3)	BL21 derivative containing a chloramphenicol-resistant plasmid supplying tRNAs for 7 rare codons (AGA, AGG, AUA, CUA, GGA, CCC, and CGG). Lysogen of λDE3 carrying a chromosomal copy of the T7 RNA polymerase gene under control of the lacUV5 promoter. F$^-$ *ompT hsdS*$_B$(r$_B^-$ m$_B^-$) *gal dcm* (DE3) pRARE2 (Cam^R) [130]
E. coli XL1 blue	Endonuclease and recombination deficient strain for improvement of plasmid preparation quality and genomic stability, respectively. *rec*A1 *end*A1 *gyr*A96 *thi*-1 *hsd*R17 *sup*E44 *rel*A1 *lac* [131]

2.1.2 Bacterial Growth Medium and Antibiotics

Bacteria were grown in LB medium (1 % NaCl, 1 % tryptone, 0.5 % yeast extract) or on LB agarose plates (containing an additional 1.3 % agarose) with the appropriate antibiotics for plasmid selection. Antibiotics were used in concentrations of 100 μg/ml ampicillin, 34 μg/ml chloramphenicol, 50 μg/ml Kanamycin, and 20 μg/ml tetracycline.

2.1.3 Polymerase Chain Reaction

Polymerase chain reactions (PCR)[132,133] were used to amplify DNA fragments for molecular cloning or site-directed mutagenesis. Specific DNA primers were used for PCR during this study (Table 3).

PCRs were set up using the Phusion Flash High-Fidelity Master Mix (Finnzymes) according to the enclosed instructions. Template DNA and primer concentrations were in the ranges of 0.3 – 0.7 ng/µl and 0.2 – 0.3 µM, respectively. Cycling conditions were adjusted to the length of the amplified DNA and the melting temperatures (T_M) of the primers.

Amplified product DNA was purified using the QIAquick® PCR Purification Kit (Qiagen) according to the enclosed protocol. 30 µl of water were used for the final elution step.

Table 3. PCR primers

Name	Sequence	Type	T_M (°C)	Construct(s)
5'NdeI-SSZ1-improved	GGA ATT CCA TAT GTC CTC TCC AGT GAT TG	forward	59	pET-28a-Ssz1
3'XhoI-STOP-SSZ1	GAA CTC GAG CTA TAA TTC ACC CTT TAC	reverse	56	pET-28a-Ssz1
5'NcoI-MG-ZUO1	CAT GCC ATG GGA ATG TTT TCT TTA CCT AC	forward	58	pET-15b-zuo50
3'XhoI-STOP-zuo50	CCG CTC GAG TCA AGA CCA GGT GTG	reverse	62	pET-15b-zuo50
5'EcoRI-ZUO1	CGG AAT TCA TGT TTT CTT TAC CTA CCC	forward	56	pMAL-c2X-Zuotin pMAL-c2X-zuo(1-X)
3'XbaI-STOP-ZUO1	GCT CTA GAT CAC ACG AAG TAG GAC AAC	reverse	59	pMAL-c2X-Zuotin pMAL-c2X-zuoR
3'XbaI-STOP-zuo(1-30)	GCT CTA GAT CAT TCG ACC GGA C	reverse	56	pMAL-c2X-zuo30
3'XbaI-STOP-zuo(1-50)	GCT CTA GAT CAA GAC CAG GTG TG	reverse	56	pMAL-c2X-zuo(X-50)
3'XbaI-STOP-zuo(1-70)	GCT CTA GAT CAG TCG ACA TTG G	reverse	55	pMAL-c2X-zuoN
5'EcoRI-zuo1(10+)	CGG AAT TCA TCA CTG TTG AAG TCA AC	forward	56	pMAL-c2X-zuo(10-40)
3'XbaI-STOP-zuo1(1-40)	GCT CTA GAT CAA GCA TGT TGC AAA AAG	reverse	59	pMAL-c2X-zuo(10-40)
5'EcoRI-zuo1(20+)	CGG AAT TCA AAA CCC ATT CG TCC	forward	56	pMAL-c2X-zuo(20-50)
5'EcoRI-zuo1(71+)	CGG AAT TCC CAG ATG AGT TGT TAT TCG	forward	59	pMAL-c2X-zuoJ
3'XbaI-STOP-zuo1(1-170)	GCT CTA GAT CAA ACA AAA TCA CAT GAG TCG	reverse	60	pMAL-c2X-zuoJ
5'EcoRI-zuo1(171+)	CGG AAT TCG CCG ATG TTC CTC CTC C	forward	62	pMAL-c2X-zuoR

2.1.4 Enzymatic DNA Restriction

DNA fragments containing specific restriction sites were treated with the corresponding endonucleases to prepare them for insertion into plasmids by DNA ligation (see 2.1.6).

Commercially available purified restriction enzymes (New England BioLabs) were used according to the manufacturer's protocols. Compatible enzymes were used during the same reactions for DNA fragments with two different restriction sites. After the reactions, the digested DNA was purified using agarose gel electrophoresis and subsequently extracted from the gel (see 2.1.5).

2.1.5   Agarose Gel Electrophoresis and Gel Extraction

Agarose gel electrophoresis was used to separate mixed DNA samples according to the sizes of the individual molecules. It was used for preparative as well as analytical purposes.

Depending on the sizes of the molecules to be separated, agarose gels contained 1 – 1.5 % (w/v) UltraPure™ Agarose (Invitrogen) in 40 mM Tris base, 20 mM acetic acid, and 2 mM EDTA pH 8 (TAE). DNA samples were mixed with an appropriate amount of 6x Loading Dye (Fermentas) and 10,000x GelRed® (Genaxxon). The gels were run in TAE. A constant voltage of 100 V was applied until the desired separation was achieved. A Gel Jet Imager 2005 (Intas) UV light gel documentation system was used to detect bands and take pictures of gels.

To extract specific DNA fragments from a gel, the corresponding bands were cut out under UV light illumination and the DNA was recovered using a QIAquick® Gel Extraction Kit (Qiagen) according to the enclosed protocol. 30 µl of water were used for the final elution step.

2.1.6   DNA Ligation

Restricted (see 2.1.4) target DNA fragments and vector backbones were enzymatically joined by DNA ligation.

T4 DNA ligase (New England BioLabs) was used according to the enclosed manual for DNA ligation reactions. If an insert was cloned for the first time, multiple reactions were set up using various ratios of insert to vector DNA to screen for optimal conditions.

2.1.7   Site-Directed Mutagenesis

Site-directed mutagenesis employs the PCR technique (see 2.1.3) to specifically alter the DNA sequence of a plasmid. To do so, an entire plasmid is amplified with primers containing the desired mutations and, subsequently, the remaining template plasmid is enzymatically degraded by the nuclease DpnI.

PCR primers were designed in a way that they carried a specific mutation and aligned to the flanking regions of the altered sequence. Sets of complementary primers were used to amplify the entire plasmid and ensure the alteration of the sequences of both strands. After the PCR, the reactions were incubated with DpnI (New England BioLabs) according to the manufacturer's manual.

2.1.8   Preparation of Calcium Competent *E. coli* Cells

A pre-culture of 5 ml LB medium was inoculated using a single colony of either *E. coli* XL1 blue or Rosetta 2 (DE3) cells and grown over night shaking at 150 rpm at 37 °C. The pre-culture was diluted 1 : 100 and grown to an optical density (OD_{600}) of 0.6 – 0.8. It was then chilled on ice for 15 min before the cells were transferred to chilled, sterile GSA tubes and centrifuged for 10 min in a SLA-1500 rotor (Sorvall) at 5,000 rpm and 4 °C. The supernatant was discarded and the cells were carefully resuspended in 50 % of the original volume of chilled 100 mM $CaCl_2$. After an incubation time of 30 min on ice, the centrifugation step was repeated, the supernatant was again discarded and the cells were carefully resuspended in 5 % of the original volume of chilled 100 mM $CaCl_2$ + 15 % glycerol. They were then distributed at 4 °C to 50 – 200 µl aliquots in chilled 1.5 ml reaction tubes, which were immediately frozen in liquid nitrogen and stored at -80 °C.

2.1.9   Transformation of Calcium Competent *E. coli* Cells

Freshly ligated plasmids (see 2.1.6), the products of site-directed mutagenesis reactions (see 2.1.7), or purified plasmids, that were to be amplified, were transformed into the *E. coli* XL1 blue cloning strain, while purified plasmids were transformed into *E. coli* Rosetta 2 (DE3) for protein expression.

10 – 100 ng of purified plasmid DNA, 5 µl of a DNA ligation reaction (see 2.1.6), or 5 µl of a site-directed mutagenesis reaction (see 2.1.7) were mixed on ice with 50 µl of competent cells. The samples were kept on ice for 2 min, transferred to a water bath at 42 °C for 30 s and immediately transferred back to the ice. 700 µl LB medium were added before the cultures were incubated at 37 °C for at least 1 h. The cells were pelleted gently by centrifugation in a centrifuge 5417 R (Eppendorf) for 2 min at 7,000 rpm, 650 µl of the supernatants were discarded and the cells were carefully resuspended in the remaining liquid before they were spread on LB plates containing the appropriate antibiotics to select for the inserted plasmid(s). The plates were incubated at 37 °C until colonies were visible.

Negative controls were done by adding water to competent cells instead of DNA. In addition, background controls were done for transformations of ligation products by adding only the ligated vector with no insert.

2.1.10 Plasmid Preparation

5 – 10 ml of LB medium containing the appropriate antibiotics to select for the desired plasmid were inoculated with a single bacterial colony. The culture was incubated over night shaking at 150 rpm at 37 °C. The plasmid DNA was then extracted from the cells using the QIAprep® Spin Miniprep Kit (Qiagen) according to the enclosed protocol. 30 µl of water were used for the final elution step.

2.1.11 Sequencing of DNA Samples

Plasmids or PCR fragments were sent to Eurofins MWG Operon (Ebersberg, Germany) for sequencing. Samples were prepared according to the company's instructions.

2.2   Protein Sample Analysis

2.2.1   Protein Precipitation

The protein content of highly diluted samples destined for SDS-PAGE analysis (see 2.2.2) were quantitatively precipitated using trichloroacetic acid (TCA).

The precipitation reactions were set up on ice and all the reagents were cooled to 4 °C. All protein samples were adjusted to a volume of 1 ml with pure water and kept on ice. 125 µl of 0.15 % sodium deoxycholate were added and, after mixing thoroughly, 125 µl of 72 % TCA were added, resulting in final concentrations of 0.015 % sodium deoxycholate and 7.2 % TCA. At this point, the samples were either stored at -20 °C to be processed later or they were incubated on ice for at least 2 h. The precipitated proteins were pelleted by centrifugation in a centrifuge 5417 R (Eppendorf) for 20 min at 14,000 rpm and 4 °C. After carefully removing the supernatants, pellets were washed with 700 µl of pure acetone chilled to -20 °C. The centrifugation step was then repeated, the supernatants were carefully removed, and the pellets were air-dried at RT for at least 15 min. The pellets were then resolved in 1x SDS sample buffer (see 2.2.2). If the color of the buffer changed to yellow, the pH value was adjusted by addition of 1 µl 1 M Tris/Cl pH 8.

2.2.2   Sodium Dodecyl Sulfate Polyacrylamide Gel Electrophoresis

Denaturing sodium dodecyl sulfate polyacrylamide gel electrophoresis (SDS-PAGE) was used to analyze protein samples by separating the individual proteins according to their sizes. The apparent molecular weights of the proteins were determined using commercial molecular weight markers.[134]

The gels were cast discontinuously, featuring a stacking and separation gel. The stacking gels contained 4 % bis-acrylamide (Rotiphorese® gel 30, Carl Roth GmbH) at a pH of 6.8, while the separation gels contained 12 or 15 % bis-acrylamide at a pH of 8.6, depending on the size range of the proteins to be analyzed. The gels contained 0.1 % (w/v) SDS. The protein samples contained 50 mM Tris base, 2 % (w/v) SDS, 0.1 % (w/v) bromophenol blue, 10 % (v/v) glycerol, 100 mM DTT, pH 6.8 (1x SDS sample buffer) and were heated to 95 °C for 2 – 5 min before being loaded into the loading chambers. The gels were run in 25 mM Tris base, 192 mM glycine, 0.1 % SDS (TGS) at a constant voltage of 200 V.

2.2.3 Staining of Protein Gels

Depending on the required sensitivity, various staining methods were applied. Default staining for low sensitivity was Coomassie Brilliant Blue. For visualization of smaller amounts of proteins SimplyBlue™ SafeStain or SYPRO® Orange Protein Gel Stain were used.

Coomassie Brilliant Blue R-250. Gels were stained in an aqueous solution of 0.25 % (w/v) Coomassie Brilliant Blue R-250 (Carl Roth GmbH), 50 % (v/v) methanol, and 10 % (v/v) acetic acid for 0.5 – 2 h and subsequently destained using 40 % (v/v) methanol and 10 % (v/v) acetic acid in water until the background was translucent and protein bands were clearly visible.

SimplyBlue™ SafeStain. Gels were transferred to 30 ml water and boiled for 60 s using a microwave oven. The water was then exchanged and the gels were boiled again. The water was discarded and the gels were boiled for 30 s in 15 ml SimplyBlue™ SafeStain (Invitrogen). They were then stored at RT until protein bands were fully visible.

SYPRO® Orange Protein Gel Stain. Gels were transferred to 7.5 % acetic acid containing 1:5,000 SYPRO® Orange Protein Gel Stain (Sigma-Aldrich) and incubated in darkness for at least 45 min. The staining solution was then discarded, the gels were washed with 7.5 % acetic acid for 30 s and subsequently transferred to water. For detection and documentation a Typhoon 9400 fluorescence scanner (Amersham Biosciences) was used at an excitation wavelength of 488 nm and a detection wavelength of 580 nm.

2.3 Protein Expression in *E. coli* and Purification of Proteins

2.3.1 Heterologous Protein Expression in *E. coli* Rosetta 2 (DE3)

The plasmid(s) (Table 4) coding for the protein(s) to be expressed were transformed (see 2.1.9) into *E. coli* Rosetta 2 (DE3). Single colonies from the transformation plates were used to inoculate 50 – 200 ml pre-cultures, that were grown over night shaking at 150 rpm and 37 °C and were then used to inoculate expression cultures at an OD_{600} of 0.05. All cultures contained the appropriate antibiotics for the selection markers of the used plasmids. The expression cultures were grown shaking at 150 rpm at 37 °C to an OD_{600} of 0.6 – 0.8 until expression was induced by the addition of 0.5 – 1.5 mM isopropyl β-D-1-thiogalactopyranoside (IPTG). The cultures were then shifted to 18 °C and incubated over night.

Cells were harvested by centrifugation for 15 min at 5,000 g and 4 °C in a SLC-6000 rotor (Sorvall). The resulting pellets were then resuspended in fresh LB medium, transferred to 50 ml tubes and pelleted again by centrifugation for 20 min at 4,460 g and 4 °C in a

ROTANTA 46 R centrifuge (Hettich) before they were frozen in liquid nitrogen and stored at -80 °C.

Table 4. Protein constructs

Name	Description	Tag (terminus)	Origin	Vector
Ssz1	wt Ssz1 (AA 1-578)	-	*C. thermophilum*	pET-28a
Ssz1	wt Ssz1 (AA 1-538)	-	*S. cerevisiae*	pET-28a
zuo10-40	Zuotin AA 10-40	MBP (N)	*S. cerevisiae*	pMal-c2X
zuo1-30	Zuotin AA 1-30	MBP (N)	*S. cerevisiae*	pMal-c2X
zuo1-50	Zuotin AA 1-50	MBP (N)	*S. cerevisiae*	pMal-c2X
zuo20-50	Zuotin AA 20-50	MBP (N)	*S. cerevisiae*	pMal-c2X
zuo50	Zuotin AA 1-50	-	*S. cerevisiae*	pET-15b
zuoJ	Zuotin AA 71-170	MBP (N)	*S. cerevisiae*	pMal-c2X
zuoN	Zuotin AA 1-70	MBP (N)	*S. cerevisiae*	pMal-c2X
zuoR	Zuotin AA 171-433	MBP (N)	*S. cerevisiae*	pMal-c2X
Zuotin	wt Zuotin (AA 1-446)	6xHis-TEV-HA (N)	*C. thermophilum*	pProEX HTb
Zuotin	wt Zuotin (AA 1-433)	-	*S. cerevisiae*	pETcoco-2
Zuotin	wt Zuotin (AA 1-433)	MBP (N)	*S. cerevisiae*	pMAL-c2x
zuoΔC	Zuotin AA 1-110	6xHis (N)	*S. cerevisiae*	pProEX HTb
zuoΔH	Zuotin AA 1-350	6xHis-TEV-HA (N)	*C. thermophilum*	pProEX HTb
zuoΔHCR	Zuotin AA 1-290	6xHis-TEV-HA (N)	*C. thermophilum*	pProEX HTb

2.3.2 Mechanical Lysis of Bacterial Cells Using a French Press

Pelleted cells (see 2.3.1) were thawed on ice and resuspended in 50 ml lysis buffer. The composition of the lysis buffer varied and is described separately for each purification strategy (see 2.3.3). A M-110L Microfluidizer Processor (Microfluidics) was equilibrated with lysis buffer before the cells were disrupted during three passes at 15,000 psi. Some grains of DNAseI (Roche) were added to the cell lysates and they were incubated on ice for 15 – 20 min before they were cleared by centrifugation for 30 min at 30,000 g and 4 °C in a SS-34 rotor (Sorvall).

2.3.3 Description of Individual Purification Strategies

2.3.3.1 Purification of S. cerevisiae RAC

S. cerevisiae RAC was purified from *E. coli* to determine its solution structure by SAXS (see 2.6.2). The purification strategy was based on the strong, opposing net charges of the negatively charged Ssz1 (pI = 4.78) and the positively charged Zuotin (pI = 8.18) near neutral pH values. This allowed for purification without any tag. RAC was first bound to an anion exchange column to concentrate the sample and remove initial impurities. This step was followed by another anion exchange chromatography and subsequent cation exchange chromatography. Any remaining impurities were then removed during size exclusion chromatography. An Äkta Purifier FPLC system (GE Healthcare) was used for all chromatography steps.

Expression of *S. cerevisiae* wild-type (wt) Ssz1 and Zuotin in *E. coli* cells was induced by the addition of 1 mM IPTG (see 2.3.1) and the cells were lysed (see 2.3.2) in 40 mM HEPES pH 7.4, 240 mM KOAc, 0.014 % β-mercapto ethanol, 1 mM PMSF, and Protease Inhibitor Cocktail Tablets (complete EDTA-free, Roche). The cleared lysate was filtered through a 0.22 µm Millex® syringe filter (Millipore) and applied to a ResourceQ anion exchange column (GE Healthcare) equilibrated with 40 mM HEPES pH 7.4 and 240 mM KOAc. Bound material was eluted using a linear gradient to 1 M KOAc over 25 CV, peak fractions were analyzed using SDS-PAGE (see 2.2.2), and RAC containing fractions were pooled. The sample was diluted 1:4 with 40 mM HEPES pH 7.4 and subsequently applied to a Poros HQ/20 anion exchange column (Applied Biosystems) equilibrated with 40 mM HEPES pH 7.4. A linear gradient to 1 M KOAc over 20 CV was used for elution, peak fractions were analyzed, and RAC containing fractions were pooled. The sample was diluted 1:6 with 40 mM HEPES pH 7.4 and subsequently applied to a Poros HS/20 cation exchange column (Applied Biosystems) equilibrated with 40 mM HEPES pH 7.4. Proteins were eluted using a linear gradient to 1 M KOAc over 20 CV, peak fractions were analyzed, and RAC containing fractions were pooled. The pooled fractions were then concentrated to a volume suitable for size exclusion chromatography using an Amicon® Ultra centrifugal filter (Millipore) with a molecular weight cut-off (MWCO) of 30 kDa at 3,500 g and 4 °C, filtered through a 0.22 µm syringe filter, and applied to a Superdex 200 size exclusion chromatography column (GE Healthcare) equilibrated with 20 mM Tris pH 7.4, 50 mM NaCl, and 2 mM DTT. Peak fractions were analyzed and fractions containing highly purified RAC were pooled and concentrated to the desired concentration.

2.3.3.2 Purification of S. cerevisiae RAC(zuoΔC)

S. cerevisiae RAC(zuoΔC) was purified from *E. coli* to determine its solution structure by SAXS (see 2.6.2). A 6xHis-tag was used for initial purification by metal ion affinity chromatography and remaining impurities were removed using size exclusion chromatography. An Äkta Purifier FPLC system (GE Healthcare) was used for all chromatography steps. Purification was done by Steffen Fliehmann during his Bachelor's thesis in the lab.

Expression of *S. cerevisiae* wild-type (wt) Ssz1 and N-terminally 6xHis-tagged zuoΔC in *E. coli* cells was induced by the addition of 1 mM IPTG (see 2.3.1) and the cells were lysed (see 2.3.2) in 40 mM HEPES pH 7.4, 240 mM KOAc, 0.014 % β-mercapto ethanol, 1 mM PMSF, and Protease Inhibitor Cocktail Tablets (complete EDTA-free, Roche). The cleared lysate was filtered through a 0.22 μm Millex® syringe filter (Millipore) and applied to a His-Trap™ HP Ni^{2+} affinity column (GE Healthcare) equilibrated with 40 mM HEPES pH 7.4 and 240 mM KOAc. After washing the column for 50 CV in the presence of 15 mM imidazole, proteins were eluted using a linear gradient to 500 mM imidazole over 20 CV. Peak fractions were analyzed using SDS-PAGE (see 2.2.2) and RAC(zuoΔC) containing fractions were pooled. The sample was then concentrated to a volume suitable for size exclusion chromatography using an Amicon® Ultra centrifugal filter (Millipore) with a molecular weight cut-off (MWCO) of 30 kDa at 3,500 g and 4 °C, filtered through a 0.22 μm syringe filter, and applied to a Superdex 200 size exclusion chromatography column (GE Healthcare) equilibrated with 20 mM Tris pH 7.4, 50 mM NaCl, and 2 mM DTT. Peak fractions were analyzed and fractions containing highly purified RAC(zuoΔC) were pooled and concentrated to the desired concentration.

2.3.3.3 Purification of S. cerevisiae HisRAC50

S. cerevisiae HisRAC50 was purified from *E. coli* for crystallization experiments (see 2.6.3) in a two-step purification procedure consisting of a metal ion affinity chromatography step followed by size exclusion chromatography.

Expression of *S. cerevisiae* full-length 6xHis-tagged Ssz1 and zuo50 in *E. coli* cells was induced by the addition of 1.5 mM IPTG (see 2.3.1) and the cells were lysed (see 2.3.2) in 20 mM Tris/HCl pH 7.4, 300 mM NaCl, 10 mM imidazole, 10 mM 2-mercaptoethanol, 1 mM PMSF, and Protease Inhibitor Cocktail Tablets (complete EDTA-free, Roche). The cleared lysate was applied to a column containing Ni-NTA resin (Qiagen) equilibrated with lysis buffer. After washing the column with lysis buffer containing 20 mM imidazole, the imidazole concentration was stepwise increased to 250 mM. All fractions were analyzed using SDS-PAGE (see 2.2.2). HisRAC50 containing fractions were pooled and concentrated to a volume suitable for size exclusion chromatography using an Amicon® Ultra centrifugal filter (Millipore) with a molecular weight cut-off (MWCO) of 10 kDa at 3,500 g and 4 °C, filtered through a 0.22 μm syringe filter, and applied to a Superdex 200 size exclusion chromatography column (GE Healthcare) equilibrated with 10 mM Tris pH 7.4, 50 mM NaCl, and 2 mM DTT. Peak fractions were analyzed and fractions containing highly purified HisRAC50 were pooled and concentrated to the desired concentration.

2.3.3.4 Purification of S. cerevisiae RAC50

S. cerevisiae RAC50 was purified from *E. coli* for crystallization experiments (see 2.6.3). The purification strategy was modified from the wt RAC purification (see 2.3.3.1). Due to the deletion of significant parts of Zuotin, the complex lost its positively charged subunit and cannot interact with cation exchange resins any more. The initial step featured a cation exchange column directly connected to an anion exchange column. Thus, many

contaminations were already removed before RAC50 was bound to the resin of the anion exchange column. Major remaining impurities were then removed using hydrophobic interaction chromatography and the final step was size exclusion chromatography.

Expression of *S. cerevisiae* wt Ssz1 and zuo50 in *E. coli* cells was induced by the addition of 1 mM IPTG (see 2.3.1) and the cells were lysed (see 2.3.2) in 50 mM Tris/HCl pH 8, 50 mM NaCl, 2 mM DTT, 1 mM PMSF, and Protease Inhibitor Cocktail Tablets (complete EDTA-free, Roche). The cleared lysate was filtered through a 0.22 µm Millex® syringe filter (Millipore) and applied to the combination of a HiTrap® SP cation exchange column (GE Healthcare) connected to a HiTrap® Q HP anion exchange column (GE Healthcare) using a peristaltic pump. Both columns had been equilibrated with 50 mM Tris/HCl pH 8, 50 mM NaCl, and 2 mM DTT. The anion exchange column was then transferred to an Äkta Purifier FPLC system (GE Healthcare) and bound proteins were eluted using a linear gradient to 1 M NaCl over 20 CV. Peak fractions were analyzed using SDS-PAGE (see 2.2.2) and RAC50 containing fractions were pooled. The sample was then slowly mixed with 2.2 M $(NH_4)_2SO_4$ to a final concentration of 1.1 M $(NH_4)_2SO_4$ and incubated on ice for 30 min. It was then filtered through a 0.22 µm syringe filter and subsequently applied to a HiTrap® PS hydrophobic interaction column (GE Healthcare) equilibrated with 50 mM Tris/HCl pH 7.6, 1 M $(NH_4)_2SO_4$, and 2 mM DTT. Proteins were eluted using a linear gradient to 50 mM Tris/HCl pH 7.6 and 2 mM DTT over 20 CV and peak fractions were analyzed. Usually, the elution of RAC50 was overlapping with a contaminating protein of roughly 100 kDa that could not be removed by size exclusion chromatography. Therefore, only those fractions that did not contain this specific contamination were pooled, concentrated to a volume suitable for size exclusion chromatography using an Amicon® Ultra centrifugal filter (Millipore) with a molecular weight cut-off (MWCO) of 10 kDa at 2,000 g and 4 °C, filtered through a 0.22 µm syringe filter, and applied to a Superdex 200 size exclusion chromatography column (GE Healthcare) equilibrated with 10 mM Tris pH 7.4, 50 mM NaCl, and 2 mM DTT. Peak fractions were analyzed and fractions containing highly purified RAC50 were pooled and concentrated to the desired concentration.

2.3.3.5 Purification of C. thermophilum RAC Truncation Constructs

C. thermophilum RAC constructs with various truncations of the Zuotin subunit were purified from *E. coli* for interaction studies (see 2.5.2) with *C. thermophilum* 80S ribosomes. The respective Zuotin truncation mutants carried an N-terminal 6xHis-tag followed by a tobacco etch virus (TEV) protease cleavage site and a HA-tag.

Expression of *C. thermophilum* wt Ssz1 and a Zuotin truncation mutant in *E. coli* cells was induced by the addition of 0.5 mM IPTG (see 2.3.1) and the cells were lysed (see 2.3.2) in 20 mM Tris/HCl pH 7, 200 mM KOAc, 7.5 mM $Mg(OAc)_2$, 15 mM imidazole, 1 mM DTT, and 1 mM PMSF. The cleared lysate was applied to 0.3 ml Ni-NTA resin (Qiagen) per 250 ml expression culture volume and washed with at least 50 CV of the lysis buffer (without PMSF) before bound proteins were eluted using 250 mM imidazole. The imidazole concentration was reduced to 15 – 20 mM during successive cycles of concentrating the sample using an

Amicon® Ultra centrifugal filter (Millipore) with a molecular weight cut-off (MWCO) of 10 kDa at 2,000 g and 4 °C and diluting it with imidazole-free buffer. The 6xHis-tag was proteolytically removed by incubation with TEV protease over night at 4 °C and the sample was then re-applied to the same amount of Ni-NTA resin as before. The flowthrough was collected and the resin was washed twice with 3 CV 20 mM Tris/HCl pH 7, 200 mM KOAc, 7.5 mM Mg(OAc)$_2$, 15 mM imidazole, and 1 mM DTT. The flowthrough of the washing steps was pooled with the flowthrough of the loading step and a PD-10 desalting column (GE Healthcare) was used to change the buffer to 20 mM Tris/HCl pH 7, 200 mM KOAc, 7.5 mM Mg(OAc)$_2$, and 2 mM DTT. The sample was then concentrated as needed and aliquots were frozen in liquid nitrogen and stored at -80 °C.

2.4   Purification of *C. thermophilum* 80S Ribosomes

C. thermophilum 80S ribosomes were prepared from the mycelium of the fungus. The purification was performed according to a standard purification protocol for yeast 80S ribosomes by Heidemarie Sieber and Dr. Thomas Becker.

The grinded mycelium (kindly provided by Stefan Amlacher, Hurt Lab, BZH, Heidelberg, Germany) was resuspended in 2 ml 20 mM HEPES/KOH pH 7.5, 100 mM KOAc, 125 mM sucrose, 7.5 mM Mg(OAc)$_2$, 1 mM DTT, and 0.5 mM PMSF per 1 g of mycelium and vortexed until no clumps remained. Insoluble material was removed by centrifugation at 4,000 rpm in a ROTANTA 46 R centrifuge (Hettich) for 10 min and subsequent centrifugation at 15,500 rpm in a SS-34 rotor (Sorvall) for 15 min. 15 – 20 ml of the cleared lysate were loaded upon a two layered high-salt sucrose cushion in a Ti-70 centrifuge tube (Beckman). The top layer of the cushion consisted of 3 ml 1.5 M sucrose, 20 mM HEPES/KOH pH 7.5, 500 mM KOAc, 5 mM Mg(OAc)2, 1 mM DTT, and 0.5 mM PMSF, while the bottom layer consisted of 3 ml of the same buffer containing 2 M sucrose. Ribosomes were pelleted by centrifugation in a Ti-70 rotor (Beckman) in an Optima L-80 XP ultra-centrifuge (Beckman Coulter) at 53,500 rpm for 18 h at 4 °C. The supernatant was discarded and the pellet was dissolved for 45 min in 200 µl 20 mM HEPES/KOH pH 7.5, 50 mM KOAc, 5 mM Mg(OAc)$_2$, 1 mM DTT, and 0.5 mM PMSF.

A sample of the recovered ribosomes was spun through a 10 – 40 % sucrose gradient. During analysis of the gradient, no 40S or 60S subunits could be detected. Therefore, no further purification steps were performed.

2.5 Interaction Studies

2.5.1 Protein Pulldown Assay

Pulldown assays were used to test various MBP-tagged Zuotin and 6xHis-tagged Ssz1 constructs from *S. cerevisiae* for interaction.

S. cerevisiae MBP-tagged Zuotin and 6xHis-tagged Ssz1 constructs were separately expressed in *E. coli* (see 2.3.1). Cells from two constructs were then mixed in a ratio to achieve stoichiometric amounts of both proteins and subsequently lysed (see 2.3.2) in 20 mM HEPES/KOH pH 7.5, 150 mM KCl, 10 mM Mg(Cl)$_2$, and 1 mM DTT. The cleared lysate was split into two aliquots. They were then processed separately. One aliquot was applied to an amylose resin (New England BioLabs) column equilibrated with lysis buffer. The column was washed with 100 CV of lysis buffer and bound proteins were eluted with 10 CV lysis buffer containing 10 mM maltose (Carl Roth GmbH). The other aliquot was adjusted to 20 mM imidazole using lysis buffer containing 120 mM imidazole and then applied to a Ni-NTA resin (Qiagen) column equilibrated with lysis buffer containing 20 mM imidazole. This column was washed with 100 CV of the same buffer and bound proteins were eluted with 10 CV lysis buffer containing 250 mM imidazole. All samples were analyzed using SDS-PAGE (see 2.2.2).

2.5.2 Co-Sedimentation Binding Assay

Co-sedimentation binding assays were used to test *C. thermophilum* RAC and various truncation constructs for interaction with 80S ribosomes.

Purified candidate molecules were mixed with purified 80S ribosomes and an appropriate binding buffer to achieve a total volume of 20-25 µl before they were incubated on ice for 10 min. Subsequently, they were loaded onto a 620 µl sucrose cushion containing 750 mM sucrose in addition to the components of the binding buffer in a SW-60 ultra-centrifuge tube (Beckman). Using the appropriate adapters, the tubes were inserted into SW-55 Ti buckets and centrifuged in the corresponding rotor (Beckman) in an Optima L-80 XP ultra-centrifuge (Beckman Coulter) at 164,000 g (40,000 rpm) for 135 min at 4 °C. Immediately after the centrifugation step, the tubes were removed from the rotor and carefully frozen in liquid nitrogen. They were then cut with a scalpel 2 cm from the bottom. The upper and the lower fragments are referred to as supernatant and pellet, respectively. The protein content of the samples was then TCA-precipitated (2.2.1), separated by SDS-PAGE (2.2.2) and visualized with SimplyBlue™ SafeStain or SYPRO® Orange (2.2.3).

Binding buffers. The binding buffer for *C. thermophilum* RAC contained 20 mM Tris/Cl pH 7, 100 mM sucrose, 7.5 mM Mg(OAc)$_2$, 2 mM DTT and variable concentrations of KOAc. The binding buffer for the *C. thermophilum* RAC truncation mutants contained 20 mM HEPES/KOH pH 7, 100 mM KOAc, 7.5 mM Mg(OAc)$_2$, and 2 mM DTT.

2.6   Structural Biology Methods

2.6.1   Cryo-EM and Single-Particle Reconstruction

The cryo-EM workflow is described for both of the projects presented in this thesis. Differences between the projects are color coded: *C. thermophilum* RAC-80S ribosome complex / *S. cerevisiae* Arx1 pre-60S particle related data is highlighted in red / blue, respectively.

2.6.1.1   Sample Preparation: C. thermophilum RAC-80S Ribosome Complex

2 pmol 80S ribosomes and 10 pmol RAC (purified by Dr. Gert Bange, Heidelberg) were mixed in the presence of 20 mM Tris/Cl pH 7, 100 mM KOAc, 100 mM sucrose, 7.5 mM $Mg(OAc)_2$, and 2 mM DTT to a total volume of 25 µl.

2.6.1.2   Sample Preparation: S. cerevisiae Arx1 pre-60S Particle

Arx1 pre-60S particles were purified from *S. cerevisiae* YPD liquid cultures grown to log phase at 30°C by tandem affinity purification (TAP) via Alb1-TAP, the binding partner of Arx1. The purification was performed by Dr. Bettina Bradatsch (Hurt Lab, BZH, Heidelberg) as described[46] with the following modifications: the purification buffer was 50 mM Tris/Cl pH 7.5, 100 mM NaCl, 5 mM $MgCl_2$, and 0.075 % (v/v) NP-40. NP-40 was only present during cells lysis. The final elution buffer was 50 mM Tris/Cl pH 7.5, 100 mM NaCl, 5 mM $MgCl_2$, 0.5 mM DTT, and 3.5 mM EGTA.

2.6.1.3   Data Collection

3.5 µl of the sample were applied to 2 nm pre-coated holey carbon supported grids (Quantifoil R3/3) and vitrified using a Vitrobot Mark IV (FEI Company). The sample was visualized on a Titan Krios TEM (FEI Company) at 200 keV under low dose conditions ($20 \ e^-/Å^2$) at a nominal magnification of 75,000x using a nominal defocus range of -3.5 to -1 µm. Images (called micrographs) were recorded on a TemCam F416 camera (4096 x 4096 pixel, 15.6 µm pixel size, 1 sec/full frame, TVIPS GmbH) with a final magnification of 148,721x at the plane of the CCD camera. The final image pixel size was 1.049 Å on the object scale. The EM-TOOLS software (TVIPS GmbH) was used for semi-automatic data collection. Grid meshes and holes were manually selected before the software automatically re-centered the beam, waited for drift, corrected the focus, and recorded images for each selected hole. Beam-shift, astigmatism, and coma were also automatically corrected by the software in regular time intervals.

Preparation of grids and data collection were performed by Charlotte Ungewickell and Dr. Otto Berninghausen.

2.6.1.4   Data Pre-Processing

The cryo-EM images were pre-processed in an interactive manner using various scripts based on the SPIDER and WEB software package[135,136]. The 16 bit 'tiff' micrographs were initially

converted into SPIDER-readable files using the 'CP FROM RAW' command, skipping 88,414 header bytes. The correct defocus and the contrast transfer function (CTF) were determined for each micrograph using the 'TF ED' command. The parameters were set to a spherical aberration constant of 2.7 mm, an electron wavelength of λ = 0.02508 Å, and an amplitude contrast ratio of 0.07. Micrographs that were closer to the focus than -1.2 μm or farther away than -3.7 / -4.2 μm were omitted. The rotational symmetry of the power spectra of the remaining micrographs was determined by calculating the internal cross-correlation of a power spectrum at 0° and 90° rotation. Micrographs with an internal cross-correlation of their power spectrum of less than 0.6 / 0.47 were also omitted. The remaining micrographs and their power spectra were visually inspected using WEB. Micrographs were excluded from the dataset if they showed serious ice contamination or a cracked mesh, or if their power spectrum showed indications for drift or astigmatism.

Particles were automatically detected using a modified version (Andreas Hauser) of the SIGNATURE software[137] with the previous low-resolution reconstruction of a *C. thermophilum* 80S ribosome / an electron density map created from the crystal structure of the *S. cerevisiae* ribosomal 60S subunit[10] as a reference. The parameters were set to a particle size of 250 / 234 pixel, a particle distance of 35 / 5 pixel, and a local correlation threshold (LCF) of 0.35. Based on the coordinates found by SIGNATURE, the corresponding particles were then windowed out from the micrographs using the SPIDER 'WI' command with a window size of 438 x 438 / 414 x 414 pixel, and their contrast was inverted. Particle images from a subset of random micrographs throughout the used defocus range were visually inspected and classified as "good-" or "non-" particles, like noise, carbon edges, ice, or other contaminations. Those particles were used as training dataset for the machine learning algorithm MAPPOS[138] which was then employed to classify all particles of the dataset accordingly.

Using the SPIDER 'AP MQ' command, the remaining particles were then aligned at 3-fold decimation to 83 projections of the initial reference using a cross-correlation-based projection matching technique. The translational search range was restricted to 17 pixel with a step size of 1 pixel, and only rings with radii from 5 – 50 pixel were analyzed. For each particle, the cross-correlation, the translational shifts (x/y-shifts), and the Eulerian angles were saved. The number of reference projections used corresponds to an angular accuracy of 15°. The micrograph-based organization of the dataset was changed to a defocus-based organization at this point. The micrographs were merged into "defocus groups" containing up to 2,000 particles according to their defocus values.

2.6.1.5 Refinement

The x/y-shifts and the Eulerian angles – and thereby the quality and resolution of the 3D reconstructions – were improved in an iterative projection matching process. During each round of refinement, all of the particles were aligned to the 3D reconstruction of the previous round and then backprojected to create an new volume. For the first round, the same reference was used as for the initial alignment. The angular increment between

reference projections (search angle) was decreased during the refinement and the reference volumes were filtered to allow for an improving accuracy of the alignment using the 'FQ' command. The Butterworth low-pass filter was selected and the pass-band and stop-band frequencies were chosen so that frequencies were removed, that were not above the noise level in the Fourier shell correlation (FSC) plot (see 2.6.1.7) of the volume. During later stages of the refinement, the reference was multiplied with a mask to restrict the alignment to the ribosomal particle, thereby avoiding the alignment of noise. The particles were aligned using the 'AP MD', 'AP RQ', 'AP RN', or 'AP RD' commands. Sub-volumes were backprojected separately from the particles of each defocus group using the 'BP 32F' command. The algorithm also created two additional volumes using randomized subsets of particles for resolution determination (see 2.6.1.7). The sub-volumes were weighted according to the number of particles that were used for the backprojection before they were CTF corrected using the theoretical CTF at the average defocus of the defocus group and combined to the final volume with the 'TF CTS' command.

2.6.1.6 Sorting

Particle-based sorting was applied to identify and separate more homogeneous subsets of particles in the dataset. It was also used to remove carbon edges and noise particles from the dataset that had not been detected during pre-processing. Reference volumes for sorting were either slightly different reconstructions from the dataset (e.g. the same volume filtered at different levels or volumes from different refinement rounds), modified volumes from the dataset, or previous reconstructions used for removal of the corresponding particles (e.g. 60S subunit or edge particle). To modify volumes (e.g. erase a ligand) the UCSF Chimera software[139] was used.

Semi-supervised sorting. Particles were aligned to up to three different reference structures and each particle was assigned to the reference structure it had the highest cross-correlation to. Every subset of particles was used to backproject its own volume as a reference for the following round. All particles were then aligned to all of the new references and separated according to cross-correlation, again. The process was repeated until the numbers of particles assigned to each reference were virtually constant for at least three rounds.

Focused sorting. Particles were treated as described for semi-supervised sorting. However, cross-correlations were determined only for a distinct part of the volume that was defined by a mask.

2.6.1.7 Resolution Determination

The resolution was determined according to the FSC = 0.5 cutoff criterion[140] for the final volume of each refinement round as well as the sub-volumes of the defocus groups. The 'RF 3' command was used with standard settings to determine the FSC between two sub-volumes consisting of random subsets of the particles that were used for the backprojection of the complete volume. The local resolution was determined by breaking up the sub-volumes into small (10 x 10 x 10 pixel) cubes and comparing corresponding cubes

with each other. The 3D distribution of local resolutions was then used to color the complete volume accordingly, using UCSF Chimera.

2.6.1.8 *Figures and Density Separation*

UCSF Chimera was used for manual separation of density and creation of figures.

2.6.2 Small-Angle X-Ray Scattering

SAXS data was collected at the X33 EMBL/DESY beamline (Hamburg, Germany). Protein concentrations were in the range of 1 – 3.4 mg/ml. The buffer controls as well as the protein samples were centrifuged before data collection. The respective buffers of the final purification steps were used for buffer correction. Two successive exposures of the same sample were compared for each sample to check for radiation damage. Raw data were analyzed and processed using the ATSAS software package[141] as described[142]. Kratky plots showed bell-shaped curves for all samples, indicating that all constructs were folded. No indication for particle interaction or aggregation was found in the datasets used for model calculation. Molecular weights were calculated from Guinier analysis by comparison of scattering intensity extrapolated to zero angle I(0) using BSA (66kDa) as a reference. The results confirmed the monomeric conformation of *S. cerevisiae* RAC, *S. cerevisiae* RAC(zuoΔC), and *C. thermophilum* RAC in solution. Rg-values were also determined from Guinier analysis. This resulted in Rg = 5.84 nm for *S. cerevisiae* RAC, Rg = 3.78 nm for *S. cerevisiae* RAC(zuoΔC), and Rg = 4.35 nm for *C. thermophilum* RAC, respectively. Sets of independent *ab initio* models were calculated using GASBOR[143]. DAMAVER[144] was then used for alignment and averaging.

SAXS data collection was performed by Dr. Gregor Witte together with Marco Gartmann and Steffen Fliehmann.

2.6.3 Protein Crystallization

2.6.3.1 *Crystallization of S. cerevisiae (His)RAC50*

Highly purified *S. cerevisiae* HisRAC50 or RAC50 (see 2.3.3.3 or 2.3.3.4) was used for vapor diffusion crystallization experiments. Initial screening was done in 96-well sitting-drop plates (Corning) with 500 nl drops and a 50 µl reservoir using a Phoenix crystallization robot (Art Robbins Instruments). Refinement of the initially found conditions was done manually using the hanging-drop technique. Reservoir size was 200 µl and the drops usually consisted of 1 µl crystallization buffer and 1 µl purified protein. Some drops were set up using 2 µl crystallization buffer and 1 µl purified protein or vice versa. For standard experiments, protein drops were set up first and the crystallization buffer was then added. All conditions were tested at 20 °C, however, some were also tested at 5, 10, or 15 °C.

2.6.3.2 Seeding Experiments

Micro seeding. Hanging-drop crystallization drops were set up as usual (see 2.6.3.1) and were allowed to equilibrate for 0.5 – 2 h. The wells were then re-opened and a cat whisker was pulled through a drop from a previous experiment containing micro-crystals or crystalline precipitate and was then pulled through the newly setup drop, before the well was closed again.

Macro seeding. Hanging-drop crystallization drops were set up as usual (see 2.6.3.1) and were allowed to equilibrate for 0.5 – 2 h. The wells were then re-opened and individual crystals were transferred from previously set-up donor drops to the equilibrated target drops using Mounted CryoLoops (Hampton Research).

2.6.3.3 Crystal Harvesting

Crystals were transferred to buffer containing cryo-protectants using Mounted CryoLoops (Hampton Research) under a light microscope. After equilibration in the cryo-protection buffer, they were again captured in the Mounted CryoLoops and frozen in liquid nitrogen.

Chapter

3 Results: Ribosome-Associated Complex

3.1 *S. cerevisiae* and *C. thermophilum* RAC are Highly Conserved

Distinct aspects of this study were investigated using RAC purified from two different organisms, namely *S. cerevisiae* and *C. thermophilum*. It was therefore a fundamental prerequisite to investigate the conservation of the chaperone complex within those organisms. The genome of *C. thermophilum* was published recently[145].
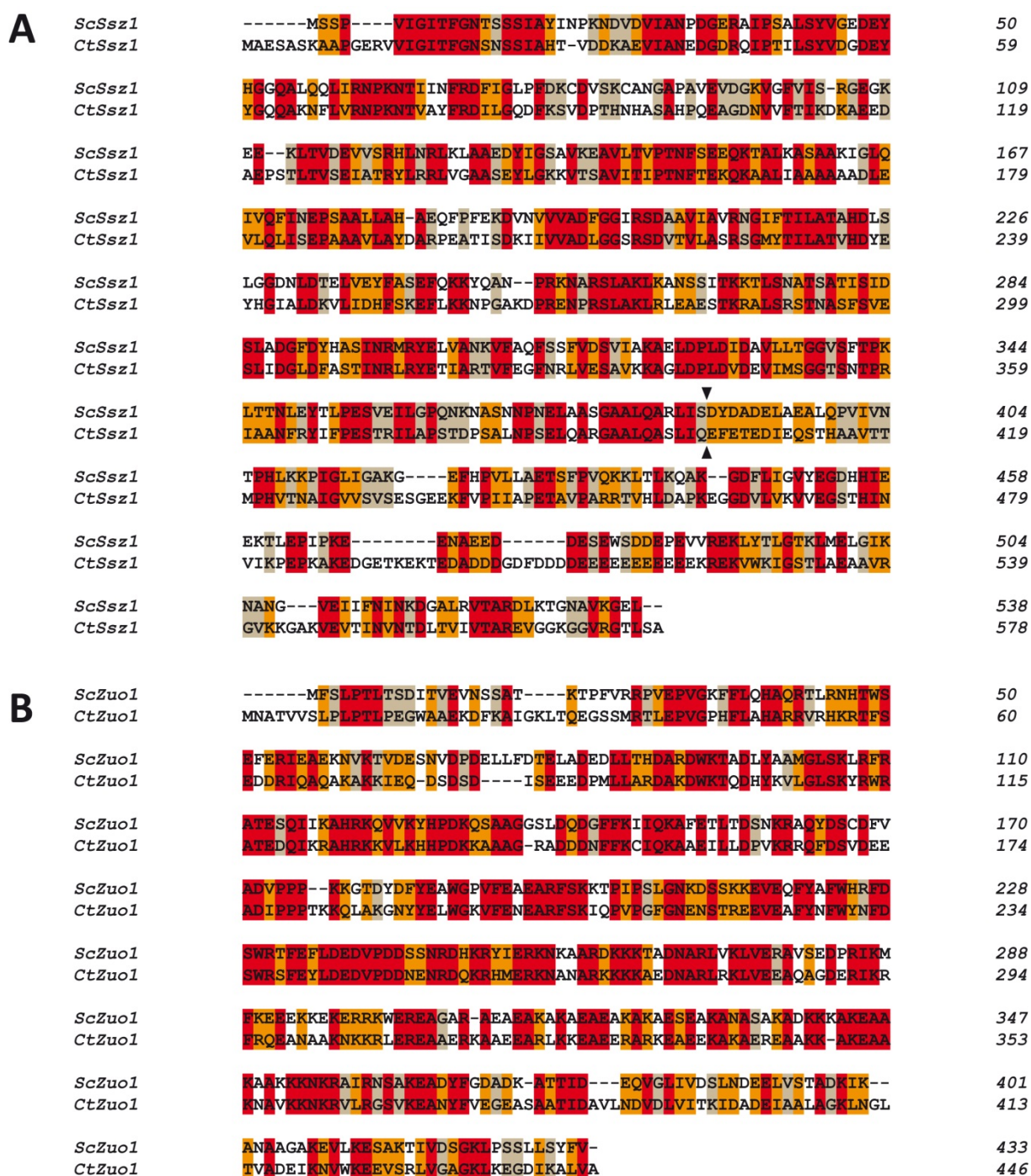

Figure 7. Protein sequence alignments for RAC's subunits from *S. cerevisiae* and *C. thermophilum*

Conserved residues are highlighted in red. Orange or grey highlighting indicates high or low similarity of the amino acids, respectively. **A.** The black triangles indicate the ends of the ATPase domains. ScSsz1: *S. cerevisiae* Ssz1; CtSsz1: *C. thermophilum* Ssz1. **B.** ScZuo1: *S. cerevisiae* Zuotin; CtZuo1: *C. thermophilum* Zuotin.

The amino acid sequences of Ssz1 and Zuotin from *S. cerevisiae* and *C. thermophilum* were aligned using the EMBL-EBI ClustalW2 web server[146,147]. Both proteins are highly similar to their respective homologs from the other species (Figure 7). The RAC subunits of *S. cerevisiae* are both slightly shorter than the *C. thermophilum* ones. *S. cerevisiae* Ssz1 comprises 538 residues, while *C. thermophilum* Ssz1 is 578 amino acids long. Their sequences share 237 identical residues, corresponding to an overall sequence identity of 44 %. With 188 conserved residues this number increases to 49 % if only the ATPase domains (residues 1-387 in *S. cerevisiae* and residues 1-402 in *C. thermophilum*, respectively) are compared (Figure 7A, see also Figure 6). *S. cerevisiae* Zuotin is 433 residues long, while *C. thermophilum* Zuotin comprises 446 amino acids. The Zuotin sequences are 50 % identical, sharing 215 conserved residues (Figure 7B). Taken together, the amino acid sequences of the RAC subunits are highly conserved between *S. cerevisiae* and *C. thermophilum*.

3.2   The cryo-EM Structure of the RAC-80S Ribosomal Complex

Previous cryo-EM analyses of RAC-80S complexes from *S. cerevisiae* (Dr. Marco Gartmann, Christoph Leidig, unpublished data) did not result in any reconstructions with a clear density for RAC. Biological molecules from *C. thermophilum* have been shown to be well suited for structural analysis[145] and the RAC-80S complex from this organism was therefore chosen for investigation in this study.
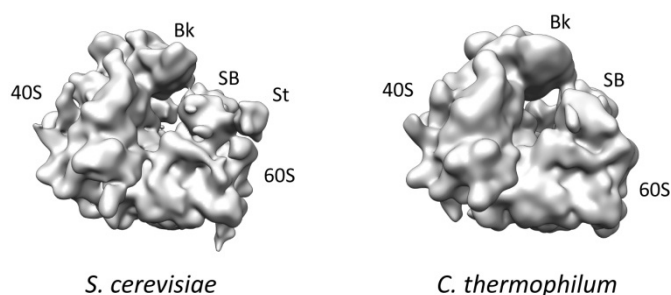

Figure 8. 3D reconstructions of 80S ribosomes from *S. cerevisiae* and *C. thermophilum*

Low-resolution reconstructions of *S. cerevisiae* and *C. thermophilum* 80S ribosomes were provided by Thomas Becker and Stephan Wickles, respectively. 40S and 60S: small and large subunit, respectively; Bk: beak; SB: stalk base; St: P-stalk.

Initially, the cryo-EM reconstruction of purified *C. thermophilum* 80S ribosomes (Stephan Wickles, unpublished data) was compared to the reconstruction of *S. cerevisiae* 80S ribosomes (Thomas Becker, unpublished data) to validate the structural similarity of the ribosomes from both species (Figure 8). No significant differences could be identified, other than the absence of the P-stalk in the *C. thermophilum* reconstruction. However, in a difference map (data not shown) between both reconstructions the P-stalk did not appear.

This indicates, that it is also present in the *C. thermophilum* 80S ribosome, but was not positioned rigidly enough to be visible in the reconstruction. The head of the small subunit, ES27^L and the L1-stalk were in differing positions in both reconstructions, respectively. However, all of these features were clearly present in *C. thermophilum*. Since RAC was suggested to interact with the ribosome close to the tunnel exit, this region was carefully compared[21]. No significant differences were found. This indicates, that structural data obtained from cryo-EM analysis of *C. thermophilum* 80S complexes can be interpreted on the basis of the *S. cerevisiae* ribosome, and additional density can be assigned to the respective ligands.
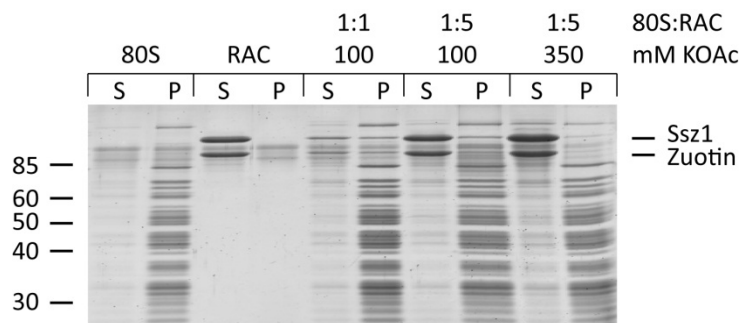

Figure 9. Binding assay for RAC to 80S ribosomes

SDS-PAGE analysis of a co-sedimentation binding assay for *C. thermophilum* RAC and 80S ribosomes. S: supernatant; P: pellet; left: molecular weight marker (kDa).

It is preferable for cryo-EM analyses to have a homogeneous and well defined sample. To achieve those prerequisites the *C. thermophilum* RAC-80S ribosomal complex was reconstituted *in vitro* from its purified components. Co-sedimentation binding assays (see 2.5.2) were used to investigate the interaction of RAC (kindly provided by Dr. Gert Bange, Sinning Lab, BZH, Heidelberg) with 80S ribosomes (see 2.4) and find suitable conditions for cryo-EM analysis. Various salt concentrations and ratios between 80S and RAC were tested (Figure 9). RAC was found to bind to 80S ribosomes in the presence of 100 mM KOAc, while the interaction was significantly reduced at a KOAc concentration of 350 mM. Thus, *C. thermophilum* RAC binds to 80S ribosomes in a salt-sensitive manner, as previously shown in *S. cerevisiae*[115]. No significant difference in the binding efficiency at 1:1 or 1:5 ratios between 80S and RAC could be detected on the protein gel. Taken together, these results indicate a hydrophilic and specific binding mode of RAC to the ribosome. Also, the dissociation speed of RAC under the tested conditions seems to be slow enough to allow significant amounts of the chaperone complex to stay associated with ribosomes during the assay, despite the absence of additional RAC in the sucrose cushion. Those conditions are therefore suitable for cryo-EM analysis of the *C. thermophilum* RAC-80S ribosomal complex, and a sample was reconstituted to collect data for single-particle analysis (see 2.6.1.1).

A dataset of 10,038 micrographs was recorded (see 2.6.1.3). After pre-processing, 6,954 micrographs remained in the dataset, and the initial reconstruction was created

from 290,740 particles (see 2.6.1.4). During two successive sorting steps, remaining non-ribosomal particles and 60S subunit particles were removed by supplying the corresponding references (see 2.6.1.6). 78,347 non-ribosomal and 51,010 60S particles were selected (Figure 10). The 3D reconstruction of the resulting 161,384 particles represented an 80S ribosome containing E-site tRNA and an additional density in the translation factor binding site. However, no additional density could be found in the tunnel exit region. The electron density map (volume) could be refined (see 2.6.1.5) to 7.6 Å resolution (see 2.6.1.7), but still no additional density that could be attributed to RAC appeared.
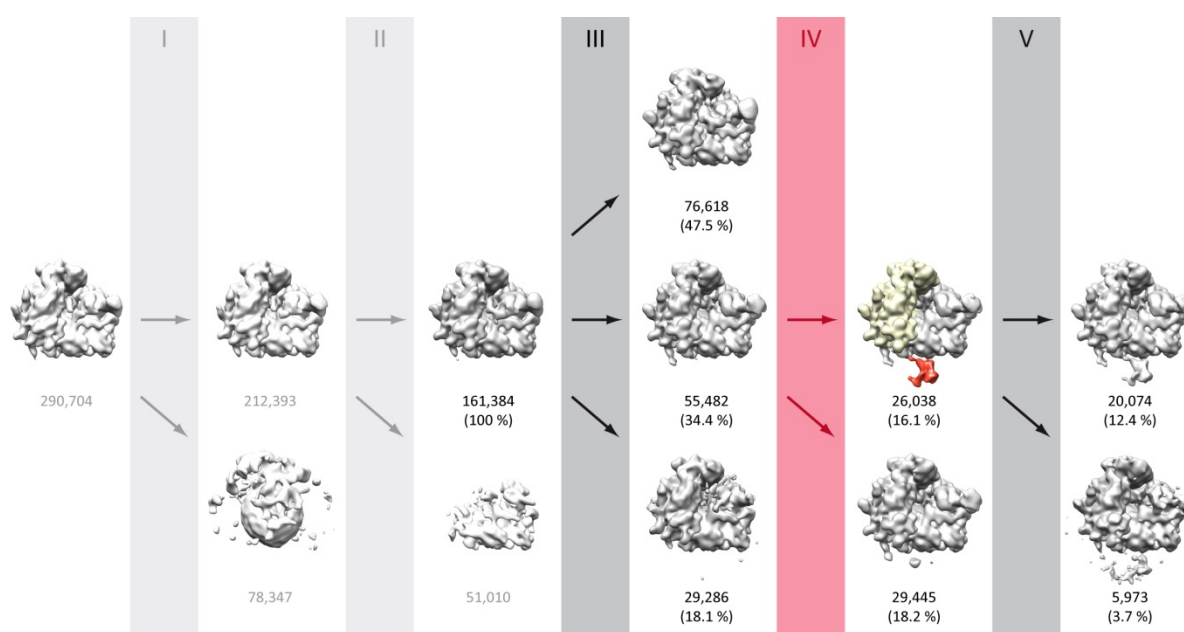

Figure 10. Sorting overview

All reconstructions were low-pass filtered between 18-20 Å using a Butterworth filter. Sorting steps are numbered using roman numbers, focused sorting is colored red. Particle numbers are indicated for each volume. Fractions are in relation to the pure 80S dataset after sorting step II.

The absence of RAC in the initial 3D reconstructions might be the result of a low occupancy or flexibility of the chaperone complex on the ribosome. Therefore, additional sorting steps were applied to find a subset of particles that might show a density for RAC. The output volumes of three different refinement rounds were used as references for sorting, resulting in stable subsets of 76,618 (A), 55,482 (B), and 29,286 (C) particles, respectively. Volume A again represented an 80S ribosome containing E-site tRNA and an additional density in the translation factor binding site, whereas this density was not present in volumes B and C (Figure 10). However, at very low contour levels, some density appeared slightly above the noise level below the tunnel exit region in volume B. The corresponding particles were therefore chosen to be analyzed by focused sorting (see 2.6.1.6). A mask restricted the cross-correlation determination to the region below the tunnel exit and all density in this region was excluded for one of the references (Figure 11A). This resulted in a subset of

29,445 particles without any significant density below the tunnel exit and a subset of 26,038 particles that showed an additional density in this region, contacting the ribosome at two sites (Figure 10). This density was assigned to RAC.

Sorting procedures using masks can lead to the creation of artifacts by aligning noise in the masked region. To verify the sorting results, the particles selected by focused sorting were backprojected using the x/y-shifts and Eulerian angles that were determined for those particles before they were sorted out of the complete dataset. No difference could be found between the resulting reconstruction and the volume created during focused sorting (Figure 11B+C). Also, the newly visible density extended outside the used mask (Figure 11A). These results indicate, that the additional density became visible due to the selection of ribosomal particles containing RAC and was not created by artificially aligning noise inside the masked region.
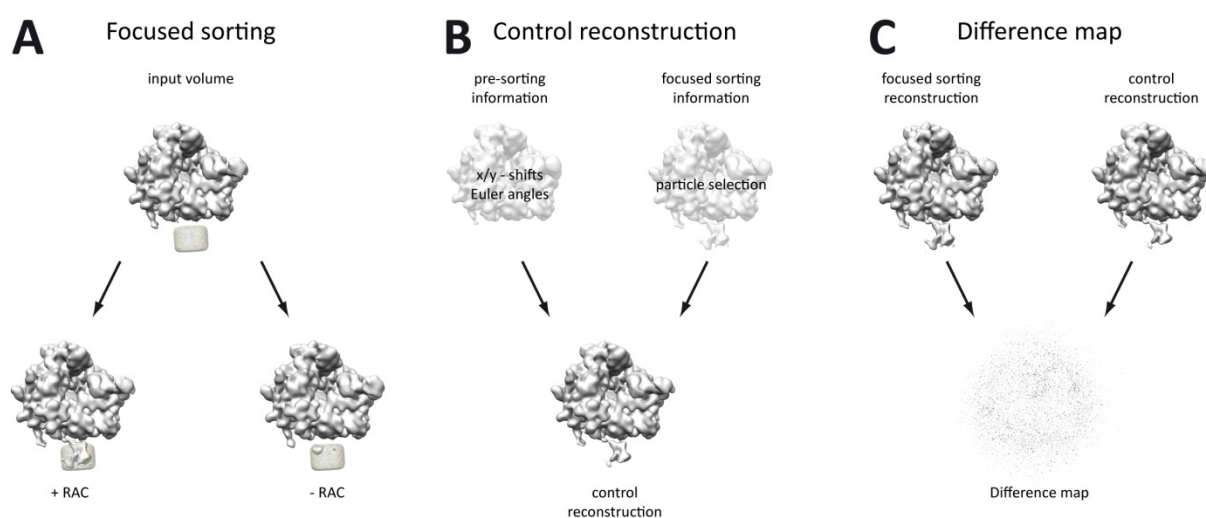

Figure 11. Focused sorting results and verification

All volumes except for the difference map were low-pass filtered between 18 – 20 Å using a Butterworth filter. **A.** Input and output volumes (grey density) of focused sorting as well as the used mask (mesh). **B.** Scheme of control reconstruction. **C.** Input and output volumes of the difference map calculation.

After focused sorting, the remaining subset of particles was once more sorted in an attempt to further improve the resolution of the 3D reconstruction. The particles were split into subsets of 20,074 and 5,973 particles, respectively. Even though a higher resolution could not be achieved, the resulting volumes still yielded some information. In the 3D reconstruction of the second volume, a series of amorphous densities indicated a possible alternative connection between RAC and the ribosome (Figure 10). The density might represent a fraction of ES27^L contacting by RAC.

The final 3D reconstruction (Figure 12) was created from the 26,038 particles that resulted from focused sorting using the best refined alignment information from before sorting. It represents the *C. thermophilum* RAC-80S complex at a resolution of 9 Å (Figure 13A,

see also 2.6.1.7). It also contains density for a tRNA in the E-site and the beginning of ES27^L is visible on the ribosome, pointing towards the tunnel exit. There is no additional density other than the L-shaped volume of RAC below the exit site, contacting the ribosome at two distinct locations.
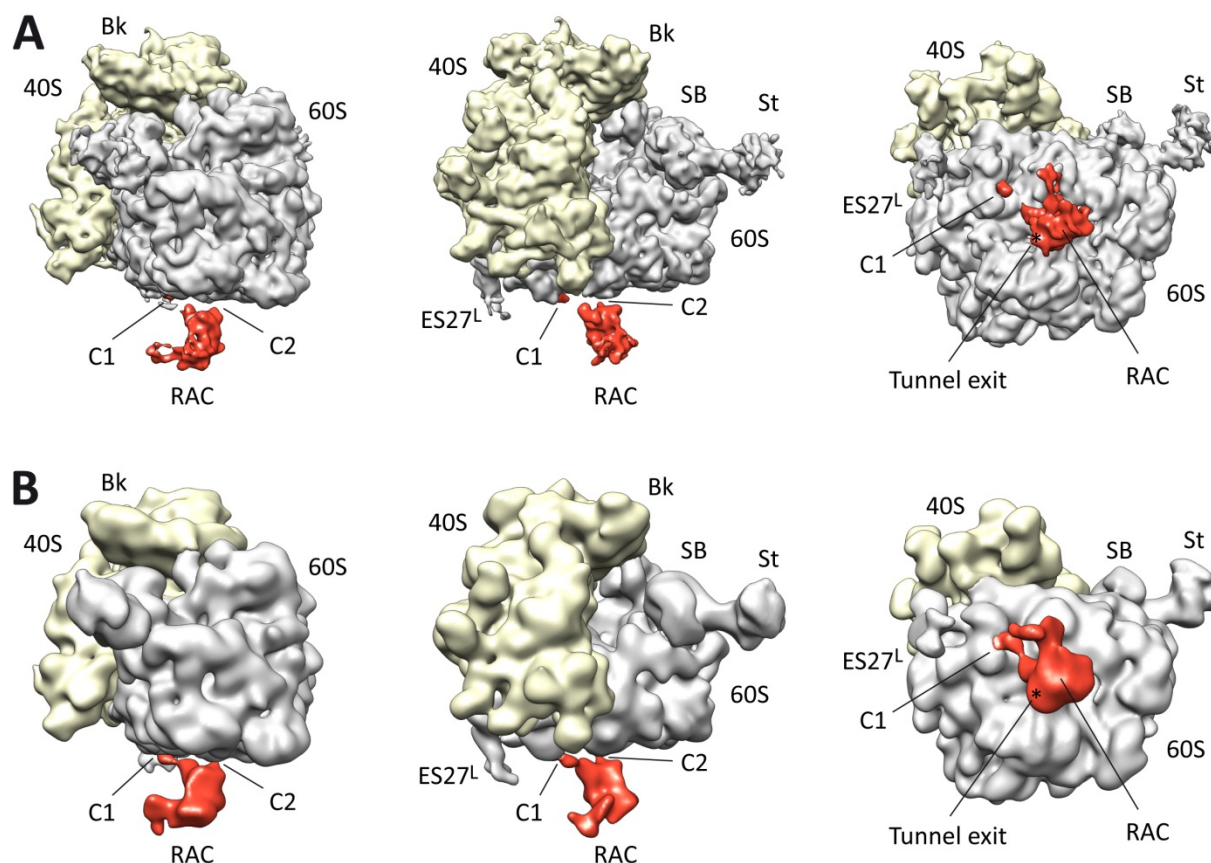

Figure 12. *C. thermophilum* **RAC-80S complex**

3D reconstruction of the *C. thermophilum* RAC-80S complex low-pass filtered at 9 – 11 Å (**A**) or 18 – 20 Å (**B**), respectively. RAC, the 60S subunit, and the 40S subunit are colored in red, grey, and yellow, respectively. Important features and the contact sites of RAC to the ribosome are labeled: beak (Bk), stalk base (SB), P-stalk (St), tunnel exit (*) and RAC contacts (C1 and C2).

The major contact seems to be formed by the elongated linker that connects the main body of the RAC density with the ribosome. In order to better describe the interaction sites, a model of the *S. cerevisiae* 60S subunit[9,148] was fit into the density. The linker contacts the ribosome between rRNA helix 59 (H59) and the ribosomal protein L22 (Rpl22) and passes in close proximity to Rpl31, that was previously shown to interact with Zuotin by cross-link studies in *S. cerevisiae*[21]. The second contact is formed between the main body of RAC and H24 of the 60S subunit (Figure 14).
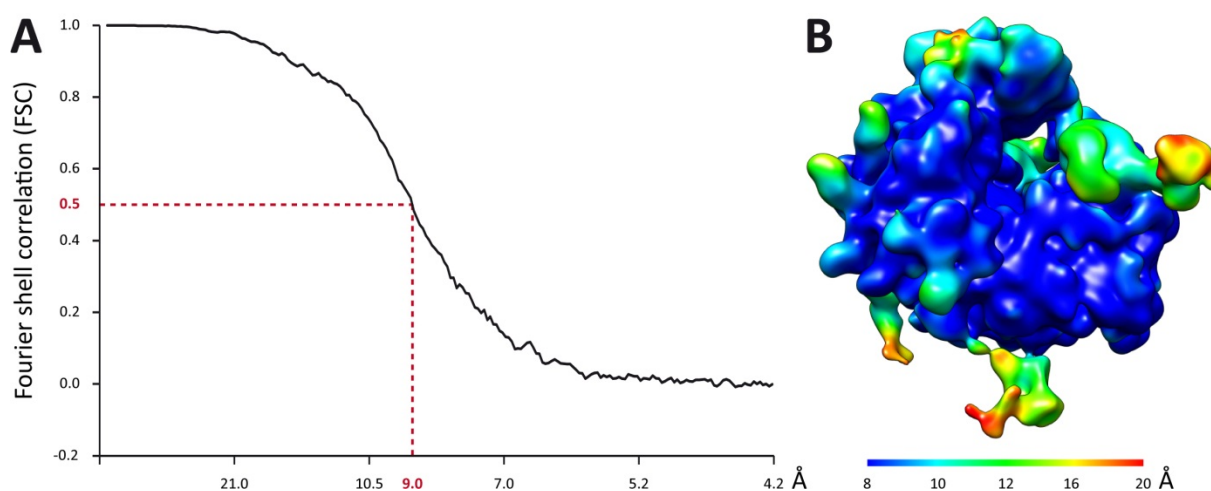
Figure 13. Resolution of the final 3D reconstruction

A. Fourier shell correlation plot of the final RAC-80S complex reconstruction. The resolution was determined at a correlation of 0.5. **B.** 3D reconstruction filtered between 18 – 20 Å. Surface was colored according to local resolution using UCSF Chimera.

The overall resolution of 9 Å was clearly not constant throughout the volume. Especially for the density assigned to RAC, the resolution seemed to be significantly lower. Clear indications were the missing linker between RAC and H59 at full resolution (Figure 12) and the fact, that no protein secondary structure elements could be identified within the RAC density. Thus, resolution values were determined locally throughout the 3D reconstruction (Figure 13B, see also 2.6.1.7). The ribosomal core is highly resolved, while flexible elements like the P-stalk, Rpl1, the head of the 40S subunit, or ES27^L show a significantly lower resolution. As expected, the resolution for RAC is also on a much lower level than the ribosomal core. Within the ligand density, the resolution is higher in close proximity to the ribosomal contacts than in the distal parts of the body. This indicates, that RAC does not adopt a completely rigid conformation and might retain a certain degree of flexibility in its ribosome bound state.
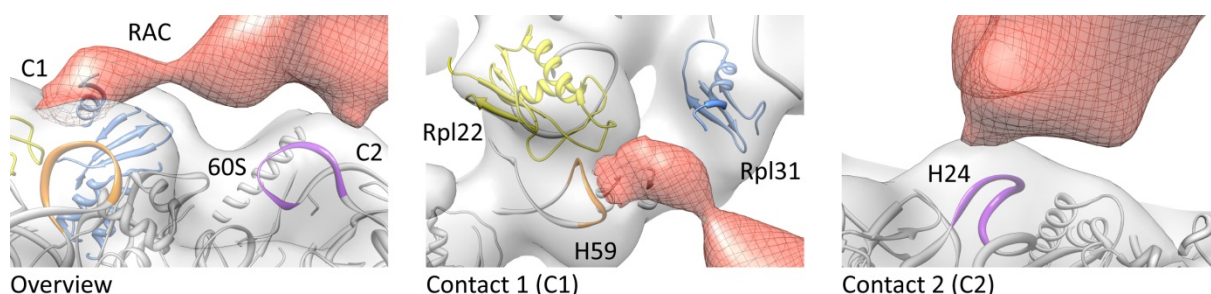

Figure 14. RAC-80S contact sites

The electron density of RAC and the 60S subunit is colored in red and grey, respectively. The map was filtered between 18 – 20 Å. *S. cerevisiae* rRNA and ribosomal protein models (grey) were fit into the density. The loops of H59 and H24 close to RAC are colored in orange and purple, respectively. Rpl22 is colored in yellow, Rpl31 in blue.

Taken together, the results obtained by cryo-EM indicate, that RAC is coordinated close to the ribosomal tunnel exit by two direct interactions with the 60S ribosomal subunit and possibly by an interaction with ES27[L]. However, the chaperone complex seems to retain some degree of flexibility. This would position the chaperone complex in a perfect location to interact with nascent polypeptide chains or other factors at the exit site, including Ssb.

3.3 SAXS Gives Insights into the Arrangement of RAC's Subunits

Cryo-EM analysis of RAC-80S complexes revealed the binding site of RAC at the ribosome. However, it was not possible to create a molecular model for RAC from the electron density. Therefore, the questions still remained whether the complete chaperone complex is visible in the cryo-EM structure and how Zuotin and Ssz1 are arranged within RAC.
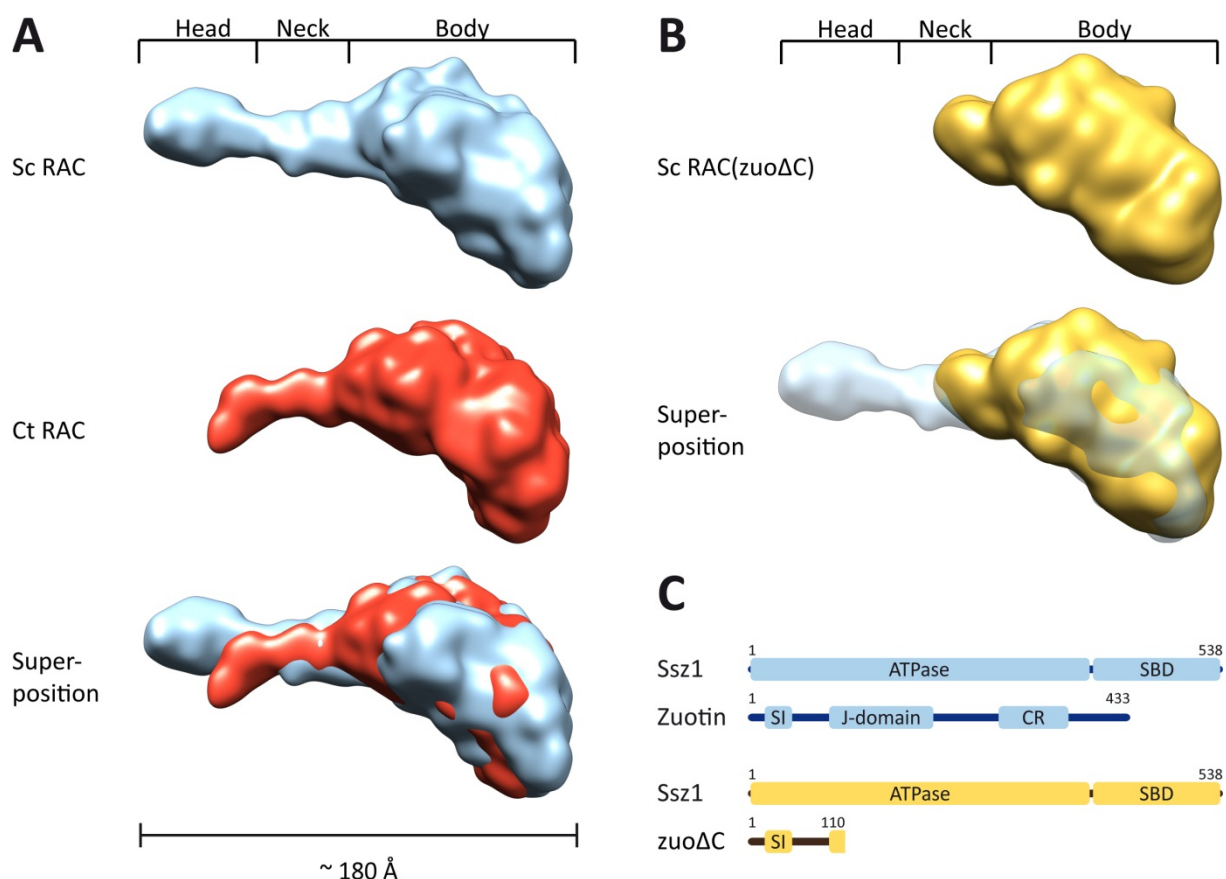
Figure 15. SAXS analysis of *S. cerevisiae* and *C. thermophilum* RAC

A & B. SAXS models of *S. cerevisiae* and *C. thermophilum* RAC, labeled Sc RAC and Ct RAC, respectively, and *S. cerevisiae* RAC(zuoΔC), labeled Sc RAC(zuoΔC). Models were filtered in UCSF Chimera using a Gaussian filter with a width of 3. **C.** Schematic overview of *S. cerevisiae* Ssz1 and Zuotin or zuoΔC. ATPase: ATPase domain; SBD: substrate binding domain; SI: Ssz1-interacting domain; CR: charged region.

To address those questions, SAXS datasets were recorded for purified *S. cerevisiae* and *C. thermophilum* RAC and their respective solution structures were calculated (see 2.6.2). Both resulting models were highly similar in shape and size. They featured a large globular part with an elongated protrusion. The globular part is referred to as body, the protrusion can be further divided into a neck and a head region. *S. cerevisiae* RAC extended for ~180 Å along its longest exit, while the model of its *C. thermophilum* counterpart was slightly shorter due to a higher overall curvature and a different angle between its body and its neck and head regions (Figure 15A). This might also indicate that the neck and head regions can move relative to the body.

A truncation mutant of *S. cerevisiae* Zuotin was created that contained residues 1-110 only. It formed a stable complex with Ssz1 that was referred to as RAC(zuoΔC) (Figure 15C). Compared to the SAXS envelope of RAC, that of the truncated complex lacked its head and part of the neck region while maintaining the body and a shortened protrusion (Figure 15B). This indicates, that the head and neck regions are formed by the C-terminal part of Zuotin and, therefore, the body is mainly constituted by Ssz1. The SAXS results also confirm the conservation of RAC (see 3.1) on a structural level.

A superposition of the solution structure of *C. thermophilum* RAC and the cryo-EM structure of the RAC-80S complex was created (Figure 16A). Due to its elongated shape, the linker with contact 1 near H59 and Rpl22 was aligned with the neck and head of the SAXS model. The two body domains comprised similar volumes, however, that of the SAXS model was slightly larger. The major difference was the angle they enclosed with their respective neck and head regions. This indicates, that most of RAC is visible in the cryo-EM structure and also suggests, that contact 1 is formed by the head region of RAC and, therefore, by the C-terminal part of Zuotin.

3.4 Zuotin's Head Domain is Crucial for Ribosome Interaction

A combination of cryo-EM and SAXS results suggested that the C-terminal part of Zuotin forms the main contact between RAC and the ribosome. Dr. Gert Bange (Sinning Lab, BZH, Heidelberg) solved the crystal structure of residues 355 – 446 of *C. thermophilum* Zuotin at a resolution of 1.3 Å (Figure 16B). The structure was composed of four α-helices with a short loop connecting α-helix 1 (α1) and α-helix 2 (α2). Some unstructured residues at the C-terminus were followed by a rudimentary α-helix ('α5').
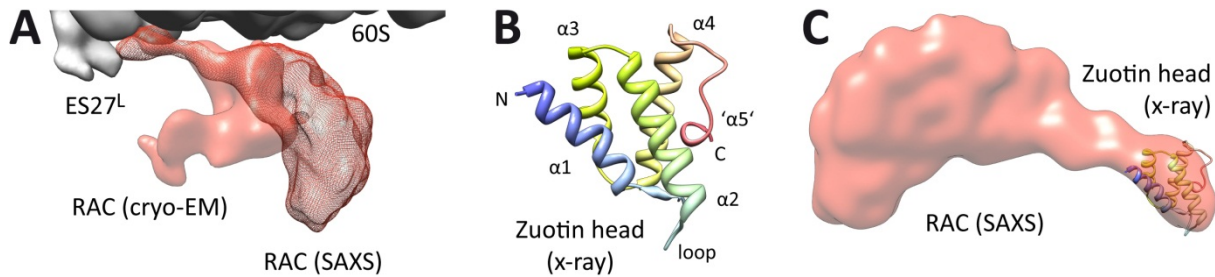
Figure 16. RAC head domain might be involved in ribosome interaction

A. Superposition of RAC model from SAXS data (mesh) and the RAC-80S complex cryo-EM map (surface) filtered between 18 – 20 Å. **B.** Crystal structure (ribbon representation) of Zuotin residues 355 – 446 crystal structure at 1.3 Å colored by residue number. Blue: N-terminus; red: C-terminus. **C.** Fit of the Zuotin C-terminus structure into the head of the RAC SAXS model.

The SAXS analysis of the Zuotin truncation experiments suggested, that the structure had to be part of the neck and head region. It could indeed be fit into the head of the SAXS model of *C. thermophilum* RAC (Figure 16C), although more than one orientation was possible (data not shown, see also Figure 28). The structure was fit so that its N-terminus pointed towards the neck region, since this is where it should be connected to the remaining part of Zuotin. A DALI search for structural homology turned up the PHAX domain, a single-stranded RNA (ssRNA) binding domain with an almost identical architecture[149,150]. These are strong indications, that the Zuotin PHAX-like domain could be essentially involved in the interaction of RAC with the ribosome. This function was, however, previously attributed to the charged region of Zuotin[21,116].
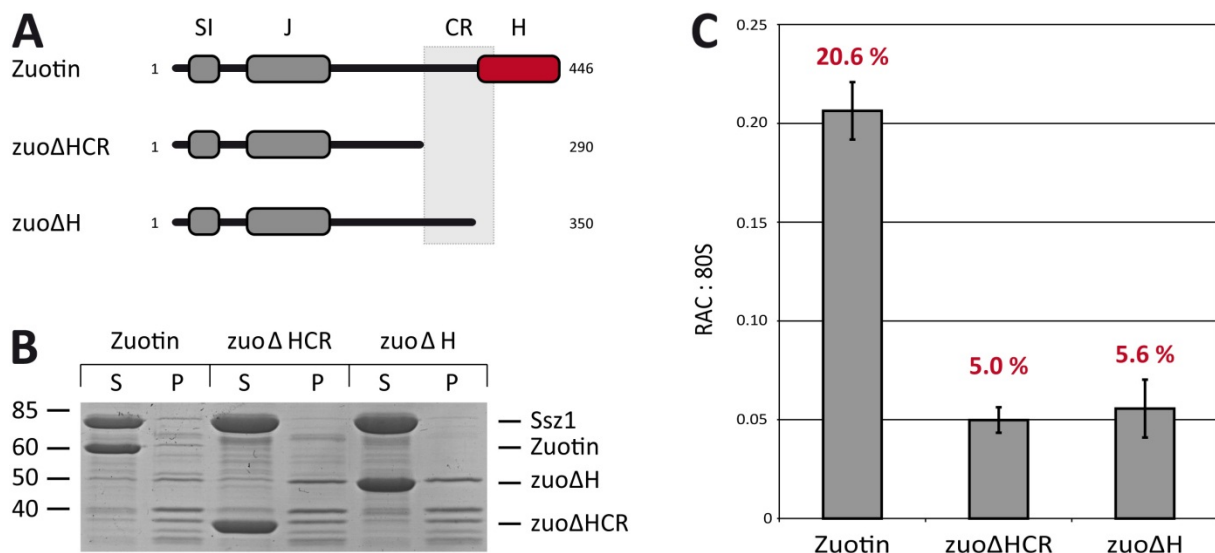
Figure 17. RAC head domain is crucial for ribosome interaction

A. Schematic overview of *C. thermophilum* Zuotin constructs. SI: Ssz1-interaction domain; J: J-domain; CR: charged region; H: head domain. **B.** Co-sedimentation binding assay for truncated RAC complexes and 80S ribosomes. S: supernatant; P: pellet; numbers: molecular weight marker (kDa). **C.** Quantification of Ssz1 bands compared to 40 kDa ribosomal band in B.

To further test this, truncation mutants of Zuotin were created and tested for ribosome binding (see 2.5.2) together with Ssz1. One of the mutants was lacking the head domain only (zuoΔH), while in the other one, the charged region was also deleted (zuoΔHCR). Both truncation mutant complexes showed significantly reduced binding to ribosomes as compared to full-length RAC (Figure 17). As a measure for binding, the respective amount of RAC in the pellets was determined. Since there were ribosomal bands running at the same height as the Zuotin constructs, the quantification was done for the Ssz1 bands of each complex in relation to the ribosomal band at 40 kDa using ImageJ[151]. The binding efficiency was reduced by a factor of 4 after deletion of the Zuotin C-terminus, while also deleting the charged region did not have any additional effect: 20.6 % of ribosomes were occupied with full-length RAC, while only 5.0 % or 5.6 % were occupied with zuoΔHCR or zuoΔH, respectively. This shows that the charged region alone is not sufficient to effectively target RAC to the ribosome and confirms the crucial role of the head region for this interaction. The fraction of wild-type RAC associated with 80S ribosomes under these conditions is in good agreement with the fraction of particles of the cryo-EM dataset that were found to carry RAC (Figure 10).

Taken together, these results show that RAC primarily, but not exclusively, interacts with the ribosome via a PHAX-like domain located in the head region of the chaperone complex.

3.5   Zuotin Interacts with Ssz1 via its N-Terminus

The results of the SAXS truncation analysis gave insights into the general arrangement of Zuotin and Ssz1 in RAC. However, the molecular details of their unique interaction remained elusive. To address this question in more detail, various fragments of *S. cerevisiae* Zuotin were tested (see 2.5.1) for interaction with Ssz1.
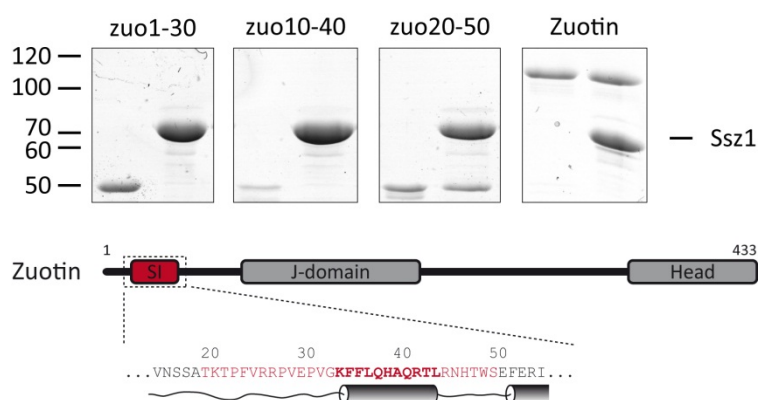

Figure 18. Interaction of Zuotin fragments with Ssz1

Gel. Pulldown assays for N-terminal MBP-tagged Zuotin fragments with immobilized Ssz1. Numbers: molecular weight marker (kDa). **Scheme.** Secondary structure prediction (cartoon) suggested an α-helix (residues 34 – 44) in the minimal interacting region (residues 20 – 50). SI: Ssz1-interation domain; numbers: residue numbers.

The Zuotin constructs were each fused to MBP-tags at their N-termini while Ssz1 carried an N-terminal 6xHis-tag. Initially, Zuotin was split into three parts: its N-terminus (zuoN), the J-domain (zuoJ) and its C-terminus (zuoR). Of those constructs, only zuoN retained the ability to interact with Ssz1 (data not shown). This construct was then further split into shorter fragments: residues 1 − 30 (zuo1-30), residues 10 − 40 (zuo10-40), residues 1 − 50 (zuo1-50) and residues 20 − 50 (zuo20-50). While zuo1-50 and zuo20-50 could be efficiently pulled down by immobilized Ssz1 (and *vice versa*), zuo1-30 and zuo10-40 did not show any interaction with Ssz1 (Figure 18). The region was then further analyzed using bioinformatics tools. Secondary structure prediction using the PredictProtein server[152] suggested that there is an α-helix in this region of Zuotin extending from AA 34 − 44 (Figure 18). An α-helix is also predicted at the corresponding position in *C. thermophilum* Zuotin and many of the residues are conserved (Figure 7B).

These results show, that residues 20 − 50 of *S. cerevisiae* Zuotin are necessary and sufficient for its interaction with Ssz1. A predicted α-helix in this region is a good candidate for the primary interaction site.

3.6 Crystallization of Truncated RAC

To understand the interaction of Zuotin and Ssz1 on a structural basis, crystallization experiments were conducted (see 2.6.3.1). Previous experiments with wt RAC did not result in any crystals[153], and since the major interest was to investigate the interaction of RAC's subunits, the complex of *S. cerevisiae* Ssz1 and zuo1-50 was used.

For the initial crystallization experiments highly purified HisRAC50 (Figure 19) was used, consisting of N-terminally 6xHis-tagged Ssz1 and zuo1-50. Crystals could be obtained from the robot screen at a concentration of 10 mg/ml HisRAC50 in condition F12 of JBScreen Classic HTS I (Jena Bioscience) after four days. This condition contains 8 % w/v PEG 8000, 200 mM LiCl, and 50 mM MgSO$_4$.

The condition was manually refined and crystals could be reproduced in several conditions. The best of those were i) 6 % w/v PEG 8000, 200 mM LiCl, and 100 mM MgSO$_4$ (Figure 19A) and ii) 6 % w/v PEG 8000, 450 mM LiCl, and 50 mM MgSO$_4$ (Figure 19B). The crystals from all conditions were similar in size and shape. Each drop yielded many crystals, growing as thin, layered plates. Many of those plates were bent, intergrown, or showed irregular edges or roundish corners. The largest ones grew to x/y-dimensions of about 90 x 90 µm (Figure 19A). Values for the z-dimension could not be determined since the crystals were too thin. Micro- and macro-seeding experiments (see 2.6.3.2) did not improve crystal quality. The largest and best defined crystals were harvested (see 2.6.3.3) and various cryo-protectants were tested: 15 % 2,3-butanediol, 30 % glycerol, 25 % ethylene glycol (ethane-1,2-diol), or 25 % MPD (2-methyl-2,4-pentanediol). The crystals were stable in 2,3-butanediol or glycerol, while they cracked and dissolved quickly in ethylene glycol or MPD. X-ray diffraction was measured for

the frozen crystals at the SLS synchrotron (Switzerland). All measured crystals were protein crystals, as could be judged from the diffraction patterns. However, the diffraction quality was very anisotropic and limited to ~10 Å along the best axis. No dataset was recorded.
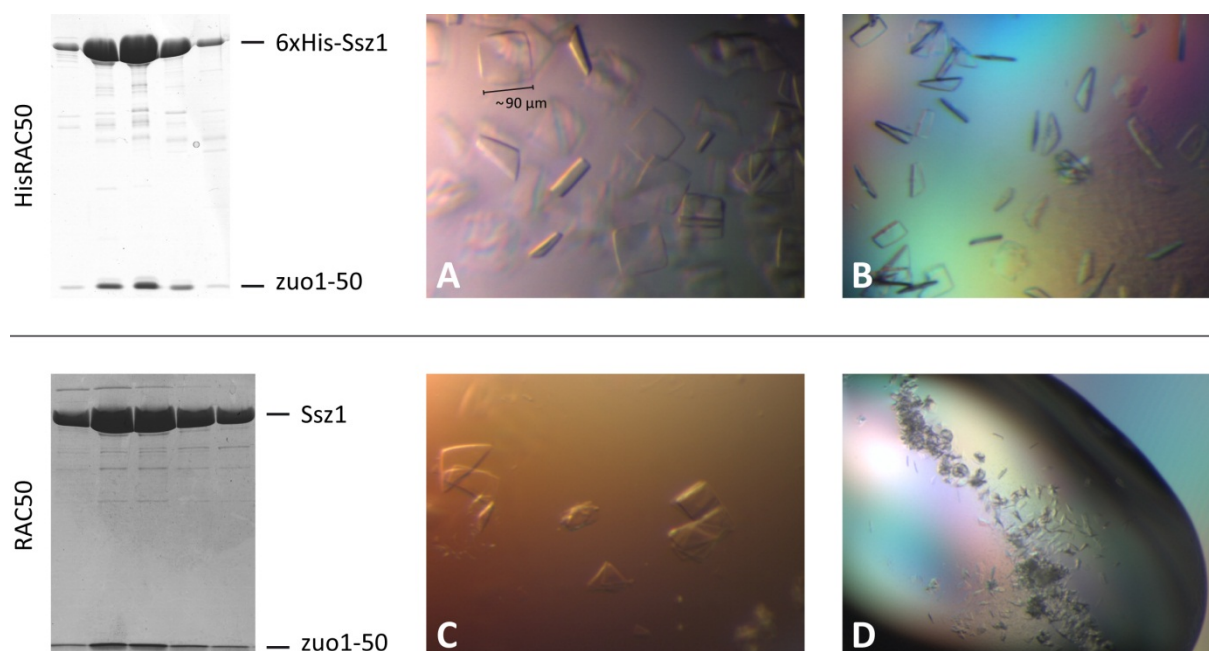

Figure 19. Crystallization of truncated RAC

Gels. SDS-PAGE analysis of gel-filtration peak fractions for representative HisRAC50 or RAC50 purifications. **A & B.** HisRAC50 crystals from manually refined conditions. **C.** RAC50 crystals with i) irregular edges and corners or ii) multiple layers. **D.** Drop with RAC50 crystals after micro-seeding. Many intergrown crystals along the streak line and some individual ones towards the sides.

In an effort to improve crystal quality, the 6xHis-tag was removed from the Ssz1 subunit on the DNA level and the complex was purified without using any tag. Crystals could be obtained from RAC50 (wt Ssz1 and zuo1-50) samples under various conditions (Table 5) at proteins concentrations between 8 – 13 mg/ml. The most promising conditions were manually refined. Crystals needed 1 – 4 days to grow. Their appearance was similar to that of the crystals obtained for purified HisRAC50. Irregular shapes and intergrown, multi-layered crystals were frequently obtained (Figure 19C). A variety of techniques was used to improve crystal quality or shape: i) micro- and macro-seeding, ii) variation of drop size and buffer to protein ratio; iii) reductive methylation of surface exposed lysine residues[154], iv) crystallization in the presence of ATP or AMPNP, v) screening for other additive compounds that might improve crystallization using Additive Screen (Hampton research), vi) screening of pH values, vii) crystallization using the NV10 compound (Expedeon), viii) incorporation of selenomethionine into the protein complex, ix) crystallization in gel[155], x) crystallization with paraffin oil covered reservoirs, and xi) screening of various crystallization temperatures. No crystals of different shape could be obtained. Micro-seeding yielded some crystals of improved quality as could be judged in the light microscope.

However, their general shape did not change, either (Figure 19D). The best crystals were obtained at a concentration of 9 mg/ml RAC50 in i) 7.1 % w/v PEG 4000, 210 mM sodium acetate pH 5.5, and 100 mM sodium citrate pH 5.5 or ii) 6.5 – 7 % w/v PEG 4000, 150 mM sodium acetate pH 5.5, and 100 mM sodium citrate pH 5.5 using micro-seeding. Selected crystals were harvested and x-ray diffraction was recorded at the ESRF (Grenoble) synchrotron. The quality of diffraction was anisotropic and most diffraction spots showed high mosaicity. With respect to the HisRAC50 crystals the diffraction slightly improved to 8 Å along the best axis, however, it was still not good enough for structure determination. No dataset was recorded.

Table 5. Commercial screen condition hits for RAC50 crystallization

Screen name – condition number	Chemical composition	Protein concentration
JBScreen Classic HTS I – D5 (Jena Bioscience)	10 % w/v PEG 4000 10 % w/v 2-propanol 100 mM sodium citrate pH 5.6	10 mg/ml
JBScreen Classic HTS I – F12	8 % w/v PEG 8000 200 mM LiCl 50 mM $MgSO_4$	13 mg/ml
JBScreen Classic HTS I – G2	10 % w/v PEG 8000 100 mM HEPES pH 7.5 200 mM $CaCl_2$	13 mg/ml
Protein Complex Suite – A5 (QUIAGEN)	15 % w/v PEG 550 MME 100 mM MES pH 6.5	13 mg/ml
Protein Complex Suite – B3	10 % w/v PEG 4000 200 mM sodium acetate 100 mM sodium citrate pH 5.5	10 mg/ml
Protein Complex Suite – D7	15 % w/v PEG 6000 100 mM sodium citrate pH 5.5	13 mg/ml
Protein Complex Suite – E2	8 % w/v PEG 8000 100 mM sodium citrate pH 5	13 mg/ml
Protein Complex Suite – E3	8 % w/v PEG 8000 200 mM NaCl 100 mM sodium cacodylate pH 6	10 mg/ml
Protein Complex Suite – F10	1 M $(NH_4)_2SO_4$ 100 mM Tris pH 8	13 mg/ml

3.7   Ssz1 ATPase Domain is Structurally Unable to Hydrolyze ATP

The crystal structure of the *C. thermophilum* Ssz1 ATPase domain was determined at 1.8 Å resolution by Dr. Gert Bange (Sinning lab, BZH, Heidelberg). It showed the typical fold of canonical Hsp70 protein ATPase domains (Figure 20A). A native, highly defined ATP-Mg^{2+} was present in the nucleotide binding cleft.
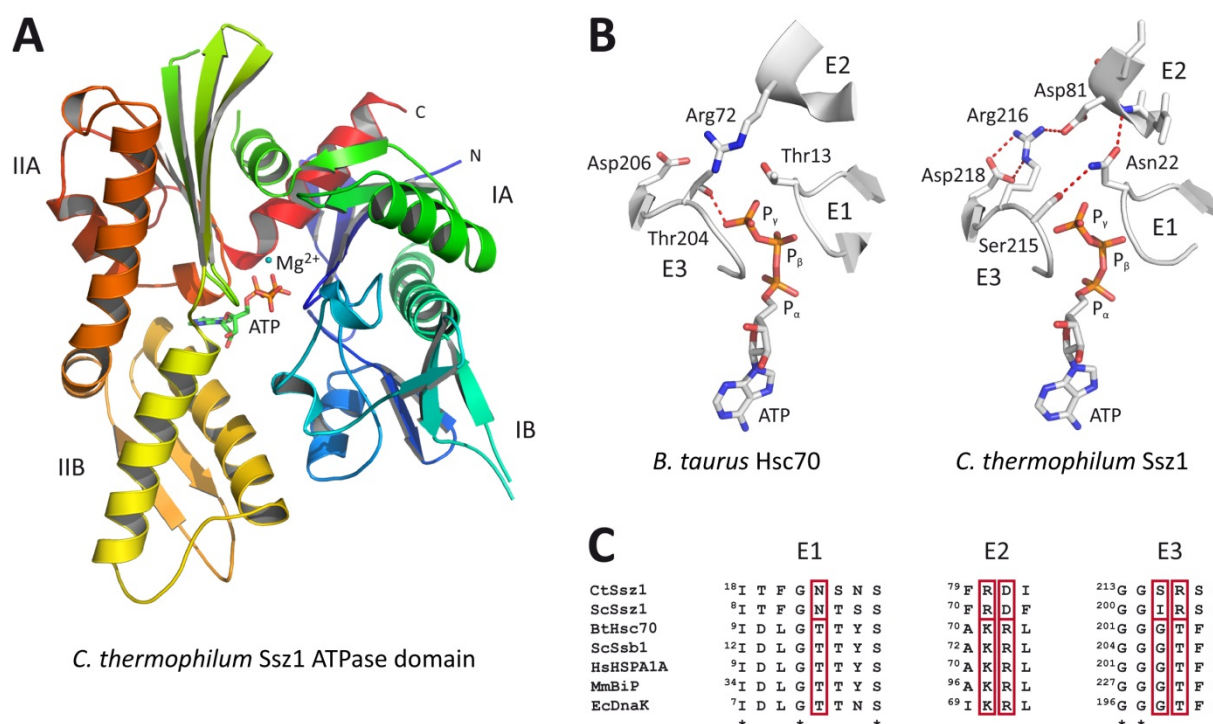
Figure 20. Structural basis for Ssz1 ATPase activity deficiency

A. Cartoon representation of the crystal structure of the *C. thermophilum* Ssz1 ATPase domain (residues 13 – 402) with native ATP-Mg^{2+}. Rainbow colored from N- to C-terminus, labeled N and C, respectively. IA – IIB: topological domains of the Hsp70 ATPase domain as previously described[156]. **B.** Comparison of the catalytic sites of *C. thermophilum* Ssz1 and the canonical Hsp70 *B. taurus* Hsc70[157] (PDB accession number 1NGE). E1 – E3: catalytically important elements. **C.** Alignment of the amino acid sequences of elements 1 – 3 of *C. thermophilum* Ssz1 (CtSsz1), *S. cerevisiae* Ssz1 (ScSsz1), *B. taurus* Hsc70 (BtHsc70), *S. cerevisiae* Ssb1 (ScSsb1), *H. sapiens* Heat shock 70 kDa protein 1A/1B (HsHSPA1A), *M. musculus* BiP (MmBiP), and *E. coli* DnaK (EcDnaK). Red boxes: catalytically active residues of canonical Hsp70 proteins that are mutated in Ssz1; *: conserved residues.

With ATP-Mg^{2+} bound in the active site, the structural basis for the previously reported catalytic inactivity[118] of the ATPase could be analyzed. The overall architecture of the catalytic center was highly conserved when compared to canonical Hsp70 chaperones (Figure 20B). There are three structural elements (E1 – E3) in the ATPase domains of Hsp70 proteins that are of major importance during ATP hydrolysis and transmission of the resulting conformational change to their substrate binding domains[158-160]. They are located closely around the phosphate moieties of the bound nucleotide (Figure 20B). Analysis of individual residues in those elements revealed, that catalytically critical residues were mutated in Szz1. At the same time, the binding pocket for the adenosine moiety was well conserved. Residue numbers for canonical Hsp70 proteins are given for *B. taurus* Hsc70, since most previous mechanistic studies for the protein family were done on this chaperone. In Element 1 (E1) of Hsp70 family proteins, the hydroxyl group of Thr13 has been shown to be crucial for ATP hydrolysis as well as the transduction of the resulting conformational change to the substrate binding domain. In Ssz1 this residue is mutated to Asn22, which creates novel interactions to the backbone of Element 2 (E2) and Ser215 in Element 3 (E3).

As a result, its hydroxyl group is unavailable for catalysis and, at the same time, all of the three elements are interlocked in a rigid conformation. This is hindering E3 to undergo the structural rearrangement it is thought to perform during ATP hydrolysis in functional Hsp70 proteins allowing the gamma phosphate to position itself for inline attack. Thr204, a catalytically important residue in E3 of Hsc70, is replaced by Arg216 in Ssz1. The arginine side chain is rotated away from the active site and is coordinated by two interactions with Asp218. It also creates an additional contact to E2, where this interaction is made possible by the mutation of Arg72 in *B. taurus* Hsc70 to Asp81 in Ssz1. Lys71 in E2 of canonical Hsp70 chaperones is essential for ATP hydrolysis. This residue is replaced by Arg80 in Ssz1.

Taken together, nearly all catalytically active residues of functional Hsp70 ATPase domains are replaced in Ssz1. At the same time, novel interactions are established, fixing formerly flexible structural elements in a rigid conformation. As a result, Ssz1 became unable to hydrolyze ATP, while maintaining the ability to bind the nucleotide in a conserved manner.

Chapter

4 Results: Arx1 pre-60S Particle

4.1   The Arx1 pre-60S Subunit Carries Scattered Additional Densities

Cryo-EM was performed to determine the 3D structure of the *S. cerevisiae* Arx1 pre-60S particle (see 2.6.1.2). A dataset of 16,616 micrographs was recorded (see 2.6.1.3), of which 6,359 remained in the dataset after pre-processing (see 2.6.1.4). The initial reconstruction was created from 222,299 particles using a mature 60S subunit as a reference. The particles were sorted (see 2.6.1.6) for mature 60S subunits and remaining non-ribosomal particles at the same time. This resulted in stable subsets containing 92,854 (A), 54,196 (B), and 75,251 (C) particles, respectively. Volume C contained the non-ribosomal particles. Even though the initial reference for volume B had been an isolated 60S subunit, volume A as well as volume B represented 60S subunits with substantial amounts of additional density. Since volume B was much better defined and contained less noise, the corresponding particles were used for further refinement. Both, volume A and volume B were used as references for the following sorting step, resulting in subsets with 29,997 and 24,200 particles, respectively. The volume of the larger subset again represented a 60S subunit with scattered additional density all over its surface, while the other volume was very noisy. The most prominent additional density were two barrel-like structures between the L1-stalk and the tunnel exit. Sorting for that feature resulted in a volume of 15,116 particles in which all of the previously observed additional densities were enhanced. Finally, those particles were analyzed by focused sorting (see 2.6.1.6) according to their density below the tunnel exit. The final volume was backprojected from 8,322 particles and had a resolution of 14.3 Å (Figure 21, see also 2.6.1.7).
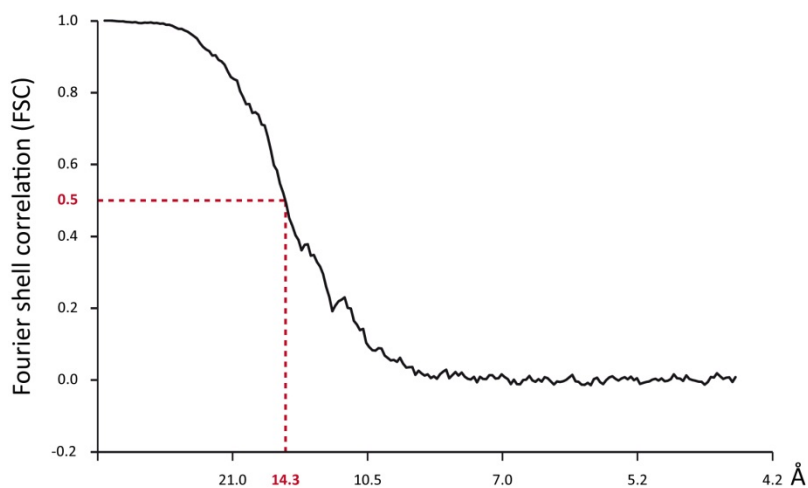
Figure 21. Fourier shell correlation plot of the Arx1 pre-60S particle

The resolution was determined from the FSC plot at a correlation of 0.5.

The volume was interpreted by comparing it to a mature 60S subunit. The core of the pre-60S particle showed no differences to the mature subunit. However, the central protuberance (CP) appeared to be in a completely different conformation and the P-stalk was absent in the pre-60S particle. As became already obvious during sorting, several

distinct additional densities could be identified (Figure 22). Additions of a green fluorescent protein (GFP) tag to Rpl25 or Rpl35 were shown to impair Arx1 interaction with 60S subunits[52] and the factor could be cross-linked to H59 as well as the tip of ES27[L] (Dr. Bettina Bradatsch, manuscript submitted). In agreement with these data, Arx1 was assigned to the red density below the tunnel exit. The position of the blue density perfectly fits the previously determined binding site for Tif6. It also resembles the factor with respect to its size and shape[62,66].
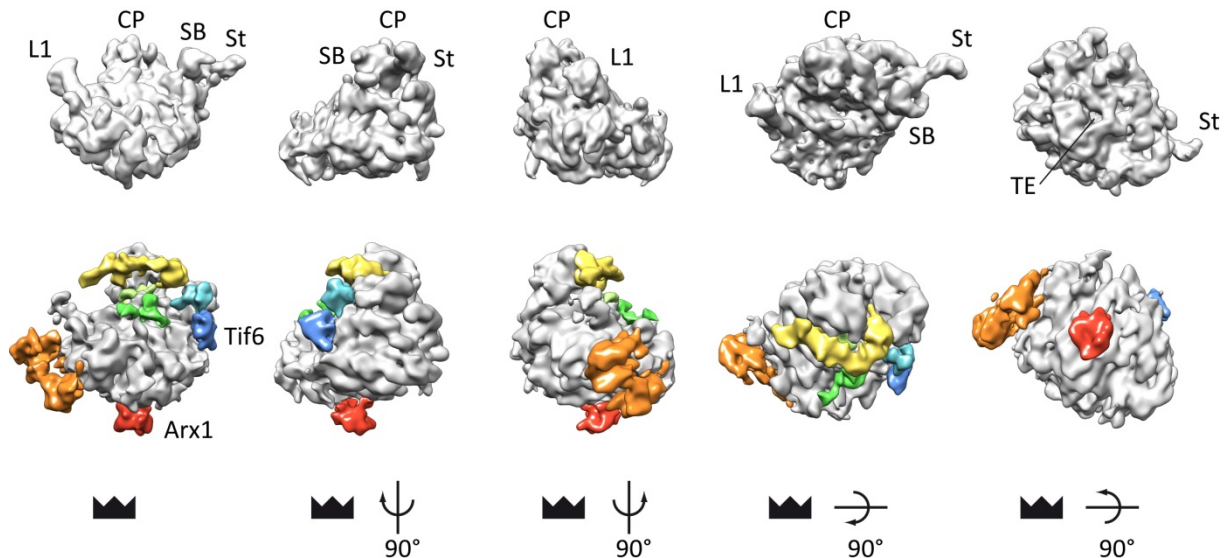
Figure 22. Cryo-EM reconstruction of the Arx1 pre-60S particle at 14.3 Å resolution

The comparison of the Arx1 pre-60S particle (lower panel) with a mature 60S subunit (upper panel, grey; isolated from *S. cerevisiae* RNC-Ssh1 complexes[161]) reveals a scattered distribution of additional densities (lower panel, red to blue) on the premature 60S subunit (lower panel; grey). The volumes were low-pass filtered at 14 – 16 Å. Rotations of the reconstructions are indicated relative to the crown view (left). The densities for Arx1 (red) and Tif6 (blue) are labeled accordingly. L1: L1-stalk; CP: central protuberance; SB: stalk base; St: P-stalk; TE: tunnel exit.

Taken together, the Arx1 pre-60S particle exhibits a scattered distribution of additional densities on the surface of a clearly premature 60S subunit. Two of those densities were identified to be the ribosomal biogenesis factors Arx1 and Tif6. Factors bound to the intersubunit surface and at the tRNA binding sites ensure translational silencing of the particle.

4.2 Towards a High-Resolution Map of the Arx1 pre-60S Particle

The 3D reconstruction of the Arx1 pre-60S particle is significantly larger and possesses a different shape than a mature 60S subunit. Therefore, the initial alignment of the particles to the mature 60S subunit was probably very inaccurate and many particles may have been

completely misaligned. Those particles would then be sorted out as non-ribosomal particles or give rise to noisy reconstructions, like those that were discarded during sorting. In an effort to increase the number of correctly aligned particles, the entire dataset was re-processed with the 3D reconstruction of the Arx1 particle as the initial reference.
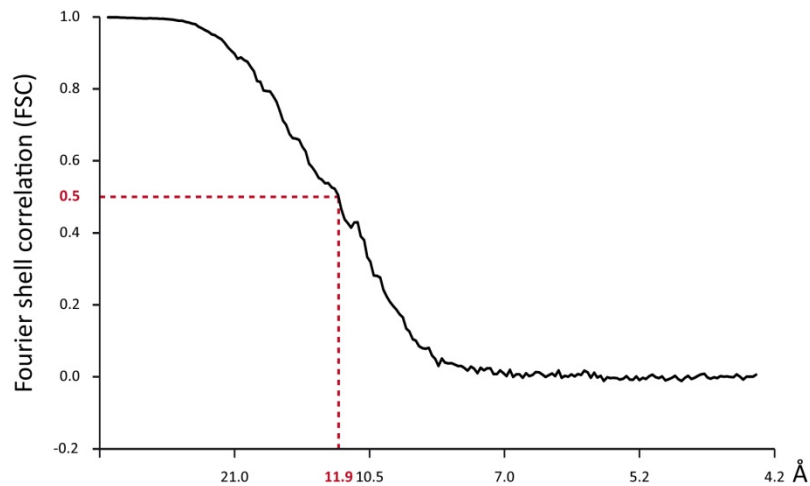

Figure 23. Fourier shell correlation plot of the Arx1 pre-60S particle

The resolution was determined from the FSC plot at a correlation of 0.5.
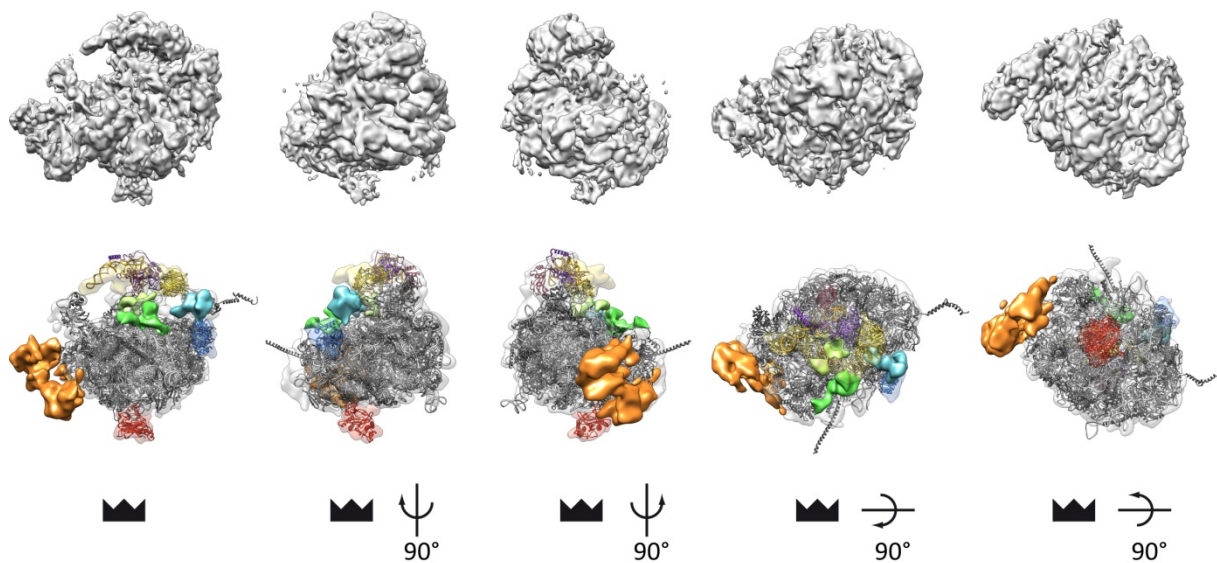
Figure 24. The Arx1 pre-60S particle

Upper panel: 3D reconstruction of the Arx1 pre-60S particle (grey) low-pass filtered at 8 – 10 Å. **Lower panel:** Model of the Arx1 pre-60S particle composed of (i) the model of the mature 60S subunit without Rpl10 and the P-stalk proteins, (ii) the model for the rearranged 5S-Rpl5-Rpl11 particle, (iii) the structures of identified factors, namely Arx1, Tif6, and Mex67-Mtr2, (iv) and the unidentified additional densities of the cryo-EM reconstruction of the Arx1 pre-60S subunit. Rotations are indicated relative to the crown view (left). Color code of the ribbon model: gold: 5S rRNA; purple: Rpl5; dark red: Rpl11; red: Arx1; yellow: Mex67-Mtr2; blue: Tif6; grey: 5.8S and 25S rRNA; black: ribosomal proteins. Color code of the cryo-EM density as in Figure 22.

The simultaneous sorting for mature 60S subunits and non-ribosomal particles resulted in subsets of 112,632 (A), 43,324 (B), and 66,994 (C) particles, respectively. In volume A all previously identified pre-ribosomal features were already visible, while volume B and volume C represented a noisy mature 60S subunit and non-ribosomal particles, respectively. In an additional sorting step, the particles of volume A were split into subsets of 63,943 and 48,691 particles, respectively. The reconstruction of the larger subset gave rise to a well resolved pre-60S particle and was further refined to a final resolution of 11.9 Å (Figure 23).

Overall, the final reconstruction after re-alignment of the data displayed the same features as the previous reconstruction (Figure 24). However, the improved resolution enabled a more detailed interpretation of the map (Figure 24, and see 4.3).

4.3   Localization of Ribosomal and non-Ribosomal Factors

An striking feature of the Arx1 pre-60S particle is its rearranged CP. The cryo-EM reconstruction reveals that several ribosomal proteins are not present in their final locations, yet. The P-stalk proteins are missing and also Rpp0 does not fit well into the observed density. Rpl12 is completely absent and Rpl10, which is buried below the CP in the mature 60S subunit, does not fit the density observed in its location. This density clearly represents RNA but not protein (Figure 25A).
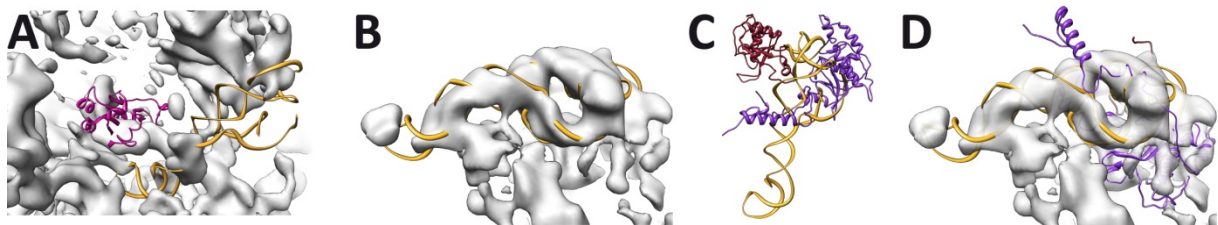
Figure 25. Localization of the 5S-Rpl5-Rpl11 particle

A. Map of the Arx1 pre-60S particle (grey) at a high contour level. Models of Rpl10 (pink) and 5S rRNA (gold) are displayed at the locations they would assume in the mature 60S subunit. The mature position of Rpl10 is occupied by a RNA density, while there is no density visible for 5S rRNA in its mature position. **B.** Rigid body fit of the mature 5S rRNA model (gold) into the density on top of the CP. **C.** Model of the complex of 5S rRNA (gold), Rpl5 (purple), and Rpl11 (dark red) isolated from the mature 60S subunit. **D.** Rigid body fit of the complex into the density on top of the CP according to the 5S rRNA position.

The 5S rRNA extends into the body of the mature 60S subunit in its final position. However, in the reconstruction of the Arx1 pre-60S particle, there is no RNA signal for this molecule (Figure 25A). Yet, a stretch of RNA could be found on top of the immature CP that was not accounted for in the model of the mature 60S subunit. The 5S rRNA perfectly fits into this density (Figure 25B). It was previously observed that the 5S rRNA is delivered to the maturing 60S subunit in complex with Rpl5 and Rpl11[35]. A model for this complex can be

isolated from the structure of the mature 60S subunit (Figure 25C). When this model is positioned into the density for the rearranged CP according to the position of the 5S rRNA, Rpl5 nicely fits into the neighboring density (Figure 25D). For Rpl11, this fit is less accurate, but the protein may still be there (data not shown). This indicates, that the 5S-Rpl5 particle, possibly already in complex with Rpl11, is positioned on top of the premature 60S subunit as a preformed entity.

Structures for several non-ribosomal factors could also be docked into the map. The model of Tif6 nicely fits into the density at the expected position, thereby confirming the previous assignment of the blue density to this factor[62,66] (Figure 26A, see also Figure 22).

A crystal structure is available of the Mex67-Mtr2 complex, comprising Mtr2 and a C-terminal fragment of Mex67[162]. Since the complex was shown to interact with 5S rRNA, it is likely to be situated inside the yellow density surrounding the rearranged CP[55]. The crystal structure was placed into the part of the density between Rpl5 and the stalk base. This region has the same size as the crystallized heterodimer and resembles its overall shape. However, it was not possible at the given resolution to unambiguously fit the structure (Figure 26B). Thus, Mex67-Mtr2 may as well be localized elsewhere on the pre-60S particle.

There is no structure available for *S. cerevisiae* Arx1. However, the crystal structure of its slightly smaller homolog from *C. thermophilum* has been solved (Dr. Gert Bange, unpublished data). This structure could be clearly fit into the red density below the tunnel exit, also confirming the previous assignment of this part of the map (Figure 26C). Arx1 contacts the premature 60S subunit between H59 and Rpl25. In addition, there may be another contact to Rpl35 (Figure 26D). This is in perfect agreement with biochemical data indicating that Arx1 binds in the vicinity of those two proteins (Hung 2006) and the previously found cross-link to H59 (Dr. Bettina Bradatsch, manuscript submitted).
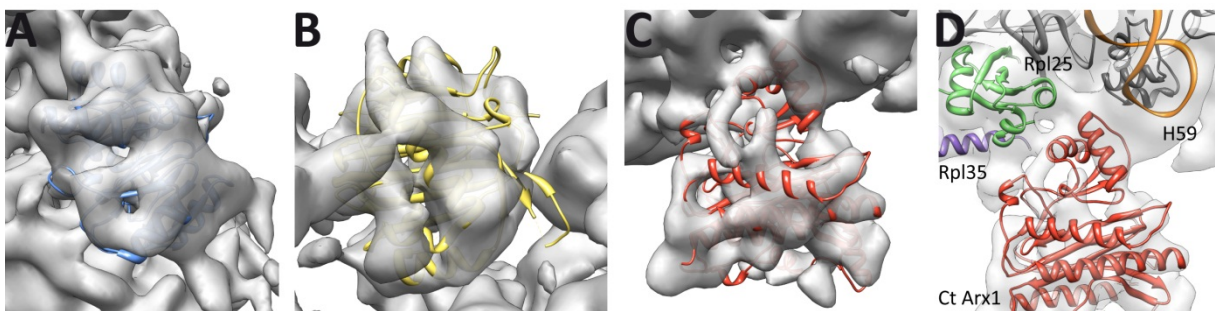
Figure 26. Positions of non-ribosomal factors on the Arx1 pre-60S particle

A. A model for Tif6 fits nicely into the density at the previously described position[62,66]. **B.** The Mex67-Mtr2 complex may be located between the rearranged CP and the stalk base. **C.** The crystal structure of *C. thermophilum* Arx1 can be unambiguously docked into the density below the tunnel exit. **D.** The structures of *C. thermophilum* Arx1 and the *S. cerevisiae* 60S subunit allow a specific description of the contact between Arx1 and the premature 60S subunit. Arx1 (Ct Arx1; red) contacts the subunit at Rpl25 (green) and H59 (orange). A contact to Rpl35 (purple) is possible.

Taken together, the cryo-EM reconstruction of the Arx1 pre-60S particle allowed the localization of several ribosomal and non-ribosomal factors on the premature 60S subunit. A preformed 5S-Rpl5 particle was located on top of the CP. The particle, that may also contain Rpl11, is arranged as it is also found in the mature 60S subunit, however, its location and orientation are completely different from this state. The proposed interaction sites of Tif6 and Arx1 on the premature subunit were confirmed, and a possible binding site for the Mex67-Mtr2 complex was suggested. Analysis of the Arx1 interaction site supports previously found evidence for interactions with H59 and Rpl25 as well as Rpl35 with structural data.

4.4 The Interaction of Arx1 and ES27^L can be Visualized by Cryo-EM

At very low contour levels ES27L extended into the direction of Arx1. When the map was low-pass filtered between 14 – 16 Å, a direct contact could be visualized. An additional round of sorting resulted in subsets of 38,730 and 25,215 particles, respectively. In the reconstruction of the second subset, the contact between Arx1 and ES27^L was even more defined (Figure 27), while no contact could be seen in the other reconstruction. This indicates, that ES27^L does interact with Arx1. However, this contact is not formed in all particles.
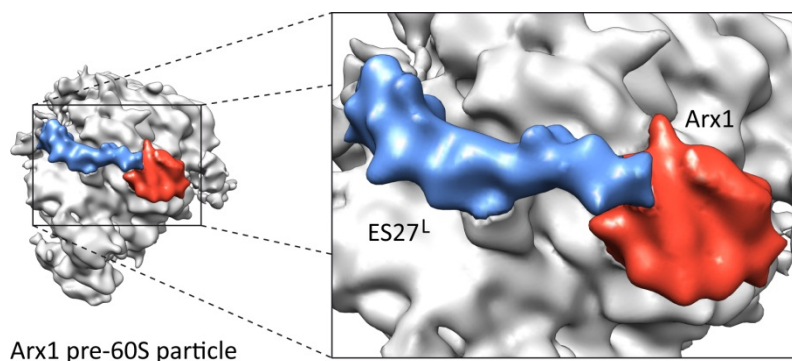

Figure 27. ES27^L contacts Arx1

Reconstruction of a subpopulation of the Arx1 pre-60S particle cryo-EM dataset low-pass filtered at 15 – 16 Å at a low contour level. ES27^L (blue) extends towards and contacts Arx1 (red). Noise has been removed using the *hide dust* function of chimera.

Chapter

5 Discussion

5.1 The Ribosome-Associated Complex

5.1.1 Ribosome Interaction of RAC

The data presented in this study suggest, that the interaction between RAC and the 80S ribosome is facilitated to a large extent by the newly described C-terminal head domain of Zuotin. This function was, however, previously attributed to the charged region of Zuotin. Deletion of the charged region has been shown to impair Zuotin's ability to bind to ribosomes[116]. Also, short peptide fragments of this region were found to interact with ribosomes[21]. In contrast, the results of this study demonstrate, that the exclusive deletion of the head domain has the same impairing effect on Zuotin's ribosome interaction as a combined deletion with the charged region. This contradiction may be explained by the finding that the charged region and the head domain partially overlap. The common sequence (residues 349 − 364 in *S. cerevisiae* or residues 355 − 370 in *C. thermophilum*) forms the α1 helix of the head domain (Figure 28A). This α-helix is, therefore, likely to be crucial for the interaction. Alternatively, deletion of the charged region could inhibit the efficient binding of Zuotin to the 80S ribosome simply by decreasing the distance between the head domain and Zuotin's second binding interface (C2), thereby preventing their simultaneous interaction. In agreement with the data presented here, the existence of such secondary binding interfaces was previously suggested[21]. This would also explain why a Zuotin mutant lacking only part of its charged region was found to be unable to interact with ribosomes[21].

Previous attempts to determine RAC's binding site on the ribosome by biochemical approaches revealed a close proximity of Zuotin to Rpl31. However, it was shown in the same study, that Rpl31 is not required for the formation of a RAC-ribosome complex. Since deletion of Rpl31 resulted in similar phenotypes as deletion of RAC, a functional relation was suggested between the proteins that is independent of the association of RAC with ribosomes[21]. In the cryo-EM reconstruction of the RAC-80S ribosome complex, a linker connects the head domain with the main body of RAC. Considering the domain architecture of Zuotin (Figure 17A), this linker is likely to contain the charged region. Although no direct contact is visible in the reconstruction, the linker passes in close proximity to Rpl31. It is tempting to speculate that such a contact may form only under specific conditions, e.g. interaction of a substrate nascent chain with RAC and/or Ssb. This would be consistent with a model in that Rpl31 is involved in signal transmission between RAC and ribosomes. It may also provide an explanation for the demonstrated interaction of short peptide fragments of the charged region with ribosomes. These fragments might readily bind to Rpl31 when taken out of the regulatory framework provided by intact RAC. However, these highly charged fragments might also interact with the ribosome in an unspecific manner and, in addition, the potentially unfolded fragments may not reflect the situation *in vivo*.
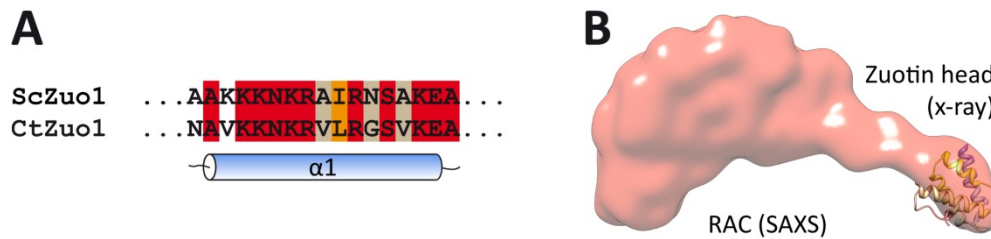
Figure 28. Zuotin head domain α1 helix may facilitate interaction with 80S ribosomes

A. Alignment of the *S. cerevisiae* (ScZuo1) and *C. thermophilum* (CtZuo1) amino acid sequences of the α1 helix of the Zuotin head domain. **B.** Fit of the *C. thermophilum* Zuotin C-terminus structure into the head of the *C. thermophilum* RAC SAXS model with the α1 helix facing outwards (compare Figure 16C).

Having identified the α1 helix of the head domain as an important element for Zuotin's ribosome interaction, the orientation of the domain in the SAXS envelope can be reconsidered. Initially, the domain was placed into the envelope according to the best fit. Considering this fit in the context of ribosome binding, α1 would be located on a surface facing away from the ribosome (Figure 16). However, it is also possible to dock the domain in a different orientation where α1 would be exposed towards the ribosome, and still achieve a reasonable fit (Figure 28B). This orientation would allow the helix to form a direct ribosomal contact.

5.1.2 A Ribosome-Associated Holding and Folding Machinery

The conserved, and seemingly directed, mutations that efficiently prevent ATP hydrolysis by Ssz1 while still permitting nucleotide binding raise the question whether this is functionally relevant. The presence of ATP in the Ssz1 NBD would lock its SBD in a low-affinity state. While low-affinity SBDs are frequently found and shown to be functionally important in Hsp40 co-chaperones, Zuotin lacks an equivalent domain[163]. A possible function of Ssz1 could be to supply its low-affinity SBD to Zuotin *in trans*. This would result in a model that can be described analogous to the canonical Hsp70 chaperone cycle (Figure 29, see also Figure 5). A substrate nascent chain would be recognized by RAC and would bind with low affinity to the SBD of Ssz1. Subsequently, interaction of the J-domain of Zuotin with Ssb and simultaneous handing over of the substrate would stimulate ATP hydrolysis by Ssb. As a result, Ssb would be tightly bound to the growing nascent chain and stay attached until it is released by downstream factors. This scenario would also explain why Zuotin can efficiently stimulate Ssb only in presence of Ssz1 and why efficient cross-links between Ssb and nascent chains require the presence of functional RAC[113,118].

The biological relevance of the Ssz1 SBD is, however, under discussion. Yeast cells expressing a Ssz1 mutant lacking its SBD were found to grow comparable to wt cells under all tested conditions[117]. In a subsequent study the phenotypes were tested more thoroughly, revealing that the truncation mutant could not completely complement the deletion of wt Ssz1 in the presence of high concentrations of paromomycin. While disruption of Ssz1's ability to bind

nucleotides does not result in an observable phenotype, the additional deletion of the SBD domain in the same mutant results in the same phenotypes as the deletion of complete Ssz1[124]. A functional relevance of the Ssz1 SBD is also supported by the finding that wt RAC displays chaperone activity *in vitro*[115]. This has also been demonstrated for the SBD-containing *E. coli* Hsp40 co-chaperone DnaJ[100]. The SBD may, however, not be required for all cellular functions of Ssz1. Taken together, these data indicate that the SBD of Ssz1 is likely to have a biological function, however, this function is not essential or may be required only under distinct conditions. This situation would be compatible with the proposed model. The absence of the SBD would occasionally lead to futile ATP hydrolysis events by Ssb and/or a slight reduction in its stimulation by RAC.
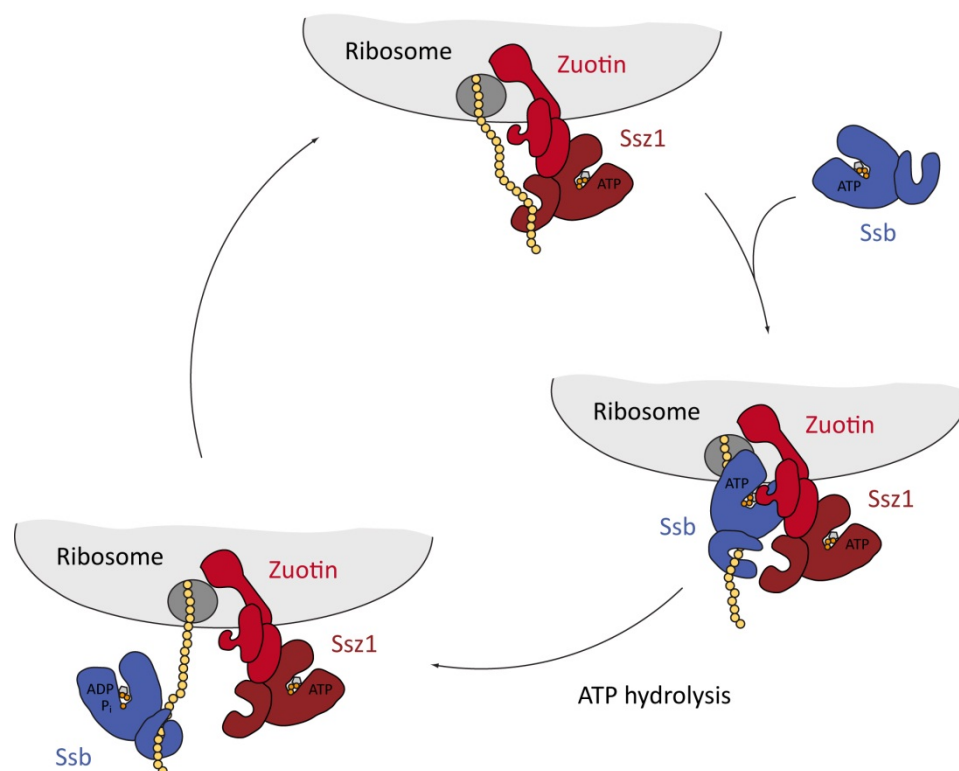
Figure 29. A ribosome-associated holding and folding machinery

A substrate nascent chain is bound with low affinity to the SBD of Ssz1. When Ssb joins the complex, interaction of the J-domain of Zuotin with Ssb and simultaneous handing over of the substrate stimulate ATP hydrolysis by Ssb. As a result, Ssb is tightly bound to the substrate and dissociates from the RAC-80S complex.

5.2   The Arx1 pre-60S Particle

Structural analysis of the Arx1 pre-60S particle yielded the first 3D cryo-EM reconstruction of an immature 60S ribosomal subunit. This reconstruction allowed the identification of bound non-ribosomal factors and revealed premature features of the subunit itself.

5.2.1 Identification of non-Ribosomal Factors

The export factor Arx1, probably in complex with Alb1, was found to bind to the pre-60S subunit directly in front of the ribosomal tunnel exit. It binds to the premature 60S subunit at the UAS1 contacting H59, Rpl25 and possibly Rpl35 (Figure 26D). A potential binding site was proposed for Mex67-Mtr2 between the CP and the stalk base (Figure 26B). The elongated, green density in the center of the intersubunit surface could not be identified (Figure 22). However, its position nicely matches the binding site identified for Nmd3 on a mature 60S subunit[51]. Such a scattered distribution of export factors would agree with the previously suggested hypothesis, that several export factors on different surfaces would be necessary to efficiently export maturing 60S subunits through the NPCs (Dr. Bettina Bradatsch, manuscript submitted). Tif6 was identified in the same position it adopts on the mature 60S subunit[62,66]. The binding sites of several other non-ribosomal factors are yet to be determined. The orange, parts of the yellow, the light green, and the cyan extra densities are still unaccounted for (Figure 22). Candidate factors would include the GTPases Nog1, Nog2, Nug1, and Lsg1 as well as the factors Mex67-Mtr2, Mrt4, Nsa2, and Rei1 (Dr. Bettina Bradatsch, manuscript submitted). Under the assumption that the position of the Mex67-Mtr2 crystal structure has been assigned correctly, the yet unidentified part of the yellow density would be the N-terminal portion of Mex67. This position would allow the previously observed interaction of Mex67 with 5S rRNA[55]. According to its size and immuno-labeling negative stain electron microscopy data (Dr. Bettina Bradatsch, manuscript submitted) the cyan density is likely to represent Nsa2.

5.2.2 The Arx1 pre-60S Subunit is not yet Translation Competent

A variety of structural features could be identified that stress the premature state of the 60S subunit. Most prominent is the placement of the 5S-Rpl5-Rpl11 particle on top of the CP. Also, H38 of the 25S rRNA (A-site finger) is not yet in its final position (data not shown) and Rpl10 is absent. These rearrangements might be an additional mechanism to prevent premature translation initiation. Analogous to the proposed function of Tif6, the presence of the 5S rRNA on the CP may block subunit association. Besides the steric prevention of the formation of an initiation complex, also the P-site is blocked by an unknown factor. Taken together, the Arx1 pre-60S particle is structurally unable to engage in active translation.

Next to the 5S rRNA, in the position where Rpl11 was placed by fitting of the 5S-Rpl5-Rpl11 particle, the electron density is more reminiscent of a short RNA fragment than of protein density. However, Rpl10 fits surprisingly well into this density. Possibly, the density map represents a mixed population of particles, resulting in overlapping RNA and protein density at this position. The RNA density could be explained by both, an alternative conformation of the A-site finger or 5S rRNA in its mature position. Another possible position for the A-site finger would be the space occupied by Rpl10 in the mature 60S subunit which is unambiguously occupied by RNA. To achieve the mature state of the 60S subunit, three steps have to occur. (i) The A-site finger needs to adopt its mature conformation, thereby

freeing the space Rpl10 will later occupy and allowing for (ii) the rotation – possibly around Rpl11 – of the 5S rRNA into its final position. This movement, that is likely to involve the release of Mex67-Mtr2, would otherwise be blocked. (iii) Finally, Rpl10 has to be inserted. A process, that was shown to be coupled to Nmd3 release[31]. The order these steps occur in, which factors they involve, and how they might be coupled or influence each other remains to be revealed by further studies.

5.3   ES27^L and the Tunnel Exit Region

In the cryo-EM reconstruction of the *C. thermophilum* RAC-80S complex some additional density is present on the body of RAC that does not seem to belong to the chaperone complex (Figure 30A, see also Figure 16A). A similar density was observed in a previous study on a C-terminal fragment of ERj1 bound to the ribosome. This density was interpreted as part of ES27^L contacting the Hsp40 chaperone[18] (Figure 30B). Accordingly, the additional density observed on RAC is very likely to represent ES27^L (Figure 30). The shape of the resulting slightly smaller density for RAC would then be more similar to the model obtained by SAXS.

When comparing the SAXS envelopes of *S. cerevisiae* and *C. thermophilum* RAC, they differ in the angle between their respective body and neck domains (Figure 15A). This angle also varies among the individual, non-averaged SAXS models calculated for the respective complexes (data not shown). This may indicate that the neck and head region can move relative to the body. The difference in this angle is even larger between the *C. thermophilum* SAXS envelope of RAC and RAC observed on the 80S ribosome by cryo-EM (Figure 16A). It is tempting to speculate about a conformational change induced by ribosome binding. Such a conformational change may also have functional relevance. It is imaginable, that movement of the RAC body – e.g. to interact with a substrate nascent chain – could induce tension in the linker. This could push parts of the linker closer to the ribosome, thereby enabling an interaction with Rpl31. In addition, an interaction of the RAC body with ES27^L could support the maintenance of this conformation.

It was previously suggested that ES27^L might facilitate the communication of ligands of the tunnel exit region with translational control or might coordinate the access of those ligands to this region[15,18]. Finding the expansion segment interacting with ribosome-associated Hsp40 chaperones, it is imaginable that ES27^L in its *exit* conformation may convey a signal for translational deceleration or pausing in the case of complex nascent proteins that require chaperone activity. This would be analogous to the translational arrest triggered by binding of the ALU-domain of SRP to the factor binding site[17,164]. Consistent with this hypothesis, ES27^L is not found in a defined conformation while SRP is bound to the ribosome[17]. In this context, the contact of ES27^L to the export factor Arx1 on the premature 60S subunit might

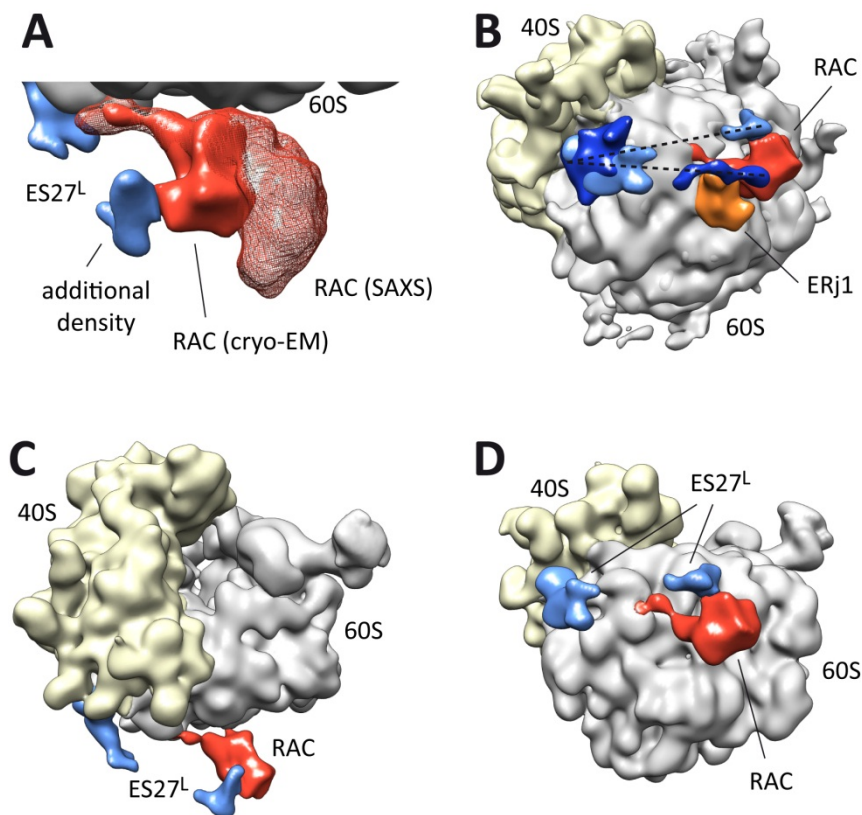be yet another mechanism to prevent premature translation activity by conveying a translational arrest signal.

Figure 30. RAC might interact with ES27^L

A. Superposition of the RAC envelope obtained by SAXS (red mesh) with the RAC-80S complex observed in cryo-EM (density map). An additional density (blue) is observed on RAC (red), that might be part of ES27^L (blue). **B.** Superposition of the complexes of RAC (red) and the ERj1 C-terminus (ERj1, orange) with the 80S ribosome (40S subunit: yellow; 60S grey: grey), respectively[18]. Additional densities are observed in both cases that were attributed to ES27^L (dark and light blue, respectively) in its *exit* conformation. Measured from the origin of ES27^L at the 60S subunit to the respective tips of the additional densities, the two slightly different ES27^L conformations enclose an angle roughly 15°. **C & D.** 3D reconstruction of the *C. thermophilum* RAC-80S complex (see also Figure 12) with coloring of ES27^L (blue). RAC, the 60S subunit, and the 40S subunit are colored in red, grey, and yellow, respectively. Electron density maps are low-pass filtered at 18 − 20 Å.

5.4 Coordination of Ribosomal Tunnel Exit Ligands

A considerable number of structures is now available for ligands at the ribosomal tunnel exit, including Arx1, ERj, RAC, Sec61, SRP[17,18,161]. Arx1 is structurally highly homologous to MAPs[52,53]. Therefore, it can be speculated that MAPs interact with ribosomes in the same way as Arx1 does. Other factors have been shown by biochemical experiments to also bind to the tunnel exit region, e.g. NAC and Oxa1[22,165]. Considering this, a simultaneous binding of those factors does not seem possible. Accordingly, RAC and NAC have been shown to compete for ribosome interaction (Julian Deeng, unpublished data), and Arx1 has already

been speculated to serve as a placeholder on the pre-60S subunit for MAP and/or other tunnel exit ligands until maturation of the subunit is completed[52]. The results of this study stress the requirement to regulate the access of ligands to the ribosomal tunnel exit site and raise the important question of how the interplay between those ligands is coordinated.

Chapter

6 Conclusion and Future Perspective

6.1 Conclusion

The work on RAC presented in this thesis shows that RAC contacts the ribosome at two distinct interaction sites and projects its major body above the ribosomal tunnel exit. RAC can be divided into a body, a neck and a head domain and it was demonstrated that the neck and head domains are exclusively constituted by Zuotin. The crystal structure of the Zuotin C-terminus was determined and identified as a structural homolog of the PHAX RNA binding domain. It was shown to fundamentally contribute to Zuotin's ribosome binding ability and was assigned to the head domain of RAC which directly contacts the ribosome. A 30 amino acid fragment in the Zuotin N-terminus was identified as the interaction site of Zuotin and Ssz1. Furthermore, the crystal structure of the Ssz1 NBD explains its inability to hydrolyze ATP. Taken together, these results suggest a *holding and folding* model for RAC at the ribosome. A possible interaction between RAC and ES27L supports hypotheses about an involvement of the expansion segment in the coordination of factors at the ribosomal tunnel exit site.

The results obtained for Arx1 pre-60S particle reveal a scattered distribution of non-ribosomal factors over the surface of the premature 60S subunit. The export factor Arx1 binds to the UAS1 at the ribosomal tunnel exit and contacts ES27^L. The initiation factor Tif6 is located close to the translation factor binding site on the intersubunit surface and Mex67-Mtr2 is possibly located between the CP and the base of the P-stalk. The pre-60S subunit displays a number of premature features, including the absence of ribosomal proteins and a significant rearrangement of the CP and neighboring regions. A pre-formed 5S-Rpl5-Rpl11 particle is located on top of the CP and Rpl10 is not yet integrated into the pre-60S subunit while the A-site finger seems to occupy its space instead. Taken together, these results emphasize the premature state of the Arx1 pre-60S particle and reveal a number of inhibitory mechanisms to prevent engagement of the maturating subunit in translation.

The interaction of ES27^L with completely unrelated ligands of the ribosomal tunnel exit suggests a general role for the essential expansion segment. Both, the coordination of ribosomal tunnel exit ligands and a role in translational control or fidelity seem possible.

6.2 Future Perspective

Despite the insights gained by this study further questions remain to be answered on both of the presented topics.

The molecular basis of the Zuotin-Szz1 interaction is not yet revealed. Especially on the side of Ssz1 very little is known. Mutagenesis studies in the identified binding region of Zuotin should be sufficient to identify the individual residues involved in the interaction. However, only a crystal structure of this region will elucidate the complete binding interface. A good

candidate construct may be the complex of Zuotin residues 20 – 50 and Ssz1. However, also truncations of Ssz1 might be necessary to achieve suitable protein crystals.

To better interpret the presented cryo-EM structure of the RAC-80S ribosome complex and to further elucidate the mechanisms of co-translational folding by RAC, visualization of the related complex of RAC, Ssb and a ribosome carrying a nascent chain should be the next target. With the information on RAC in hand, additional density could be assigned to Ssb and possible conformational changes upon substrate interaction might be observed.

Multiple factors bound to the Arx1 pre-60S particle remain to be identified. The collection of additional cryo-EM data might enable a further refinement of the structure to an even higher resolution. The unambiguous visualization of the protein secondary structures of these ligands would contribute greatly to revealing their identity. In addition, the reconstruction of earlier and later 60S maturation intermediates – i.e. exclusively nucleoplasmic or cytoplasmic pre-60S particles, respectively – could provide a structural view of ribosomal subunit biogenesis. In particular, the structural rearrangements of the CP would be a highly interesting process to observe.

The role of ES27[L] is another highly interesting topic worth thorough investigation. Biochemical experiments will have to be designed to elucidate its function and describe its interplay with the factors binding to the ribosomal tunnel exit. The visualization of the ribosomal complexes of additional ligands, e.g. MAP and NAT, and analysis with respect to ES27[L] might also provide valuable information.

References

1   Melnikov, S. *et al.* One core, two shells: bacterial and eukaryotic ribosomes. *Nat Struct Mol Biol* **19**, 560-567, doi:10.1038/nsmb.2313 (2012).

2   Frank, J. *et al.* Three-dimensional reconstruction of the 70S Escherichia coli ribosome in ice: the distribution of ribosomal RNA. *J Cell Biol* **115**, 597-605 (1991).

3   Verschoor, A. *et al.* Three-dimensional structure of the yeast ribosome. *Nucleic Acids Res* **26**, 655-661 (1998).

4   Ban, N. *et al.* The complete atomic structure of the large ribosomal subunit at 2.4 A resolution. *Science* **289**, 905-920 (2000).

5   Schluenzen, F. *et al.* Structure of functionally activated small ribosomal subunit at 3.3 angstroms resolution. *Cell* **102**, 615-623 (2000).

6   Carter, A. P. *et al.* Functional insights from the structure of the 30S ribosomal subunit and its interactions with antibiotics. *Nature* **407**, 340-348, doi:10.1038/35030019 (2000).

7   Wimberly, B. T. *et al.* Structure of the 30S ribosomal subunit. *Nature* **407**, 327-339, doi:10.1038/35030006 (2000).

8   Yusupov, M. M. *et al.* Crystal structure of the ribosome at 5.5 A resolution. *Science* **292**, 883-896, doi:10.1126/science.1060089 (2001).

9   Armache, J. P. *et al.* Cryo-EM structure and rRNA model of a translating eukaryotic 80S ribosome at 5.5-A resolution. *Proc Natl Acad Sci U S A* **107**, 19748-19753, doi:10.1073/pnas.1009999107 (2010).

10   Ben-Shem, A. *et al.* Crystal structure of the eukaryotic ribosome. *Science* **330**, 1203-1209, doi:10.1126/science.1194294 (2010).

11   Ben-Shem, A. *et al.* The structure of the eukaryotic ribosome at 3.0 A resolution. *Science* **334**, 1524-1529, doi:10.1126/science.1212642 (2011).

12   Nissen, P. *et al.* The structural basis of ribosome activity in peptide bond synthesis. *Science* **289**, 920-930 (2000).

13   Spahn, C. M. *et al.* Structure of the 80S ribosome from Saccharomyces cerevisiae--tRNA-ribosome and subunit-subunit interactions. *Cell* **107**, 373-386 (2001).

14   Smith, T. F. *et al.* The origin and evolution of the ribosome. *Biol Direct* **3**, 16, doi:10.1186/1745-6150-3-16 (2008).

15   Beckmann, R. *et al.* Architecture of the protein-conducting channel associated with the translating 80S ribosome. *Cell* **107**, 361-372 (2001).

16   Kramer, G. *et al.* L23 protein functions as a chaperone docking site on the ribosome. *Nature* **419**, 171-174, doi:10.1038/nature01047 (2002).

17   Halic, M. *et al.* Structure of the signal recognition particle interacting with the elongation-arrested ribosome. *Nature* **427**, 808-814, doi:10.1038/nature02342 (2004).

18   Blau, M. *et al.* ERj1p uses a universal ribosomal adaptor site to coordinate the 80S ribosome at the membrane. *Nat Struct Mol Biol* **12**, 1015-1016, doi:10.1038/nsmb998 (2005).

19   Kohler, R. *et al.* YidC and Oxa1 form dimeric insertion pores on the translating ribosome. *Mol Cell* **34**, 344-353, doi:10.1016/j.molcel.2009.04.019 (2009).

20   Halic, M. *et al.* Signal recognition particle receptor exposes the ribosomal translocon binding site. *Science* **312**, 745-747, doi:10.1126/science.1124864 (2006).

21   Peisker, K. *et al.* Ribosome-associated complex binds to ribosomes in close proximity of Rpl31 at the exit of the polypeptide tunnel in yeast. *Mol Biol Cell* **19**, 5279-5288, doi:10.1091/mbc.E08-06-0661 (2008).

22   Pech, M. *et al.* Dual binding mode of the nascent polypeptide-associated complex reveals a novel universal adapter site on the ribosome. *J Biol Chem* **285**, 19679-19687, doi:10.1074/jbc.M109.092536 (2010).

23   Beckmann, R. *et al.* Alignment of conduits for the nascent polypeptide chain in the ribosome-Sec61 complex. *Science* **278**, 2123-2126 (1997).

24   Sweeney, R. *et al.* An rRNA variable region has an evolutionarily conserved essential role despite sequence divergence. *Mol Cell Biol* **14**, 4203-4215 (1994).

25   Jeeninga, R. E. *et al.* Variable regions V13 and V3 of Saccharomyces cerevisiae contain structural features essential for normal biogenesis and stability of 5.8S and 25S rRNA. *RNA* **3**, 476-488 (1997).

26   Seidelt, B. *et al.* Structural insight into nascent polypeptide chain-mediated translational stalling. *Science* **326**, 1412-1415, doi:10.1126/science.1177662 (2009).

27   Selmer, M. *et al.* Structure of the 70S ribosome complexed with mRNA and tRNA. *Science* **313**, 1935-1942, doi:10.1126/science.1131127 (2006).

28   Rheinberger, H. J. in *Protein Synthesis and Ribosome Structure* (eds K. H. Nierhaus & D. N. Wilson) Ch. Ribosome Assembly, 85-144 (WILEY-VCH Verlag GmbH & Co. KGaA, 2004).

29   Dinman, J. D. The eukaryotic ribosome: current status and challenges. *J Biol Chem* **284**, 11761-11765, doi:10.1074/jbc.R800074200 (2009).

30   Fatica, A. & Tollervey, D. Making ribosomes. *Curr Opin Cell Biol* **14**, 313-318 (2002).

31   Zemp, I. & Kutay, U. Nuclear export and cytoplasmic maturation of ribosomal subunits. *FEBS Lett* **581**, 2783-2793, doi:10.1016/j.febslet.2007.05.013 (2007).

32   Henras, A. K. *et al.* The post-transcriptional steps of eukaryotic ribosome biogenesis. *Cell Mol Life Sci* **65**, 2334-2359, doi:10.1007/s00018-008-8027-0 (2008).

33   Grandi, P. *et al.* 90S pre-ribosomes include the 35S pre-rRNA, the U3 snoRNP, and 40S subunit processing factors but predominantly lack 60S synthesis factors. *Mol Cell* **10**, 105-115 (2002).

34   Cmarko, D. *et al.* Nucleolus: the ribosome factory. *Histol Histopathol* **23**, 1291-1298 (2008).

35   Zhang, J. *et al.* Assembly factors Rpf2 and Rrs1 recruit 5S rRNA and ribosomal proteins rpL5 and rpL11 into nascent ribosomes. *Genes Dev* **21**, 2580-2592, doi:10.1101/gad.1569307 (2007).

36   Ciganda, M. & Williams, N. Eukaryotic 5S rRNA biogenesis. *Wiley Interdiscip Rev RNA* **2**, 523-533, doi:10.1002/wrna.74 (2011).

37   Venema, J. & Tollervey, D. Ribosome synthesis in Saccharomyces cerevisiae. *Annu Rev Genet* **33**, 261-311, doi:10.1146/annurev.genet.33.1.261 (1999).

38   Schafer, T. *et al.* The path from nucleolar 90S to cytoplasmic 40S pre-ribosomes. *EMBO J* **22**, 1370-1380, doi:10.1093/emboj/cdg121 (2003).

39   Moy, T. I. & Silver, P. A. Nuclear export of the small ribosomal subunit requires the ran-GTPase cycle and certain nucleoporins. *Genes Dev* **13**, 2118-2133 (1999).

40   Moy, T. I. & Silver, P. A. Requirements for the nuclear export of the small ribosomal subunit. *J Cell Sci* **115**, 2985-2995 (2002).

41   Oeffinger, M. *et al.* A pre-ribosome-associated HEAT-repeat protein is required for export of both ribosomal subunits. *Genes Dev* **18**, 196-209, doi:10.1101/gad.285604 (2004).

42   Schafer, T. *et al.* Hrr25-dependent phosphorylation state regulates organization of the pre-40S subunit. *Nature* **441**, 651-655, doi:10.1038/nature04840 (2006).

43   Fatica, A. *et al.* Nob1p is required for cleavage of the 3' end of 18S rRNA. *Mol Cell Biol* **23**, 1798-1807 (2003).

44   Granneman, S. *et al.* The putative NTPase Fap7 mediates cytoplasmic 20S pre-rRNA processing through a direct interaction with Rps14. *Mol Cell Biol* **25**, 10352-10364, doi:10.1128/mcb.25.23.10352-10364.2005 (2005).

45   Strunk, B. S. *et al.* Ribosome assembly factors prevent premature translation initiation by 40S assembly intermediates. *Science* **333**, 1449-1453, doi:10.1126/science.1208245 (2011).

46   Nissan, T. A. *et al.* 60S pre-ribosome formation viewed from assembly in the nucleolus until export to the cytoplasm. *EMBO J* **21**, 5539-5547 (2002).

47   Hurt, E. *et al.* A novel in vivo assay reveals inhibition of ribosomal nuclear export in ran-cycle and nucleoporin mutants. *J Cell Biol* **144**, 389-401 (1999).

48   Ho, J. H. *et al.* Nmd3p is a Crm1p-dependent adapter protein for nuclear export of the large ribosomal subunit. *J Cell Biol* **151**, 1057-1066 (2000).

49   Stage-Zimmermann, T. *et al.* Factors affecting nuclear export of the 60S ribosomal subunit in vivo. *Mol Biol Cell* **11**, 3777-3789 (2000).

50   Gadal, O. *et al.* Nuclear export of 60s ribosomal subunits depends on Xpo1p and requires a nuclear export sequence-containing factor, Nmd3p, that associates with the large subunit protein Rpl10p. *Mol Cell Biol* **21**, 3405-3415, doi:10.1128/mcb.21.10.3405-3415.2001 (2001).

51   Sengupta, J. *et al.* Characterization of the nuclear export adaptor protein Nmd3 in association with the 60S ribosomal subunit. *J Cell Biol* **189**, 1079-1086, doi:10.1083/jcb.201001124 (2010).

52   Hung, N. J. & Johnson, A. W. Nuclear recycling of the pre-60S ribosomal subunit-associated factor Arx1 depends on Rei1 in Saccharomyces cerevisiae. *Mol Cell Biol* **26**, 3718-3727, doi:10.1128/mcb.26.10.3718-3727.2006 (2006).

53   Bradatsch, B. *et al.* Arx1 functions as an unorthodox nuclear export receptor for the 60S preribosomal subunit. *Mol Cell* **27**, 767-779, doi:10.1016/j.molcel.2007.06.034 (2007).

54   Hung, N. J. *et al.* Arx1 is a nuclear export receptor for the 60S ribosomal subunit in yeast. *Mol Biol Cell* **19**, 735-744, doi:10.1091/mbc.E07-09-0968 (2008).

55   Yao, W. *et al.* Nuclear export of ribosomal 60S subunits by the general mRNA export receptor Mex67-Mtr2. *Mol Cell* **26**, 51-62, doi:10.1016/j.molcel.2007.02.018 (2007).

56   Yao, W. *et al.* A versatile interaction platform on the Mex67-Mtr2 receptor creates an overlap between mRNA and ribosome export. *EMBO J* **27**, 6-16, doi:10.1038/sj.emboj.7601947 (2008).

57   Gavin, A. C. *et al.* Functional organization of the yeast proteome by systematic analysis of protein complexes. *Nature* **415**, 141-147, doi:10.1038/415141a (2002).

58   Yao, Y. *et al.* Ecm1 is a new pre-ribosomal factor involved in pre-60S particle export. *RNA* **16**, 1007-1017, doi:10.1261/rna.2012310 (2010).

59   Hackmann, A. *et al.* The mRNA export factor Npl3 mediates the nuclear export of large ribosomal subunits. *EMBO Rep* **12**, 1024-1031, doi:10.1038/embor.2011.155 (2011).

60   Hedges, J. *et al.* Release of the export adapter, Nmd3p, from the 60S ribosomal subunit requires Rpl10p and the cytoplasmic GTPase Lsg1p. *EMBO J* **24**, 567-579, doi:10.1038/sj.emboj.7600547 (2005).

61   West, M. *et al.* Defining the order in which Nmd3p and Rpl10p load onto nascent 60S ribosomal subunits. *Mol Cell Biol* **25**, 3802-3813, doi:10.1128/mcb.25.9.3802-3813.2005 (2005).

62   Gartmann, M. *et al.* Mechanism of eIF6-mediated inhibition of ribosomal subunit joining. *J Biol Chem* **285**, 14848-14851, doi:10.1074/jbc.C109.096057 (2010).

63   Senger, B. *et al.* The nucle(ol)ar Tif6p and Efl1p are required for a late cytoplasmic step of ribosome synthesis. *Mol Cell* **8**, 1363-1373 (2001).

64   Lebreton, A. *et al.* A functional network involved in the recycling of nucleocytoplasmic pre-60S factors. *J Cell Biol* **173**, 349-360, doi:10.1083/jcb.200510080 (2006).

65   Meyer, A. E. *et al.* The specialized cytosolic J-protein, Jjj1, functions in 60S ribosomal subunit biogenesis. *Proc Natl Acad Sci U S A* **104**, 1558-1563, doi:10.1073/pnas.0610704104 (2007).

66   Klinge, S. *et al.* Crystal structure of the eukaryotic 60S ribosomal subunit in complex with initiation factor 6. *Science* **334**, 941-948, doi:10.1126/science.1211204 (2011).

67   Nissan, T. A. *et al.* A pre-ribosome with a tadpole-like structure functions in ATP-dependent maturation of 60S subunits. *Mol Cell* **15**, 295-301, doi:10.1016/j.molcel.2004.06.033 (2004).

68   Ulbrich, C. *et al.* Mechanochemical removal of ribosome biogenesis factors from nascent 60S ribosomal subunits. *Cell* **138**, 911-922, doi:10.1016/j.cell.2009.06.045 (2009).

69   Shine, J. & Dalgarno, L. The 3'-terminal sequence of Escherichia coli 16S ribosomal RNA: complementarity to nonsense triplets and ribosome binding sites. *Proc Natl Acad Sci U S A* **71**, 1342-1346 (1974).

70   Klinge, S. *et al.* Atomic structures of the eukaryotic ribosome. *Trends Biochem Sci* **37**, 189-198, doi:10.1016/j.tibs.2012.02.007 (2012).

71   Simonetti, A. *et al.* A structural view of translation initiation in bacteria. *Cell Mol Life Sci* **66**, 423-436, doi:10.1007/s00018-008-8416-4 (2009).

72   Gao, Y. G. *et al.* The structure of the ribosome with elongation factor G trapped in the posttranslocational state. *Science* **326**, 694-699, doi:10.1126/science.1179709 (2009).

73   Schmeing, T. M. *et al.* The crystal structure of the ribosome bound to EF-Tu and aminoacyl-tRNA. *Science* **326**, 688-694, doi:10.1126/science.1179700 (2009).

74   Brandt, F. *et al.* The three-dimensional organization of polyribosomes in intact human cells. *Mol Cell* **39**, 560-569, doi:10.1016/j.molcel.2010.08.003 (2010).

75   Petry, S. *et al.* The termination of translation. *Curr Opin Struct Biol* **18**, 70-77, doi:10.1016/j.sbi.2007.11.005 (2008).

76   Zavialov, A. V. *et al.* Splitting of the posttermination ribosome into subunits by the concerted action of RRF and EF-G. *Mol Cell* **18**, 675-686, doi:10.1016/j.molcel.2005.05.016 (2005).

77   Gao, N. *et al.* Specific interaction between EF-G and RRF and its implication for GTP-dependent ribosome splitting into subunits. *J Mol Biol* **374**, 1345-1358, doi:10.1016/j.jmb.2007.10.021 (2007).

78   Jackson, R. J. *et al.* The mechanism of eukaryotic translation initiation and principles of its regulation. *Nat Rev Mol Cell Biol* **11**, 113-127, doi:10.1038/nrm2838 (2010).

79   Pisarev, A. V. *et al.* The role of ABCE1 in eukaryotic posttermination ribosomal recycling. *Mol Cell* **37**, 196-210, doi:10.1016/j.molcel.2009.12.034 (2010).

80   Leopold, P. E. *et al.* Protein folding funnels: a kinetic approach to the sequence-structure relationship. *Proc Natl Acad Sci U S A* **89**, 8721-8725 (1992).

81   Whitford, P. C. *et al.* Biomolecular dynamics: order-disorder transitions and energy landscapes. *Rep Prog Phys* **75**, 076601, doi:10.1088/0034-4885/75/7/076601 (2012).

82   Carrell, R. W. & Lomas, D. A. Conformational disease. *Lancet* **350**, 134-138, doi:10.1016/s0140-6736(97)02073-4 (1997).

83   Vogel, C. *et al.* Structure, function and evolution of multidomain proteins. *Curr Opin Struct Biol* **14**, 208-216, doi:10.1016/j.sbi.2004.03.011 (2004).

84   Bukau, B. & Horwich, A. L. The Hsp70 and Hsp60 chaperone machines. *Cell* **92**, 351-366 (1998).

85   Mayhew, M. *et al.* Protein folding in the central cavity of the GroEL-GroES chaperonin complex. *Nature* **379**, 420-426, doi:10.1038/379420a0 (1996).

86   Schmid, D. *et al.* Kinetics of molecular chaperone action. *Science* **263**, 971-973 (1994).

87   Zhu, X. *et al.* Structural analysis of substrate binding by the molecular chaperone DnaK. *Science* **272**, 1606-1614 (1996).

88   Szabo, A. *et al.* The ATP hydrolysis-dependent reaction cycle of the Escherichia coli Hsp70 system DnaK, DnaJ, and GrpE. *Proc Natl Acad Sci U S A* **91**, 10345-10349 (1994).

89   Buchberger, A. *et al.* Substrate shuttling between the DnaK and GroEL systems indicates a chaperone network promoting protein folding. *J Mol Biol* **261**, 328-333, doi:10.1006/jmbi.1996.0465 (1996).

90   Palleros, D. R. *et al.* ATP-induced protein-Hsp70 complex dissociation requires K+ but not ATP hydrolysis. *Nature* **365**, 664-666, doi:10.1038/365664a0 (1993).

91   McCarty, J. S. *et al.* The role of ATP in the functional cycle of the DnaK chaperone system. *J Mol Biol* **249**, 126-137, doi:10.1006/jmbi.1995.0284 (1995).

92   Theyssen, H. *et al.* The second step of ATP binding to DnaK induces peptide release. *J Mol Biol* **263**, 657-670 (1996).

93   Pierpaoli, E. V. *et al.* The power stroke of the DnaK/DnaJ/GrpE molecular chaperone system. *J Mol Biol* **269**, 757-768, doi:10.1006/jmbi.1997.1072 (1997).

94   Flynn, G. C. *et al.* Peptide binding and release by proteins implicated as catalysts of protein assembly. *Science* **245**, 385-390 (1989).

95   Ha, J. H. & McKay, D. B. ATPase kinetics of recombinant bovine 70 kDa heat shock cognate protein and its amino-terminal ATPase domain. *Biochemistry* **33**, 14625-14635 (1994).

96   Liberek, K. *et al.* Escherichia coli DnaJ and GrpE heat shock proteins jointly stimulate ATPase activity of DnaK. *Proc Natl Acad Sci U S A* **88**, 2874-2878 (1991).

97   Wall, D. *et al.* The NH2-terminal 108 amino acids of the Escherichia coli DnaJ protein stimulate the ATPase activity of DnaK and are sufficient for lambda replication. *J Biol Chem* **269**, 5446-5451 (1994).

98   Karzai, A. W. & McMacken, R. A bipartite signaling mechanism involved in DnaJ-mediated activation of the Escherichia coli DnaK protein. *J Biol Chem* **271**, 11236-11246 (1996).

99   Szabo, A. *et al.* A zinc finger-like domain of the molecular chaperone DnaJ is involved in binding to denatured protein substrates. *EMBO J* **15**, 408-417 (1996).

100   Langer, T. *et al.* Successive action of DnaK, DnaJ and GroEL along the pathway of chaperone-mediated protein folding. *Nature* **356**, 683-689, doi:10.1038/356683a0 (1992).

101   Schroder, H. *et al.* DnaK, DnaJ and GrpE form a cellular chaperone machinery capable of repairing heat-induced protein damage. *EMBO J* **12**, 4137-4144 (1993).

102   Gamer, J. *et al.* A cycle of binding and release of the DnaK, DnaJ and GrpE chaperones regulates activity of the Escherichia coli heat shock transcription factor sigma32. *EMBO J* **15**, 607-617 (1996).

103   Kramer, G. *et al.* The ribosome as a platform for co-translational processing, folding and targeting of newly synthesized proteins. *Nat Struct Mol Biol* **16**, 589-597, doi:10.1038/nsmb.1614 (2009).

104   Adams, J. M. On the release of the formyl group from nascent protein. *J Mol Biol* **33**, 571-589 (1968).

105   Housman, D. *et al.* Removal of formyl-methionine residue from nascent bacteriophage f2 protein. *J Mol Biol* **65**, 163-166 (1972).

106   Giglione, C. *et al.* Protein N-terminal methionine excision. *Cell Mol Life Sci* **61**, 1455-1474, doi:10.1007/s00018-004-3466-8 (2004).

107   Lowther, W. T. & Matthews, B. W. Structure and function of the methionine aminopeptidases. *Biochim Biophys Acta* **1477**, 157-167 (2000).

108   Polevoda, B. & Sherman, F. Composition and function of the eukaryotic N-terminal acetyltransferase subunits. *Biochem Biophys Res Commun* **308**, 1-11 (2003).

109   Jaenicke, R. Protein folding: local structures, domains, subunits, and assemblies. *Biochemistry* **30**, 3147-3161 (1991).

110   Deuerling, E. *et al.* Trigger factor and DnaK cooperate in folding of newly synthesized proteins. *Nature* **400**, 693-696, doi:10.1038/23301 (1999).

111   Teter, S. A. *et al.* Polypeptide flux through bacterial Hsp70: DnaK cooperates with trigger factor in chaperoning nascent chains. *Cell* **97**, 755-765 (1999).

112   Wiedmann, B. *et al.* A protein complex required for signal-sequence-specific sorting and translocation. *Nature* **370**, 434-440, doi:10.1038/370434a0 (1994).

113   Gautschi, M. *et al.* A functional chaperone triad on the yeast ribosome. *Proc Natl Acad Sci U S A* **99**, 4209-4214, doi:10.1073/pnas.062048599 (2002).

114   Carla Fama, M. *et al.* The Saccharomyces cerevisiae YFR041C/ERJ5 gene encoding a type I membrane protein with a J domain is required to preserve the folding capacity of the endoplasmic reticulum. *Biochim Biophys Acta* **1773**, 232-242, doi:10.1016/j.bbamcr.2006.10.011 (2007).

115   Gautschi, M. *et al.* RAC, a stable ribosome-associated complex in yeast formed by the DnaK-DnaJ homologs Ssz1p and zuotin. *Proc Natl Acad Sci U S A* **98**, 3762-3767, doi:10.1073/pnas.071057198 (2001).

116   Yan, W. *et al.* Zuotin, a ribosome-associated DnaJ molecular chaperone. *EMBO J* **17**, 4809-4817, doi:10.1093/emboj/17.16.4809 (1998).

117   Hundley, H. *et al.* The in vivo function of the ribosome-associated Hsp70, Ssz1, does not require its putative peptide-binding domain. *Proc Natl Acad Sci U S A* **99**, 4203-4208, doi:10.1073/pnas.062048399 (2002).

118   Huang, P. *et al.* The Hsp70 Ssz1 modulates the function of the ribosome-associated J-protein Zuo1. *Nat Struct Mol Biol* **12**, 497-504, doi:10.1038/nsmb942 (2005).

119   Pfund, C. *et al.* The molecular chaperone Ssb from Saccharomyces cerevisiae is a component of the ribosome-nascent chain complex. *EMBO J* **17**, 3981-3989, doi:10.1093/emboj/17.14.3981 (1998).

120   Pfund, C. *et al.* Divergent functional properties of the ribosome-associated molecular chaperone Ssb compared with other Hsp70s. *Mol Biol Cell* **12**, 3773-3782 (2001).

121   Zhang, S. *et al.* Zuotin, a putative Z-DNA binding protein in Saccharomyces cerevisiae. *EMBO J* **11**, 3787-3796 (1992).

122   Wilhelm, M. L. *et al.* Transfer RNA binding protein in the nucleus of Saccharomyces cerevisiae. *FEBS Lett* **349**, 260-264 (1994).

123   Raychaudhuri, S. *et al.* Zuotin, a DnaJ molecular chaperone, stimulates cap-independent translation in yeast. *Biochem Biophys Res Commun* **350**, 788-795, doi:10.1016/j.bbrc.2006.09.124 (2006).

124   Conz, C. *et al.* Functional characterization of the atypical Hsp70 subunit of yeast ribosome-associated complex. *J Biol Chem* **282**, 33977-33984, doi:10.1074/jbc.M706737200 (2007).

125   Muldoon-Jacobs, K. L. & Dinman, J. D. Specific effects of ribosome-tethered molecular chaperones on programmed -1 ribosomal frameshifting. *Eukaryot Cell* **5**, 762-770, doi:10.1128/ec.5.4.762-770.2006 (2006).

126   Motohashi, K. *et al.* Isolation of the stable hexameric DnaK.DnaJ complex from Thermus thermophilus. *J Biol Chem* **269**, 27074-27079 (1994).

127   Otto, H. *et al.* The chaperones MPP11 and Hsp70L1 form the mammalian ribosome-associated complex. *Proc Natl Acad Sci U S A* **102**, 10064-10069, doi:10.1073/pnas.0504400102 (2005).

128   Fiaux, J. *et al.* Structural analysis of the ribosome-associated complex (RAC) reveals an unusual Hsp70/Hsp40 interaction. *J Biol Chem* **285**, 3227-3234, doi:10.1074/jbc.M109.075804 (2010).

129   Klingelschild. It's all about me. (2012).

130   Merck. *Rosetta 2 (DE3) genotype*, <http://www.merckmillipore.com/germany/life-science-research/rosetta-2-competent-cell-set/EMD_BIO-71405/p_XGSb.s1OgJoAAAEjSxl9.zLX> (2012).

131   EcoliWiki. *XL1 Blue genotype*, <http://ecoliwiki.net/colipedia/index.php/XL-1_Blue> (2009).

132   Scharf, S. J. *et al.* Direct cloning and sequence analysis of enzymatically amplified genomic sequences. *Science* **233**, 1076-1078 (1986).

133   Saiki, R. K. *et al.* Primer-directed enzymatic amplification of DNA with a thermostable DNA polymerase. *Science* **239**, 487-491 (1988).

134   Weber, K. & Osborn, M. The reliability of molecular weight determinations by dodecyl sulfate-polyacrylamide gel electrophoresis. *J Biol Chem* **244**, 4406-4412 (1969).

135   Frank, J. *et al.* SPIDER and WEB: processing and visualization of images in 3D electron microscopy and related fields. *J Struct Biol* **116**, 190-199, doi:10.1006/jsbi.1996.0030 (1996).

136   Becker, T. *et al.* Structural basis of highly conserved ribosome recycling in eukaryotes and archaea. *Nature* **482**, 501-506, doi:10.1038/nature10829 (2012).

137   Chen, J. Z. & Grigorieff, N. SIGNATURE: a single-particle selection system for molecular electron microscopy. *J Struct Biol* **157**, 168-173, doi:10.1016/j.jsb.2006.06.001 (2007).

138   Norousi, R. *et al. Automatic post-picking improves particle image detection from Cryo-EM micrographs*, <http://arxiv.org/abs/1112.3173v2> (2011).

139   Pettersen, E. F. *et al.* UCSF Chimera--a visualization system for exploratory research and analysis. *J Comput Chem* **25**, 1605-1612, doi:10.1002/jcc.20084 (2004).

140   Frank, J. Single-particle imaging of macromolecules by cryo-electron microscopy. *Annu Rev Biophys Biomol Struct* **31**, 303-319, doi:10.1146/annurev.biophys.31.082901.134202 (2002).

141   Konarev, P. V. *et al.* PRIMUS: a Windows PC-based system for small-angle scattering data analysis. *Journal of Applied Crystallography* **36**, 1277-1282, doi:doi:10.1107/S0021889803012779 (2003).

142   Putnam, C. D. *et al.* X-ray solution scattering (SAXS) combined with crystallography and computation: defining accurate macromolecular structures, conformations and assemblies in solution. *Q Rev Biophys* **40**, 191-285, doi:10.1017/s0033583507004635 (2007).

143   Svergun, D. I. *et al.* Determination of domain structure of proteins from X-ray solution scattering. *Biophys J* **80**, 2946-2953, doi:10.1016/s0006-3495(01)76260-1 (2001).

144   Volkov, V. V. & Svergun, D. I. Uniqueness of ab initio shape determination in small-angle scattering. *Journal of Applied Crystallography* **36**, 860-864, doi:doi:10.1107/S0021889803000268 (2003).

145   Amlacher, S. *et al.* Insight into structure and assembly of the nuclear pore complex by utilizing the genome of a eukaryotic thermophile. *Cell* **146**, 277-289, doi:10.1016/j.cell.2011.06.039 (2011).

146   Larkin, M. A. *et al.* Clustal W and Clustal X version 2.0. *Bioinformatics* **23**, 2947-2948, doi:10.1093/bioinformatics/btm404 (2007).

147   Goujon, M. *et al.* A new bioinformatics analysis tools framework at EMBL-EBI. *Nucleic Acids Res* **38**, W695-699, doi:10.1093/nar/gkq313 (2010).

148   Armache, J. P. *et al.* Localization of eukaryote-specific ribosomal proteins in a 5.5-A cryo-EM map of the 80S eukaryotic ribosome. *Proc Natl Acad Sci U S A* **107**, 19754-19759, doi:10.1073/pnas.1010005107 (2010).

149   Segref, A. *et al.* The evolutionarily conserved region of the U snRNA export mediator PHAX is a novel RNA-binding domain that is essential for U snRNA export. *RNA* **7**, 351-360 (2001).

150   Mourao, A. *et al.* Structure and RNA recognition by the snRNA and snoRNA transport factor PHAX. *RNA* **16**, 1205-1216, doi:10.1261/rna.2009910 (2010).

151   Abràmoff, M. D. *et al.* Image Processing with ImageJ. *Biophotonics International* **11**, 36-42 (2004).

152   Rost, B. *et al.* The PredictProtein server. *Nucleic Acids Res* **32**, W321-326, doi:10.1093/nar/gkh377 (2004).

153   Leidig, C. *Structural and functional characterization of the S. cerevisiae ribosome associated complex (RAC)* Master of Science (Biochemistry) thesis, Ludwig-Maximilians-Universität München, (2008).

154   Walter, T. S. *et al.* Lysine methylation as a routine rescue strategy for protein crystallization. *Structure* **14**, 1617-1622, doi:10.1016/j.str.2006.09.005 (2006).

155   Lorber, B. *et al.* Crystal growth of proteins, nucleic acids, and viruses in gels. *Prog Biophys Mol Biol* **101**, 13-25, doi:10.1016/j.pbiomolbio.2009.12.002 (2009).

156   Flaherty, K. M. *et al.* Three-dimensional structure of the ATPase fragment of a 70K heat-shock cognate protein. *Nature* **346**, 623-628, doi:10.1038/346623a0 (1990).

157   Flaherty, K. M. *et al.* Structural basis of the 70-kilodalton heat shock cognate protein ATP hydrolytic activity. II. Structure of the active site with ADP or ATP bound to wild type and mutant ATPase fragment. *J Biol Chem* **269**, 12899-12907 (1994).

158   Johnson, E. R. & McKay, D. B. Mapping the role of active site residues for transducing an ATP-induced conformational change in the bovine 70-kDa heat shock cognate protein. *Biochemistry* **38**, 10823-10830, doi:10.1021/bi990816g (1999).

159   O'Brien, M. C. *et al.* Lysine 71 of the chaperone protein Hsc70 Is essential for ATP hydrolysis. *J Biol Chem* **271**, 15874-15878 (1996).

160   Sousa, M. C. & McKay, D. B. The hydroxyl of threonine 13 of the bovine 70-kDa heat shock cognate protein is essential for transducing the ATP-induced conformational change. *Biochemistry* **37**, 15392-15399, doi:10.1021/bi981510x (1998).

161   Becker, T. *et al.* Structure of monomeric yeast and mammalian Sec61 complexes interacting with the translating ribosome. *Science* **326**, 1369-1373, doi:10.1126/science.1178535 (2009).

162   Fribourg, S. & Conti, E. Structural similarity in the absence of sequence homology of the messenger RNA export factors Mtr2 and p15. *EMBO Rep* **4**, 699-703, doi:10.1038/sj.embor.embor883 (2003).

163   Vembar, S. S. *et al.* The mammalian Hsp40 ERdj3 requires its Hsp70 interaction and substrate-binding properties to complement various yeast Hsp40-dependent functions. *J Biol Chem* **284**, 32462-32471, doi:10.1074/jbc.M109.000729 (2009).

164   Siegel, V. & Walter, P. Removal of the Alu structural domain from signal recognition particle leaves its protein translocation activity intact. *Nature* **320**, 81-84, doi:10.1038/320081a0 (1986).

165   Jia, L. *et al.* Mapping of the Saccharomyces cerevisiae Oxa1-mitochondrial ribosome interface and identification of MrpL40, a ribosomal protein in close proximity to Oxa1 and critical for oxidative phosphorylation complex assembly. *Eukaryot Cell* **8**, 1792-1802, doi:10.1128/ec.00219-09 (2009).

Acknowledgements

Wow, it is done! It has been a pretty long time in the lab and there are lots of people that I would like to thank for their various contributions and support during this time. I will begin with what this section is all about: a huge *THANK YOU* to everyone who is mentioned here. So even if you do not find those words directly associated with your name, they are still meant for you!

First of all, I would like to thank Prof. Dr. Roland Beckmann for giving me the opportunity to do my PhD in his lab and for providing the probably best working environment I could imagine. Naturally, there have been ups and downs, but retrospectively I had a great time in his lab. Marco introduced me to the lab and the RAC project when I started as a Master's student. He provided me with a solid basis to finally finish this long-lasting project. A special thanks goes to Gert. I did much of my work on the RAC project in a highly productive collaboration with him and I am grateful for many stimulating discussions and brilliant advice. I learned much from that. I would like to thank Charlotte and Otto for making tons of grids, collecting all the data and for their excellent support with anything concerning cryo-EM. Stephan, Thomas, Alex and Jean-Paul were always there when I had any processing questions or computer problems and Andy was brilliantly managing the cluster. I would like to thank Stephan and Julian for sharing their brilliant Titan processing and focused sorting as well as local resolution determination scripts, respectively. Gregor introduced me to SAXS and invested lots of time in explaining things to me. Together with Diana, he also helped me a lot with crystallization setups. I am grateful to Alex, Eli, Diana and Birgitta for taking the time to proof-read the drafts of this thesis and excellent suggestions for corrections.

I would like to thank the entire Beckmann and Wilson labs for providing an enjoyable and productive working environment during my time here. Very special thanks go to Heidi, Joanna and Andrea. Without their constant effort to keep the lab running as smoothly as it does, I would probably still be at my bench instead of writing this thesis. At the same time I would like to thank Ingegerd for brilliantly organizing all of the non-lab tasks. Thank you Alex, Sibylle and Stephan for all the nice lunch breaks with the delicious food we prepared and enjoyed together.

I am also very grateful to all the people that made my life outside the lab so nice and beautiful. Diana, you went with me almost throughout my thesis constantly encouraging and supporting me. Thank you for that! I owe some of my most enjoyable holidays to the "Iceland and Scotland Crew". It was great and I hope we will at some point manage to finally have another trip together! Thanks to all the people that went to the mountains with me for climbing, skiing or hiking.

Last, but by far not least, I would like to thank my parents for unquestioningly supporting me throughout my life – regardless of what I decided to do. You made this possible for me!